Fall 2021

Energy Management and Size Optimization of Hybrid Energy Systems

Mohammadreza Babaei Jamnani
University of Windsor

Energy Management and Size Optimization of Hybrid Energy Systems

by

Mohammadreza Babaei Jamnani

A Thesis

Submitted to the Faculty of Graduate Studies

through the Department of Mechanical, Automotive and Materials Engineering

in Partial Fulfilment of the Requirements for

the Degree of Master of Applied Science at the

University of Windsor

Windsor, Ontario, Canada

2021

Energy Management and Size Optimization of Hybrid Energy Systems

by

Mohammadreza Babaei Jamnani

APPROVED BY:

J. Johrendt

Department of Mechanical, Automotive & Materials Engineering

R. Ruparathna

Department of Civil and Environmental Engineering

D. S-K. Ting, Co-Advisor

Department of Mechanical, Automotive & Materials Engineering

R. Carriveau, Co-Advisor

Department of Civil and Environmental Engineering

August 30th, 2021

DECLARATION OF CO-AUTHORSHIP/ PREVIOUS PUBLICATIONS

I.   Co-Authorship

I hereby declare that this thesis incorporates material that is the result of joint research, as
follows:

- *Chapter II, III, and IV of this thesis also incorporate the outcome of research under the
  supervision of Dr. David S-K. Ting, Dr. and Rupp Carriveau, .In all cases, the author
  performed the key ideas, primary contributions, data analysis, processing, and
  interpretation.*

I am aware of the University of Windsor Senate Policy on Authorship, and I certify that I
have properly acknowledged the contribution of other researchers to my thesis and have obtained
written permission from each of the co-author(s) to include the above material(s) in my thesis.

I certify that, with the above qualification, this thesis, and the research to which it refers,
is the product of my own work.

This thesis includes three original paper that has been previously submitted for publication
in peer-reviewed journals, as follows:

Thesis chapter	Publication Title	Publication status
Chapter II	*Mohammadreza Babaei Jamnani, David S-K. Ting, Rupp Carriveau. Feasibility and optimal sizing analysis of stand-alone hybrid energy systems coupled with various battery technologies: A case study of Pelee Island, Journal of Renewable Energy*	*Under review*
Chapter III	*Mohammadreza Babaei Jamnani, David S-K. Ting, Rupp Carriveau.Dispatch strategies-based feasibility analysis of grid-connected hybrid energy systems using sun-tracking PV modules, Journal of Cleaner Production*	*Submitted*
Chapter IV	*Mohammadreza Babaei Jamnani, David S-K. Ting, Rupp Carriveau.Optimal planning of off-grid hybrid microgrids in energy-poor islands using sustainable hydrogen production, International Journal of Hydrogen Energy*	*Submitted*

I certify that I have obtained a written permission from the copyright owner(s) to include the above-published material(s) in my thesis. I certify that the above material describes work completed during my registration as a graduate student at the University of Windsor.

III.   General

I declare that, to the best of my knowledge, my thesis does not infringe upon anyone's copyright nor violate any proprietary rights and that any ideas, techniques, quotations, or any other material from the work of other people included in my thesis, published or otherwise, are fully acknowledged in accordance with the standard referencing practices. Furthermore, to the extent that I have included copyrighted material that surpasses the bounds of fair dealing within the meaning of the Canada Copyright Act, I certify that I have obtained a written permission from the copyright owner(s) to include such material(s) in my thesis.

I declare that this is a true copy of my thesis, including any final revisions, as approved by my thesis committee and the Graduate Studies office, and that this thesis has not been submitted for a higher degree to any other University or Institution.

ABSTRACT

Electricity is assumed as a significant driving force in people's lives, ensuring comfort and boosting the quality of life. However, some remote communities have the least access to the national grid due to the far distance to the province's s industrial and electrical sector. The lack of grid connection has led to antiquated methods of power production, which increases reliance on carbon-based fuels and pollutes the atmosphere. This study focuses on the techno-econo-environmental aspects of introducing hybrid renewable energy systems (HRES) in three energy-poor islands in Eastern Canada. the proposed HRES have been simulated based on real-time field data of solar irradiation, wind speed, ambient temperature, and load demand during 8760 hours in a year. Chapter II examines Pelee Island's reliable and economical hybrid energy solutions by comparing conventional and state-of-the-art storage technologies, namely 1kWh Lead Acid, 1kWh Li-Ion, 100kWh Li-Ion, and Scenario IV: 2.5 kWh PowerSafe SBS (SBS). The optimization results indicate that 152 kW PV module, 200 kW DG, 190 kW CNV, when integrated with 853 1kWh Li-Ion batteries, have the lowest NPC. Fuel price and irradiance of Lead Acid -based systems have a greater impact on renewable fraction but have a lower effect on LCOE. Chapter III evaluates the ability of grid-connected renewable energy solutions to implement four different PV tracking technologies controlled by two energy management strategies(CC and LF). The assumed sun-tracking PV modules contain horizontal-axis monthly adjustment (HMA), horizontal-axis continuous adjustment (HCA), Vertical-Axis continuous adjustment (VCA), and Dual-axis-tracker (DAT). The results indicate that a CC-controlled system equipped with a vertical-axis PV tracker has the optimal solution. The LF-controlled system with a similar tracker has a higher net present cost (NPC), cost of energy (COE), and renewable fraction by ~$0.02M, ~$0.002/kWh and 7.6%, respectively. In Chapter IV, techno-economic feasibility evaluation of simultaneous hydrogen and electricity production is discussed in three energy-poor islands in Canada: Pelee, Saint Pierre, and Wolfe Island, all located in separate directions in Eastern Canada. The optimal sizing for the electric load of 50 residential households and hydrogen for 50 fuel cell electric cars will be conducted in each location. The results show that the impact of load value in minimizing NPC is higher than the expected inflation rate. Paying attention to these research findings highly depends on the location and techno-economic data of the project.

CONTRIBUTION

This thesis shows reliable and cost-effective hybrid renewable energy systems for electrification and hydrogen purposes in various remote localities. The principal contributions of this thesis are:

- Fuel price and irradiance of LA-based systems have a greater impact on renewable fraction but lower LCOE.

- 1 kWh Li-Ion battery-based hybrid options maintain their lowest LCOE and NPC over variation of fuel price, irradiance and required load.

- When comparing storage throughput, it is expected that 100 kWh Li-Ion batteries would be more efficient and have a longer service life than 2.5 kWh SBS batteries.

- NPC of HMA and COE of HVA-based systems controlled with CC dispatch strategies are the most sensitive cases to SOC_{min} fluctuation.

- As a result of load variation, the largest and lowest decrease in energy cost, respectively, is observed in HVA and DA trackers controlled by the CC dispatch strategy.

- LF-controlled systems show more volatility toward albedo variation than CC-controlled systems. The albedo of ~60% obtains the appropriate results compared to all other ground cover types based on the economic perspectives.

- Analyzing the volatility in resource assessment indicates that predicting the energy cost over a short-term project is challenging

- The salvage share in the long-term project is more than that of the short-term, indicating that the long-term project is more cost-effective for the government.

DEDICATION

I dedicate this work to my parents and beautiful sister, who have supported me throughout this endeavour.

ACKNOWLEDGEMENTS

I would like to acknowledge the invaluable guidance, wisdom, and patience provided by my co-advisors, Dr. David S-K Ting and Dr. Rupp Carriveau. I appreciated the support that they provided during the past year was crucial in my personal improvement. I have truly enjoyed working with them in the Turbulence & Energy Laboratory, and I have found them to be accommodating and knowledgeable whenever I've sought their insight. I hope our relationship continues to grow in the future.

TABLE OF CONTENTS

LIST OF TABLES

CHAPTER IV: Conclusions and recommendations

LIST OF FIGURES

CHAPTER IV: Optimal Planning of Off-grid Hybrid Renewable Microgrids Using Sustainable Hydrogen Production

CHAPTER I

Introduction

1.1. Background

The threat of climate change, which is spelled by the combustion of fossil fuels, is one of humanity's greatest challenges today. Established fossil-fuel-based power production technologies are unsustainable and have resulted in the accumulation of greenhouse gases and an increase in global temperature [1]. Moreover, the globally increasing population and equally energy demand acceleration in these areas call for a reliable and cost-effective alternative [2]. In this regard, the employment of renewable power options (i.e. solar, wind, biomass, hydrogen) as natural, accessible, clean, and easily replenished energy sources is necessary to respond to emission production and ever-increasing global energy consumption [3]. However, implementing such renewable technologies is highly site-specific and dependent on locally available renewable resources and load demand. Hence, it is crucial to undertake the resource assessment as precisely as possible. The wind speed, solar irradiation, amount of biomass, and annual frequency are key parameters that identify the output of the energy components. Similarly, at each specific location, the application of renewable energy technologies requires a thorough resource assessment.

Many communities are currently suffering load constraints, which has caused infrastructure growth to be halted. There are over 292 remote communities with no access to commercial forms of energy in Canada, many of which rely on diesel generators for a power source [4]. The use of renewables can help improve conditions for people living in these remote and difficult-to-reach communities. In some situations, it can lower operating costs through minimization of fuel consumption, increases in system efficiency, and reduced pollution and noise [5]. The definition of "remote area" varies from region to region; for instance, "remote areas" in the first-world nations are denoted by the localities with a long physical distance from the nearest town or service center [6]. Technical constraints to electrify remote areas can be factors like uneven terrains, limited transmission, dispersed and sparse populations. Higher initial cost and output intermittency in renewable energy technologies are often challenged to establish more sustainable and critically reliable energy systems.

There are some potential issues with grid-connected electrification in Ontario. Firstly, grid-delivered electricity in Ontario has an alarming carbon intensity of 77 g/kWh [7], which made this province boost Made-in-Ontario green energy systems to lower emissions [8]. Secondly, It has been estimated that cleaning up Ontario's grid saved $4.4 billion per annum in health, financial, and environmental costs [9]. Meanwhile, since Ontario has not shown its promising emissions rate, some policies called "back stop" have already been applied to this territory. One of them is maximizing the carbon tax by 566% during ten years($30 tonne/emissions in 2020 to $170 tonne/emissions in 2030) [10].

Among remote places in Canada, Pelee Island is Canada's southernmost community, located in Essex County, Ontario. It sits near the middle of Lake Erie and has diverse ecological significance critical to Canada's national heritage. Pelee residents are currently dependent on a 26-kilometer underwater cable that typically fails when residents need it most, especially during the tourist season. Beyond this, despite the fact that three-phase power is the standard in Canada's business and agricultural sectors, the cable only delivers single-phase power. Also, according to Canadian Ambient Air Quality Standards (CAAQS), in three consecutive years (2015-2017), Essex County, Ontario, and its surrounding places, which includes Pelee Island, have not met CAAQS ozone standard [18]. Agriculture and tourism are the major sources of revenue on Pelee Island. Bringing independent commercial forms of energy is a key to poverty eradication, risk avoidance, environmental protection, and sustainable economic growth. The availability of commercial energy via renewables can also promote economic growth via job creation, product transportation to market, and grows education and the provision of health services. More importantly, local renewable solutions serve as an intriguing non-wires alternative to upgrading the compromised underwater cable and connected substations.

1.2. Objectives and Scope

This work aims to: (i) determine the reliable and cost-effective hybrid solutions through renewable components in Pelee Island via cost optimization technique (ii) investigate techno-econo-environmental parameters of various battery and solar tracking technologies coupled with each system (iii) study connectivity status on the operation and cost of the optimal results (iv) compare operation based on the energy management controllers and (v) impacts of the project lifetime through the production of sustainable hydrogen and electricity via renewables.

A brief outline of all the chapters that follow is presented next.

Chapter II: Review of Literature

A review of the research findings close to this research is presented. It evaluates the various renewable energy sources and technologies with their current status and potential. Technologies to harness these renewable sources are outlined, along with a brief description of microgrids and optimization procedures.

Chapter II: Autonomous Hybrid Renewable Energy Systems (HRES) – Impacts of battery technologies. This chapter introduces the concept of off-grid renewable energy systems under conventional and state-of-art battery types and analyzes their techno-economic features in detail. The renewable resources involved in this chapter contain solar irradiation and wind speed with/without diesel generator. Impacts of volatility in solar irradiance, required load, and fuel price values on each battery-based hybrid solution have not been compared in many findings.

Chapter III: Dispatch strategies-based analysis of grid-connected HRES – Impacts of sun-tracking modules

The compatibility of various PV tracking technologies operating with CC and LF dispatch strategies under grid-connected systems will be discussed in this chapter. Cost and efficiency optimization of the feasible results is conducted via HOMER software.

Chapter IV: Optimal planning of off-grid HRES – Sustainable Hydrogen production

This chapter evaluates three energy-poor islands, namely, Pelee, Saint Pierre, and Wolfe Island, all of which are located in separate directions in Eastern Canada. The optimal sizing for the electric load of 50 residential households and hydrogen for 25 fuel cell electric cars will be compared in each location.

Chapter IV: Conclusions and Recommendations

Firstly, a comparison procedure of optimal planning and financial results for the previous chapters will be conducted to other analogous works worldwide. Then, based on previous chapters' sensitivity analysis and research findings, optimal and appropriate suggestions will be offered.

References

[1]   M. GRANOVSKII, I. DINCER, and M. ROSEN, "Greenhouse gas emissions reduction by use of wind and solar energies for hydrogen and electricity production: Economic factors," *Int. J. Hydrogen Energy*, vol. 32, no. 8, pp. 927–931, Jun. 2007, doi: 10.1016/j.ijhydene.2006.09.029.

[2]   H. El-houari, A. Allouhi, S. Rehman, and M. S. Buker, "Design, Simulation, and Economic Optimization of an O ff -Grid Photovoltaic System for Rural Electrification."

[3]   M. Shabani and J. Mahmoudimehr, "Techno-economic role of PV tracking technology in a hybrid PV-hydroelectric standalone power system," *Appl. Energy*, vol. 212, pp. 84–108, Feb. 2018, doi: 10.1016/j.apenergy.2017.12.030.

[4]   K. Karanasios and P. Parker, "Recent Developments in Renewable Energy in Remote AboriginalKaranasios, K., & Parker, P. (n.d.). Recent Developments in Renewable Energy in Remote Aboriginal Communities, Ontario, Canada. PCED (Vol. 16). Retrieved from http://www.hydroone.com/OurCommitmen," *Pap. Can. Econ. Dev.*, vol. 16, pp. 82–97, 2016.

[5]   F. Diab, H. Lan, L. Zhang, and S. Ali, "An environmentally friendly factory in Egypt based on hybrid photovoltaic/wind/diesel/battery system," *J. Clean. Prod.*, vol. 112, pp. 3884–3894, 2016, doi: 10.1016/j.jclepro.2015.07.008.

[6]   T. Jamal, T. Urmee, M. Calais, G. M. Shafiullah, and C. Carter, "Technical challenges of PV deployment into remote Australian electricity networks: A review," *Renew. Sustain. Energy Rev.*, vol. 77, no. xxxx, pp. 1309–1325, 2017, doi: 10.1016/j.rser.2017.02.080.

[7]   L. C. Buildings, "Carbon intensity and the Ontario electrical grid," *Arborus consulting*, 2016. [Online]. Available: http://arborus.ca/2016/05/carbon-intensity-and-the-ontario-electrical-grid/#:~:text=However%2C grid-delivered electricity in,generate most of Ontario's electricity.

[8]   J. Thornton, "The Future of Ontario's Electricity Grid. Charging Forward," *Environ. Def. Canada*, 2020, doi: 10.1115/1.2012-aug-2.

[9]   "Ontario Ministry of Energy, Northern Development and Mines (2017). The End of Coal," 2017. [Online]. Available: https://www.ontario.ca/page/end-coal.

[10]   A. Harvie, M. Collett, G. Smeijers, and Mélissa Devost, "Canada to increase carbon taxes by 566%," *Norton Rose Fulbright*, 2020. [Online]. Available: https://www.nortonrosefulbright.com/en/knowledge/publications/d58ef644/canada-to-increase-carbon-taxes-by-566.

CHAPTER II

Feasibility and optimal sizing analysis of stand-alone hybrid energy systems coupled with various battery technologies: A case study of Pelee Island

2.1. Introduction

In 2018, the environmental and economic benefits of a renewable energy transition motivated a number of countries to pursue generating more than 20% of their electricity from solar photovoltaics and wind power. According to planning scenarios, the distribution of clean energy in the final energy supply is more likely to develop as 17% by 2030 and 25% by 2050 [11], [12].

To improve reliability, these renewable energy converters are often coupled with low-cost storage systems such as batteries as a backup and stabilizer of energy supply to meet the peak load demands when sun and wind are not available [13], [14]. However, from a techno-economic standpoint, the planning and optimal sizing of such a stand-alone design are challenging since getting a continuous power supply from renewable resources such as solar and wind is impossible [15].In this regard, stand-alone systems are frequently either oversized or undersized to satisfy energy demands. Oversizing a system increases costs and generates excess energy, whereas undersizing a system results in power supply failure to meet load requirements.

Several studies have modelled and analyzed hybrid energy designs with different storage technologies: Lead-acid [16]–[19], Li-ion [20], [21], and vanadium redox flow [22], [23]. Lead-acid (LA) is a very well-established rechargeable battery that still competes with modern battery technologies owing to higher operational safety, lower capital expenditure, and relatively better portable implementation [24]–[27]. The integration of PV and wind energy into existing energy infrastructure receives more attention every year [28]; subsequently, Li-Ion batteries are increasingly being adopted to provide better storage capacity and ancillary services [29]. A third battery type, SBS, is also being implemented to cope with elevated temperatures and harsh environments, made possible by advanced thin plate, pure lead technology, and unique manufacturing methods [30], [31]. The rapid acceleration of battery technology has led to confusion over what design is feasible and which is most technoeconomically suited to serve commercial or residential system applications.

This study focuses on the western side of Pelee Island as it is home to the Island's key loads, which are the backbone of this small community. This study examines the potential for reliable and economical hybrid energy solutions for Pelee Island by comparing conventional and state-of-the-art storage technologies. Further, it provides details of the environmental, technical, and financial features for the optimal designs for the 25 year study period. The study has the potential to serve as a reference point for electrification designs for communities with broadly similar characteristics.

2.2. Methodology

HOMER is a well-known Hybrid Energy System modelling tool. The most important input data to support accurate simulations are meteorological data like temperature and number of daylight hours, renewable resources availability such as solar irradiance and wind speed, load details, technical and financial information. These details are fed into HOMER as monthly averages or time-series data to analyze the output energy of the components based on them [32]. Considering these factors, potential systems are introduced based on a combination of renewable and non-renewable solutions. A non-trivial technical challenge for off-grid hybrid systems is the dispatch strategy or a set of rules that govern the operation of the battery storage and diesel generator(s) [33]. In this research, the cycle charging (CC) dispatch strategy is implemented. As is presented in Fig. 2.1, when the DG is switched on, it runs at its maximum rated capacity to meet the net load and charges the battery with excess energy. In other words, if the produced power by renewable resources and stored energy by the batteries are not sufficient to supply the required demand, the diesel generator is employed to satisfy the electrical load.

The cost of discharging the batteries is calculated using [34].

$$C_{discharging} = C_{battery,wear} + C_{battery,energy} \qquad (2.1)$$

Assuming time step n , battery energy cost, $C_{battery,energy}$ (\$/kWh) and $C_{battery,wear}$, battery wear cost (\$/kWh) are calculated by the following equations:

$$C_{battery,energy,n} = \frac{\sum_{i=1}^{n-1} C_{cc,i}}{\sum_{i=1}^{n-1} E_{cc,i}} \qquad (2.2)$$

where $C_{cc,i}$ is the cost of cycle charging in time step i (\$), and $E_{cc,i}$ is the quantity of energy put into the batteries in time step i (kWh).

$$C_{battery,wear} = \frac{C_{battery,replacement}}{N_{battery}Q_{life}\sqrt{\eta_{rt}}} \qquad (2.3)$$

Where $C_{battery,replacement}$ is the battery replacement cost ($), $N_{battery}$ is the number of batteries in the storage bank, Q_{life} is the single battery throughput (kWh), and η_{th} is the battery round trip efficiency (%). The cost of running the generator at maximum capacity to meet the net load and charge the battery is calculated using the following equation.

$$C_{gen,ch} = C_{gen} + C_{cc} - C_{batt,energy} \qquad (2.4)$$

where C_{cc} here refers to the cost of cycle charge in the current time step, which is calculated by the following equation [34]:

$$C_{cc} = C_{gen,marginal} + C_{battery,wear} \qquad (2.5)$$

$C_{gen,marginal}$ is the marginal cost of the generator ($/kWh), which is calculated using the following expression:

$$C_{gen,marginal} = \frac{F_{slope}F_{price}}{\eta_{th}} \qquad (2.6)$$

where F_{slope} is the slope of fuel curve (L/kWh).
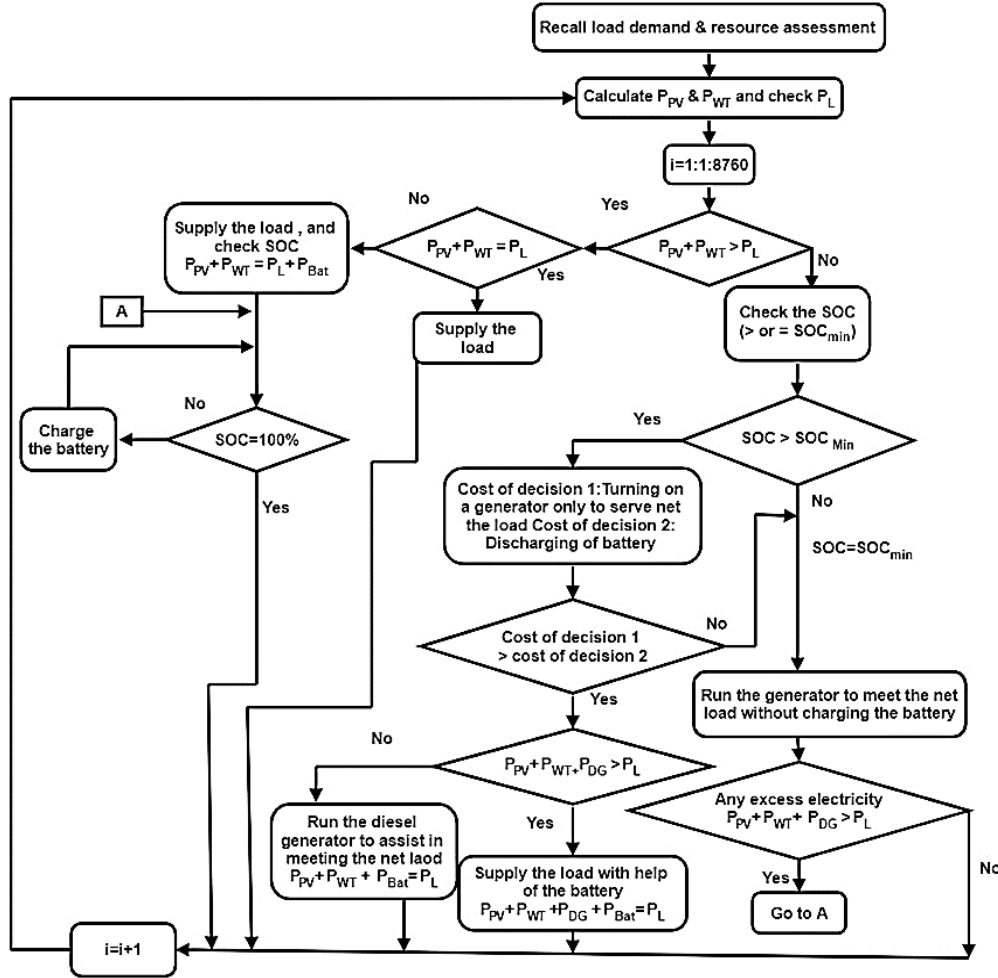
Fig. 2.1. CC dispatch strategy flowchart for off-grid PV/WT/DG system

2.3. Description of the studied area

2.3.1. Renewable resource data

Pelee Island, Ontario, Canada (41.77° N, -82.65° W) is located near the middle of Lake Erie and has an area of approximately 11.2 km², a population of 300 (permanent),1500 (seasonal) residents, and has a cold climate designation [35]. Due to the southerly location and Lake Erie's moderating effect, Pelee Island typically has a slightly milder climate pattern, with relatively notable solar irradiance and wind intensity, compared to the rest of inland Ontario. Fig. 2.2 is provided to present the monthly key data of the site. The climate information has been collected from the "NASA surface meteorology and solar energy database" [36]. The clearness index is a measurement of the atmosphere's clearness. It is the proportion of solar energy that passes through the atmosphere and reaches the Earth's surface. The annual average and maximum irradiance are estimated to be 3.77

8

kWh/m²/day and 6.01 kWh/m²/day, respectively. The irradiance peaks from May to August, varying from 5.28 kWh/m²/day to 6.01 kWh/m²/day. It then reaches a minimum of 1.44 kWh/m²/day in December, which has the lowest cleanness index of 0.411. Also, fall and winter are the windiest periods of the year on the island, from October to March, wind average is observed about 7.9 m/s. The wind rose also depicts wind speed, directions, and wind duration per year. Based on the wind duration, the southern and eastern parts are the windiest and calmest directions on the island, respectively. This study assumes the western side of Pelee Islnad, wherein wind blows for more than 750 hours per year.
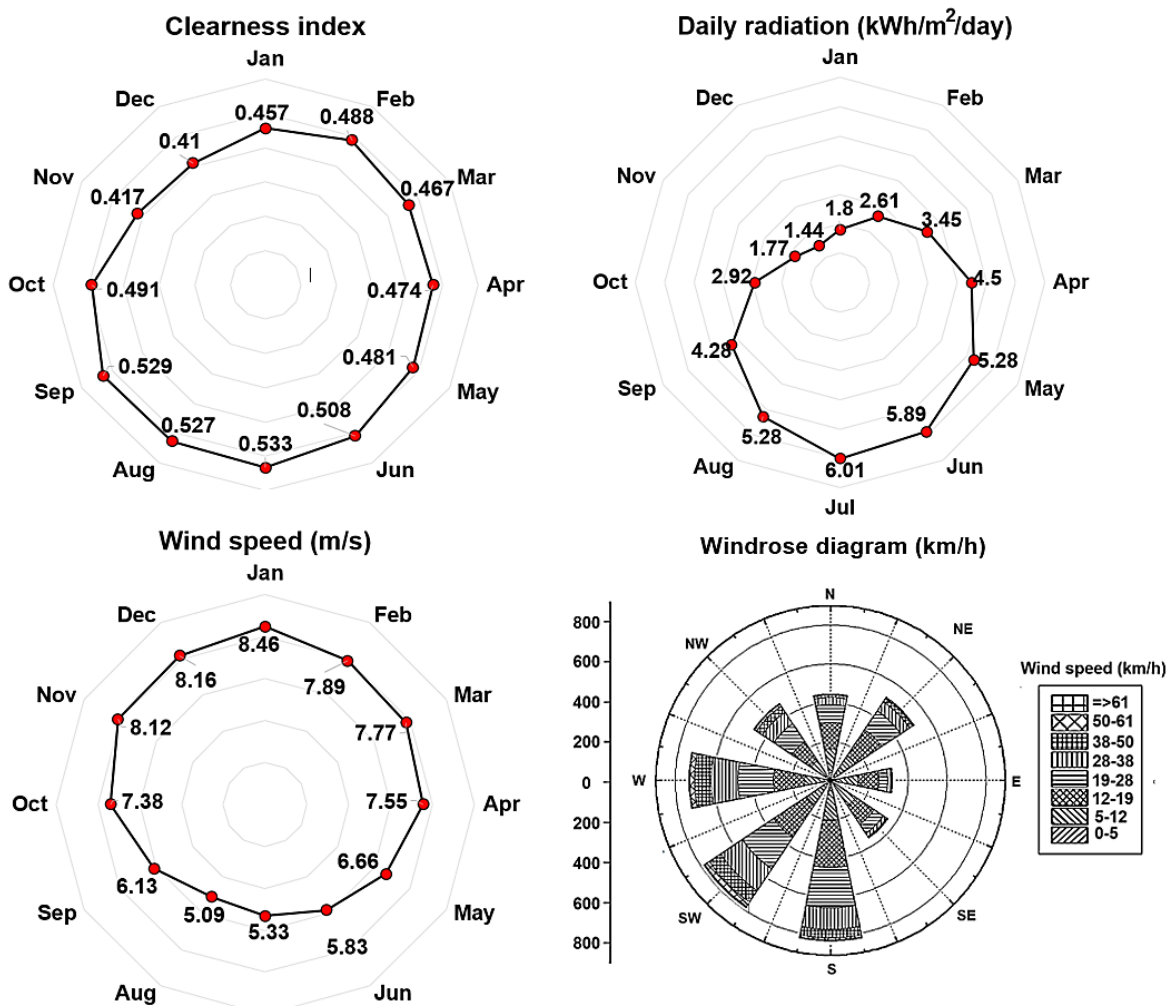
Fig. 2.2. Summary of averaged meteorological data and wind rose in Pelee Island

2.3.2. Electric load data

Table 2.1 categorizes a summary of the property's power needs in western Pelee Island based on the type and average daily consumption. The site's total electricity consumption is estimated to reach a maximum of 2235 kWh/day, which occurs during summer. Less than seventy residential houses, five micro, seven small, and one medium business are located in this area, each of them needs an average of 25,15, 35, and 90 kWh per day, respectively. Considering load details over a year in Fig 2.3(a), it is evident that the highest loads are consumed mostly in the summer with a peak and average of nearly 400 kW and 120 kW, respectively. This peak is due to increased travel and tourism and longer working hours than the rest of the months. On colder days, power consumption of the Pelee residents hovers around 70 kW during winter. Fig 2.3(b) demonstrates the load range versus frequency distribution as well as the cumulative percent of the load. Consumption of 20 to 50 kW/year occurs 50% of the time, while less than 2% of the time, the load ranges between 50 to 80 kW/year and/or beyond 230 kW/year.

Table 2.1. Summary of properties and their average electricity consumption

Type of load	Name of the place	Electricity consumption (kWh/day)
	50 houses	1,250
	Pelee Island Public School	25
	Township of Pelee Municipal Office	25
Residential	Stone House 1891	25
	Driftwood Bed & Bagel	25
	The Gathering Place B&B	25
	Royal Canadian Legion Branch 403	25
	Medical clinic	25
	Pelee Island Coneheads (shop)	15
	Pelee Art Works	15
Micro business	Our Lady, Star of the Sea Church	15
	Comfortech Bicycle Rental	15
	Down the Lane Boutique and Gifts	15
	LCBO	35
	Public Washrooms	35
	Stonehill Bed & Breakfast	35
Small business	Pelee Island Pheasant Farm	35
	At the Farm Table	35
	Anchor and Wheel Inn	35
	The Bakery - Pelee Island	35
Medium business	Pelee Island Winery Pavilion + Pelee Island Vineyards	901
Additional	Streetlights, new properties, improving facilities etc.	400
Total	-	2,235
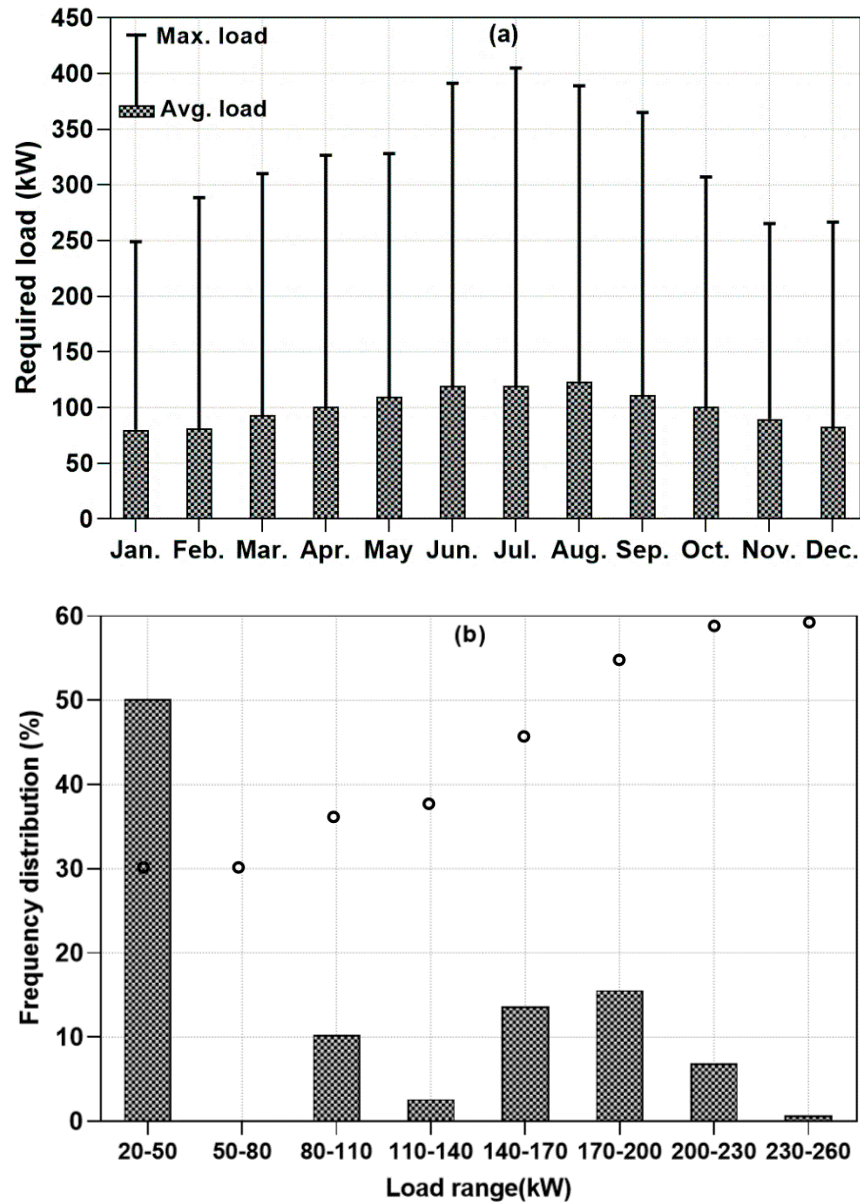
Fig. 2.3. Presentation of (a) probability density mass of load demands and (b) cumulative density of load demands

2.4. System description

Fig. 4 illustrates the possible components of the off-grid HES, which can are investigated to find the winning solutions. It consists of a 200 kW diesel generator, variable size of 1 kW flat-plate PV,10 kW wind turbine, system converter, and four defined 1 kWh battery technologies. The supply priority is set based on the CC dispatch strategy. Table 2.2 presents the defined case

scenarios from I to IV sorted based on battery designs:1kWh LA, 1kWh Li-Ion, 100 kWh Li-Ion, and 2.57 kWh SBS. While schemes here vary depending on the set of system components used to satisfy the load. PV module is assumed to be the primary component in each scheme, and scheme (c) is considered to be the cleanest configuration
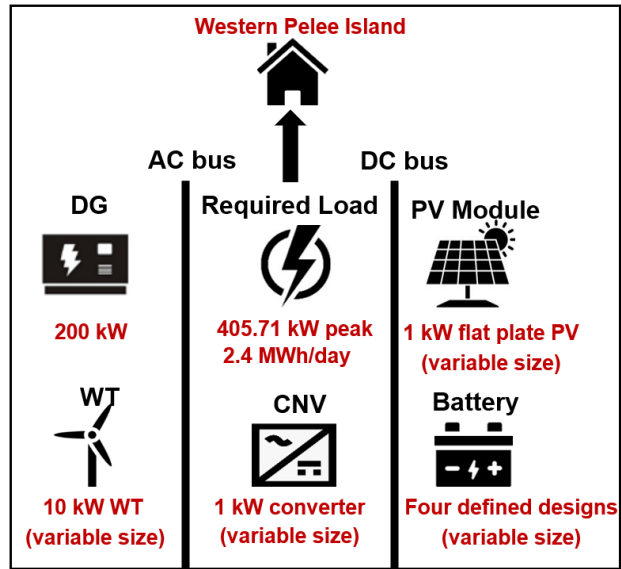
Fig. 2.4. The off-grid set of components

Table 2.2. Definition of scenarios and schemes involved for electrification

Scenario	Scheme	Technologies involved
I	a	PV/DG/CNV/1kWh LA battery
	b	PV/WT/DG/CNV/1kWh LA battery
	c	PV/WT/CNV/1kWh LA battery
II	a	PV/DG/CNV/1kWh Li-Ion battery
	b	PV/WT/DG/CNV/1kWh Li-Ion battery
	c	PV/WT/CNV/1kWh Li-Ion battery
III	a	PV/DG/CNV/100kWh Li-Ion battery
	b	PV/WT/DG/CNV/100kWh Li-Ion battery
	c	PV/WT/CNV/100kWh Li-Ion battery
IV	a	PV/WT/DG/CNV/2.5 kWh SBS battery
	b	PV/WT/DG/CNV/2.5 kWh SBS battery
	c	PV/WT/CNV/2.5 kWh SBS battery

2.4.1. Diesel generator

In order to provide dependable power while considering sustainability simultaneously, backup generation (here in the form of diesel) can be integrated with an HES. Utilizing a Diesel Generator

(DG) also can save initial, operating, and maintenance costs. Here a CAT-250kVA-50Hz-PP DG is selected to firm up power from the renewable components. The diesel generator specs are listed in Table 2.3.

Table 2.3. Technical and economic data of considered diesel generator

Parameter	Value
Name	CAT-250kVA-50Hz-PP
Fuel price ($/L)	0.76
Capacity (kW)	20
Fuel curve intercept (L/hr)	6.68
Fuel curve slope (L/hr/kW)	0.22
LHV (MJ/kg)	43.2
Density (kg/m^3)	820
Carbon content (%)	88
Minimum load ratio (%)	0.25
Lifetime (hours)	15,000

The following equation defines the diesel generator efficiency:

$$\eta_g = \frac{3600 \, P_e}{\rho_f (P_{gen} F_0 + P_e F_1)} \tag{2.7}$$

Where η_g is the generator efficiency(%), P_e is the output power(kW), ρ_f is the fuel density (kg/m^3), P_{gen} is the rated generator power(kW), F_0 is the generator fuel curve intercept co-efficient(L/h/rated kW or m^3/h/rated kW), and F_1 is the fuel curve slope(L/h/ output kW or, m^3/h/output kW). HOMER assumes that the fuel curve is a straight line. The following relation calculates the real generator's fuel consumption in L/h [37]:

$$\dot{m}_{fuel} = F_0 Y_{gen} + F_1 P_{gen} \tag{2.8}$$

where Y_{gen} is the rated capacity of the generator (kW)

2.4.2. PV module

The PV module harvests DC electricity in direct proportion to the solar irradiance incident upon it. The derating factor represents the reduced output in real-world operating conditions as a result of dust accumulation, shading snow cover, wiring losses, and aging [38]. Since Pelee Island has a

relatively high precipitation rate and climate variability, the derating factor was assumed to be 80%. The power output of a solar panel can be calculated using the following equation [62]:

$$p_{PV} = W_{PV} f_{PV} \frac{G_T}{G_S} [1 + \alpha_p (T_C - T_S)] \tag{2.9}$$

where W_{pv} is the peak power output of PV array (kW), f_{pv} is the PV derating factor (%), G_T is the solar radiation incident in the current hour (kW/m^2), G_S is the incident radiation at standard test conditions(1 kW/m^2), α_p is the temperature coefficient (%/°C), T_C is the PV module temperature in the current time step (°C), and T_S is the PV module temperature in standard test condition(25 °C). The number of solar PV panels is assumed to be variable, with each 1 kW generic flat plate with specifications presented in Table 2.4.

Table 2.4. Technical and economic data of considered PV module

Parameter	Value
Related capacity(kW)	1
Temperature coefficient(%/°C)	-0.5
Nominal operating cell temperature (°C)	47
Efficiency at standard test conditions (%)	13
Lifetime(years)	25
Capital cost ($)	2,500
Replacement cost ($)	2,500
O&M cost($/year)	10

2.4.3. Wind Energy Conversion System (WECS)

A 10 kW AC voltage wind turbine is selected for this area. The selection is based on the cut-in and cut-out wind speed values, wind turbine cost, and hub height. The power output for the wind turbine can be calculated by employing the following equation [39]:

$$P = \frac{1}{2} \rho A V^3 C_{PC} \tag{2.10}$$

where ρ is the air density (1.225 kg/m3), V is the wind speed (m/s), A is the rotor swept area (m^2), and C_{pc} is the maximum power coefficient. The technical key data of the selected wind turbine is prepared in Table 2.5.

Table 2.5. Technical and economic data of considered wind turbine

Parameter	Value
Rated capacity(kW)	10
Number of blades	3
Lifetime (years)	20
Hub height (m)	24
Capital cost($)	50,000
Replacement cost($)	50,000
O&M cost($/year)	500

2.4.4. Battery Storage

The battery stores electricity in a chemical form, and subsequently, this stored energy can be recharged and reused to supply continuous operation as required. For the longevity of the battery bank, the maintenance of the battery charge within 20% is very necessary [40]. Four battery technologies are assumed for this research, and the specification of each of them is presented in Table 2.6.

Table 2.6. Technical and economic data of considered battery designs[1] [41]

Parameter	1kWh Li-Ion	1kWh LA	100kWh Li-Ion	2.57 kWh SBS[2]
Nominal voltage (V)	6	12	600	12
Nominal capacity (kWh)	1	1	100	2.57
Capital cost ($)	550	300	70,000	1,400
Replacement ($)	550	300	70,000	1,400
O&M ($/year)	10	10	1,000	20
Lifetime (years)	15	15	15	15
Max. charge/discharge current (A)	167-500	16.7-24.3	167-500	190-983
Min. state of charge (%)	20	40	20	30

The following equation shows how values of battery energy can be estimated [18].

$$Q_{battery} = Q_{battery,0} + \int_0^\tau V_{battery} I_{battery} \, dt \qquad (2.11)$$

$Q_{battery,0}$(kWh) is the initial battery charge, $V_{battery}$(V) is the battery voltage and $I_{battery}$(A) is the battery current

The state of battery charge is expressed by the equation (2.12).

$$B_{soc} = \frac{Q_{battery}}{Q_{battery,max}} \times 100(\%) \qquad (2.12)$$

2.4.5. Converter

The converter maintains the flow of energy between DC and AC, here equivalent to either an inverter or rectifier. The converter converts DC power from the PV module and battery output into AC. In the case of excess wind energy generation, a rectifier converts AC power to DC to be stored in the battery storage system[42]. Table 2.7 supplies the general data of the selected power converter. The power rating of the converters can be obtained from the following equation [43]:

$$P_{inv} = \frac{P_{peak}}{\eta_{inv}} \qquad (2.13)$$

where P$_{peak}$ is the peak load demand, and η$_{inv}$ is inverter efficiency.

Table 2.7. Technical and economic data of considered converter

Parameter	Value
Inverter efficiency(%)	95
Rectifier efficiency(%)	95
Capital cost($/battery)	300
Replacement cost($/battery)	300
O&M cost($/battery/year)	10
Inverter lifetime(years)	15

2.4.6. Economic parameters definition

The system's life cycle total cost can be characterized by NPC, which involves the initial, O&M, replacement and resource-related costs such as fuel cost over the project lifetime. The total NPC ($) is measured by the following equation [44], [45]:

$$C_{npc,tot} = \frac{C_{ann,tot}}{CRF(i, R_{proj})} \tag{2.14}$$

Here, $C_{ann,tot}$ is the total annualized cost (\$/year), i is the annual real interest rate (%), and $CRF(i, n)$ is the capital recovery factor, which is calculated by Eq. 15 [46]:

$$CRF(i, n) = \frac{i(1 + i)^n}{(1 + i)^n - 1} \tag{2.15}$$

which n is the lifetime of the project (year), and i is the annual real interest rate, which is determined by Eq. 6

$$i = \frac{i - f}{1 + f} \tag{2.16}$$

where i is the nominal interest rate (%), and f is the annual inflation rate(%).To measure the LCOE (\$/kWh), the following equation is used [47]:

$$LCOE = \frac{C_{ann,tot}}{L_{ann,load}} \tag{2.17}$$

Here, $L_{ann,load}$ is the total electricity consumption per year (kWh/year), and $C_{ann,tot}$ is the total annualized cost (\$/year)

2.5. Results and discussion

2.5.1. Optimization results

Several stand-alone HES's are modeled to fulfill small-scale residential and commercial energy needs in western Pelee Island. Each hybridized power solution is determined under the CC dispatch method. Further, PV is selected as a mandatory component of generation in each scheme. As specified in Table 8, scheme (a) in scenario II, which is comprised of 152 kW PV arrays, 200 DG, 190 kW CNV, and 853 Li-Ion batteries, has the lowest NPC and LCOE by \$3.67M and 0.321\$/kWh, respectively. This configuration minimizes NPC by \$250,000, \$160,000, and \$270,000 compared to similar schemes in scenarios I, III, and IV. If the diesel generator is neglected, costs will escalate. Namely, scheme (c) is perceived as the optimal design without the generator, followed by the lowest NPC and LCOE of \$14.2 M and 1.24 \$/kWh, respectively. Fig. 5 demonstrates the overall NPC optimization profile versus the variation of CO_2 emissions among the viable options under scenario II. Each feasible configuration is optimized to reach the

appropriate design with the lowest NPC. Among all of the optimized solutions, just one case contributes to the lowest NPC (lowest dot), which here is recognized as the optimal configuration (i.e., winning scheme). This option produces 583 tonnes/year emissions, which is higher than the rest of the feasible options in scenario II and lower than the similar schemes of other scenarios, which is also visible in Table 2.8.

Table 2.8. Parameters of optimized scenarios based on sensitivity variables

	Scheme	PV (kW)	WT (No)	DG (kW)	CNV (kW)	Battery (No)	NPC (M$)	LCOE ($/kWh)	Fuel rate (m^3/yr)	CO$_2$ (t/yr)
Scenario I	a	139	-	200	227	1,104	3.92	0.343	239.8	632.5
	b	147	1	200	231	1,067	3.93	0.343	234.7	619.0
	c	1,942	194	-	452	6,354	21.8	1.91	-	-
Scenario II	a	152	-	200	190	853	3.67	0.321	221.3	583.8
	b	234	3	200	225	731	3.78	0.330	200.8	529.6
	c	2,170	39	-	502	6,640	14.2	1.24	-	-
Scenario III	a	204	-	200	248	7	3.83	0.334	217.3	572.7
	b	121	1	200	249	8	3.85	0.336	224.2	591.4
	c	2,471	34	-	468	64	15.8	1.38	-	-
Scenario IV	a	149	-	200	233	325	3.94	0.344	240.2	633.5
	b	32.5	1	200	233	325	4.01	0.350	250	659.5
	c	2,003	36	-	498	3,072	14.4	1.26	-	-
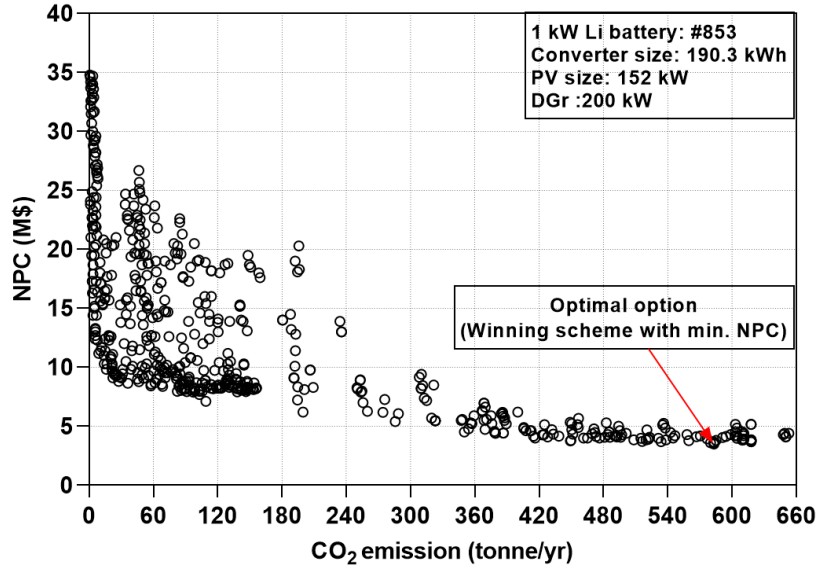
Fig. 2.5. Optimization plot of the NPC against CO_2 emissions

2.5.2.1 Sensitivity analysis

Given the stochasticity of the island climate and the variation of diesel prices in Ontario (0.76 $/L to 1 $/L depending on the location), the proposed HES are evaluated by differing sensitivity variables. These include the diesel fuel price (0.7, 0.8, 0.9, 1, 1.1, 1.2 $/L), average solar radiation (1.8, 3.7, 4.50, 5.20, 6.0, 1.80 kWh/m^2/day), and ambient temperature (-1, 2, 10, 15, 20 °C).Table 11 shows the sensitivity analysis variations of the scheme (a) in scenario II (optimal system), here sorted from lower to higher fuel cost. The nominal discount rate was 8%, with a 2% inflation rate. Nearly 898,864 solutions were simulated, among which 405,527 solutions were feasible, and 493,337 were not, owing to non-optimal utilization of the converter or insufficient power sources. The first three optimal data points for each fuel price at an average irradiance were considered to maintain simplicity. As the ambient temperature rises, the number of battery units, NPC, LCOE and emissions of all hybrid options increase. Wind turbines are used at a fuel cost higher than $1.1/L, where the optimizer ignores DG due to having lower cost-effective solutions. As shown in Table 2.9, both NPC and LCOE increase from $3.6M to $50M when the fuel cost rate shifts from 0.7 $/L to 1.2 $/L. Moreover, here we see the fixed fuel price of 1 $/L when the ambient temperature changes from -1 °C to 15 °C; the NPC and LCOE increase from $4.43M to $45M and 0.387 $/kWh to 0.389 $/kWh, respectively. A summary of the cost breakdown in the optimal scheme (PV-DG) of each scenario is presented in Table 2.10. Nearly 50% of the initial cost in scenario III is tied up in battery storage, namely 100kWh Li-Ion, which is higher than the other

similar scenarios. Using DG, compared to the other components in the system, leads to major O&M costs. O&M under the optimal scheme in scenario I (1kWh Lead-Acid battery) is estimated to be $103.10 k, $96.90 k, and $43.60 k higher than scheme (a) in scenario II, III, and IV, respectively. Further, the lowest diesel fuel cost appears in scenario III as $2133 k, while this scenario owing to high initial equipment cost, can not be economical. PV arrays integrated with the 1 kWh Li-Ion battery (scenario I) represent the lowest overall cost of $366.10 k as compared to the rest of the scenarios. At the end of the project, the remaining cost expressed as salvage cost under scenario III is shown to be $55.7k, which is higher than other scenarios.

Table 2.9. Variation of sensitivity variables against size variation and cost type for the optimal scheme

Fuel cost ($/L)	Ambient temperature (°C)	PV (kW)	WT (kW)	DG (kW)	Battery (No.)	CNV (kW)	NPC (M$)	LCOE ($/kWh)	CO_2 rate (t/yr)
0.7	-1	151.6	-	200	853	190.3	3.67	0.321	583.9
0.7	10	100	-	200	956	213.1	3.71	0.330	529.6
0.7	15	103.5	-	200	959	213	3.72	0.334	637.4
0.8	-1	164.9	-	200	907	183.4	3.84	0.336	565.0
0.8	10	172.8	-	200	891	221.	3.87	0.339	610.6
0.8	15	148.5	-	200	941	218.9	3.89	0.353	636.9
0.9	-1	276.4	-	200	845	183.7	4.18	0.366	533.3
0.9	10	273	-	200	853	203	4.22	0.366	636.3
0.9	15	162	-	200	985	285.2	4.26	0.383	610.1
1	-1	264.6	-	200	845	192.3	4.43	0.388	541.2
1	10	264.4	-	200	875	188.6	4.49	0.389	636.1
1	15	288.2	-	200	853	196.6	4.51	0.409	627.3
1.1	-1	466.8	3	200	472	227.2	4.69	0.410	532.6
1.1	10	519.5	3	200	495	203.5	4.79	0.420	618.2
1.1	15	215.8	1	200	988	182.5	4.83	0.441	635.8
1.2	-1	461.5	4	200	491	204.8	4.91	0.429	445.0
1.2	10	479.5	7	200	405	239.3	5.00	0.434	635.6
1.2	15	352.2	12	200	840	200.7	5.21	0.470	618.1

Table 2.10. Comparison of cost breakdown of scheme (a) designs under four scenarios

	Cost type	DG (k$)	Battery units (k$)	PV system (k$)	Converter (k$)	Total (k$)
Scenario I	Capital	60	331.2	34.8	68	807.3
	Replacement	60.1	292.6	-	28.8	381.5
	O&M	231	142.7	18	29.3	421.1
	Fuel	2356.3	-	-	-	2356.3
	Salvage	0.3	39.6	-	5.4	45.4
Scenario II	Capital	60	469.1	379.2	57	965.4
	Replacement	46	199	-	24.2	269.1
	O&M	163.4	110.2	19.6	24.6	318

	Fuel	2175	-	-	-	2175
	Salvage	12.8	37.5	-	4559	54.8
	System	2,431.5	741	398	101.3	3,672.7
Scenario III	Capital	60	469.1	379.2	57	965.4
	Replacement	46	199	-	24.2	269.1
	O&M	163.4	110.2	19.6	24.6	318
	Fuel	2175	-	-	-	2175
	Salvage	12.8	37.5	-	4559	54.8
	System	2,431.5	741	398	101.3	3,672.7
Scenario IV	Capital	60	455	371.8	70	956.8
	Replacement	77.6	193	-	29.6	300.4
	O&M	244.1	84	19.2	30.1	377.5
	Fuel	2360	-	-	-	2360
	Salvage	12.2	36.3	-	5.5	54.1
	System	2,729.5	695.7	391	124.210	3,940.6

2.5.2.2. Sensitivity analysis of optimal scheme of each scenario

The yearly load profile of the site plays a significant role in estimating NPC and LCOE of the autonomous hybrid power options. Fig. 2.6 (a) and (b) are provided to signify the impacts of the island's average load variation versus NPC and LCOE when the optimized scheme of each defined scenario is utilized. Larger loads lead to increased NPC since the component size will rise. Scenario II(1 kWh Li-Ion-based system) is estimated to be a cost-effective choice. Scenario IV(SBS-based systems) has higher NPC values, although using scenario I (LA-based systems) results in higher LCOE. It is observed that by growing the required load, the associated LCOE can be cheaper so that the highest LCOE is 0.45 $/kWh in scenario I under 840 kWh/day load demand.
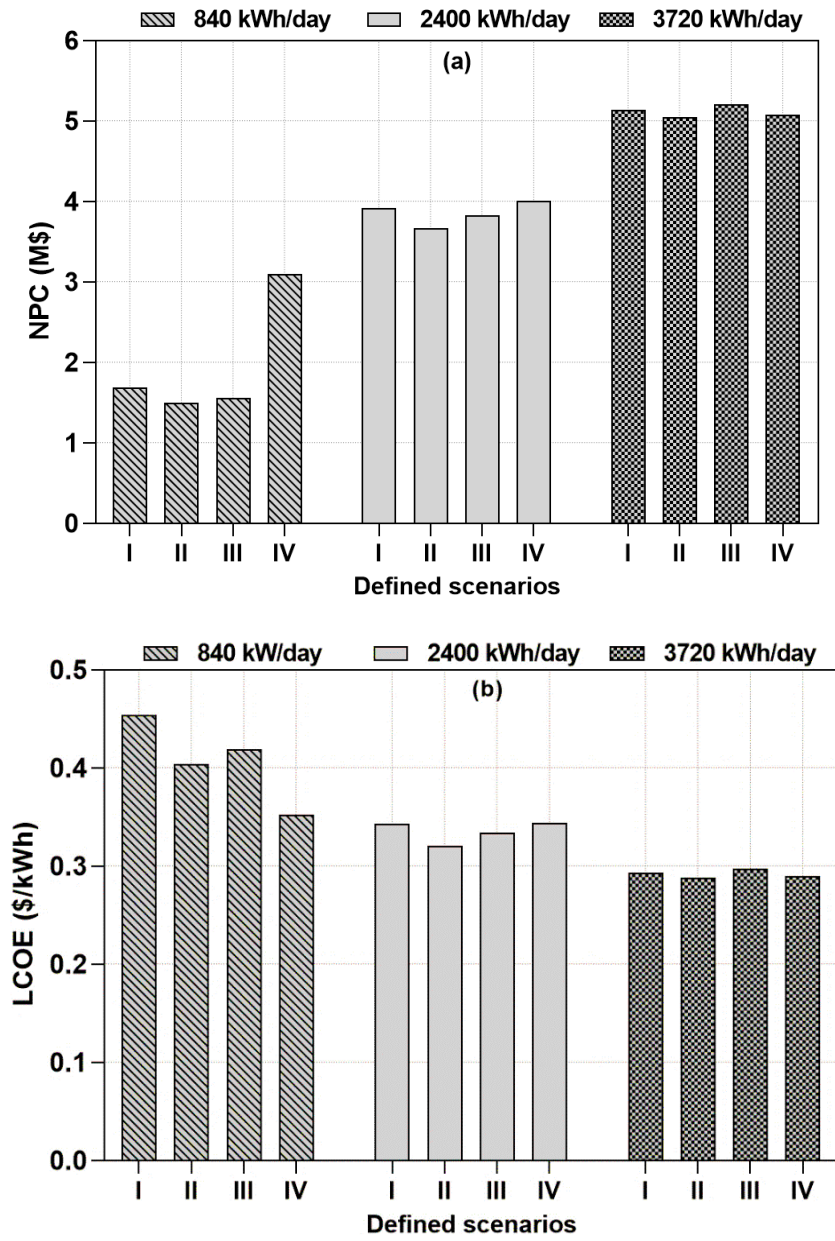
Fig. 2.6. Effects of load demands on NPC (a) and LCOE (b) optimal option of each scenario

Fig. 2.7 (a) and (b) illustrate how significantly solar irradiance can shift the LCOE and renewable fraction for DG/PV configuration. An increment in irradiance values will lower the LCOE and increase renewable fraction in all battery designs since the hybrid system implements more solar modules and minimizes its dependence on DG. Over this variation, LA battery-based HES has the highest increase in renewable fraction by 44.3%, and also 1 kWh Li-Ion battery-based HES witnesses the highest LCOE reduction by 29.4%. Fig. .8 (a) and (b) show fuel price volatility on LCOE and the renewable fraction of the PV/DG system. Among the considered battery

technologies, 1 kWh Li-Ion battery-based HES maintains their lowest LCOE values and halves from $0.206/kWh to $0.407/kWh. Fuel price growth also decreases the operation time of DG in all of the hybrid PV/DG solutions. The renewable fraction of LA battery-based HES is more sensitive to fuel price than other options.
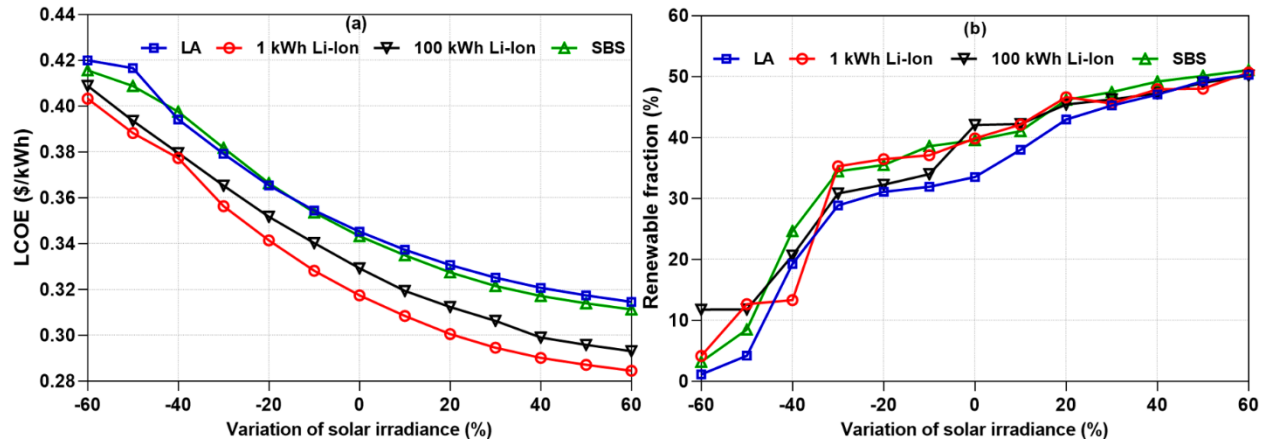
Fig 2.7. Impact of solar irradiance variation versus (a) LCOE and (b)renewable fraction of PV/DG system
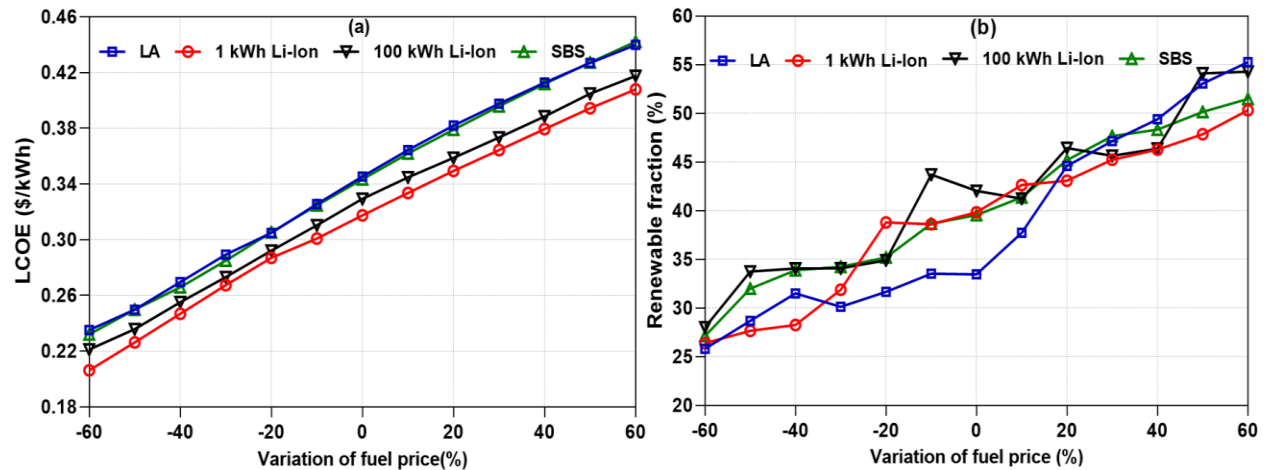
Fig 2.8. Impact of fuel price variation versus (a) LCOE and (b)renewable fraction of PV/DG system

2.5.3. Comparison of scenarios on unmet load and energy in/out

HES design iterations that leave unmet electric load and the lack of capacity must be firmed up so that power is always available [48]. Unmet electric load specifies information on the load that went unserved owing to insufficient production. Besides, the PV size can either be enhanced or reduced based on the magnitude of the unmet electric load and renewable fraction set in the scheme. As

23

depicted in Fig. 2.9, since all designs have unmet loads, they are assumed to be reliable with different features. Scheme (b) in Scenario III is the most reliable case due to its lowest unmet load, estimated to be 286 kWh/year. Conversely, scheme (c) under scenario II and IV are the worst design from this standpoint at nearly 600 kWh/year. Moreover, the storage throughput (kWh) is expressed as the total energy that cycles through the storage bank for one year. Battery throughput is approximated by the average energy (kWh) between energy in and out. Fig. 2.10 depicts the circumstances of input/output energy under various hybrid configurations. In point of fact, battery throughput per battery can enlighten points regarding the battery's operational lifetime; there is an indirect correlation between the annual throughput and the battery's lifespan. The lowest and highest energy throughputs are found in scenario III(100 kWh Li-Ion-based HES) and scenario IV (2.5 kWh SBS-based HES), respectively. Therefore, It is predicted that 100 kWh Li-Ion, can efficiently operate at a higher service lifetime than 2.5 SBS batteries. Moreover, schemes (c), comprising of PV/WT configurations, are more compatible with their batteries over the higher lifetime.
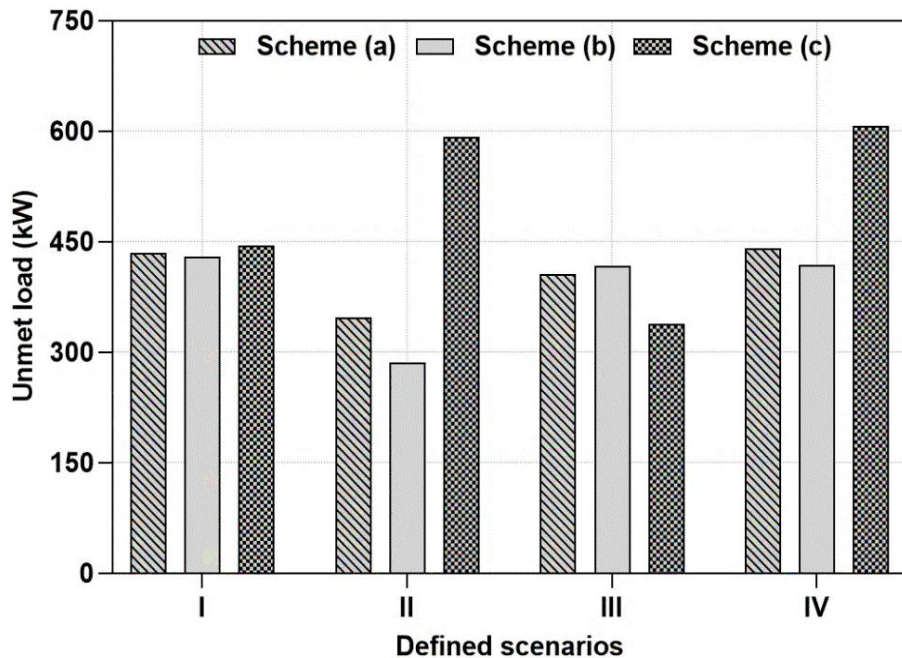
Fig. 2.9. Variation of unmet load under defined scenarios
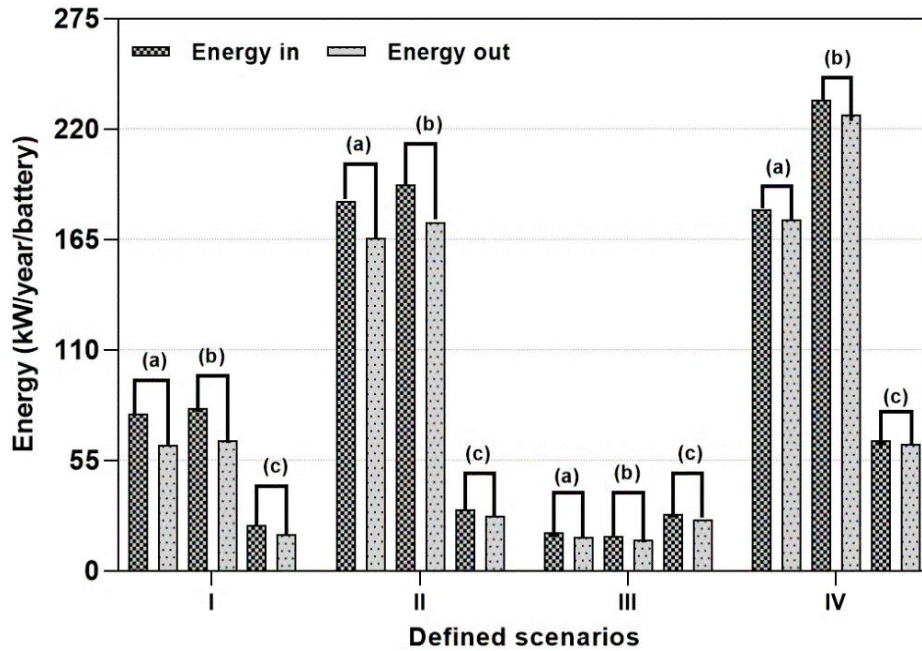
Fig. 2.10. Variation of Input/output energy under defined scenarios

2.5.4. Sample of energy balance under the optimal scheme

In this subsection, to better understand the system performance, a sample of the hourly simulation in the optimized option is depicted in Fig. 2.11. Since May has a moderate climate pattern, HES outputs, AC load, and the battery status from the beginning of May 26th to the end of May 27th are analyzed as a sample of the hourly simulation for the site. At the beginning of the day (3480 to 3484 hour), storage discharges its power to meet the load alone until the diesel generator is implemented. At noon (3482 hour), when solar irradiance is sufficient, the PV module begins generating power, reducing the DG output. Under strong daylight, the DG and PV array restart to charge the battery (from 3486 to 3489). When the SOC reaches its lowest value, such as the hours of 3483, 3504, and 3511, the generator starts to work to meet the site's required load. Here we note that the PV module is able to produce up to nearly 50 kW/h during the days to assist the generator during the daily peak demands (hours of 3492 to 3504 and 3514 to 3528). That is why the generator output drops slightly at these specified periods. From hours of 3492 to 3504 as well as 3522 to 3528, the battery is discharged to maintain the generator and PV system in the satisfying load. Beyond this, Fig. 2.12 (a) and (b) illustrate the distribution of renewable energy supplies during January and July, which are the coldest and warmest periods of the year, respectively. Even though inhabitants consume different load types over the winter and summer, the summation of produced

25

electricity by renewables still varies between 90 kW to 110 kW. It is also observed that wind farm outperforms PV arrays by generating twofold more power in January. Conversely, the energy production coming from the PV array reaches 90 kW in mid-July. It should be noted that both components generate power consistently during the month and effectively complement each other whenever one source is faced with a low energy density.
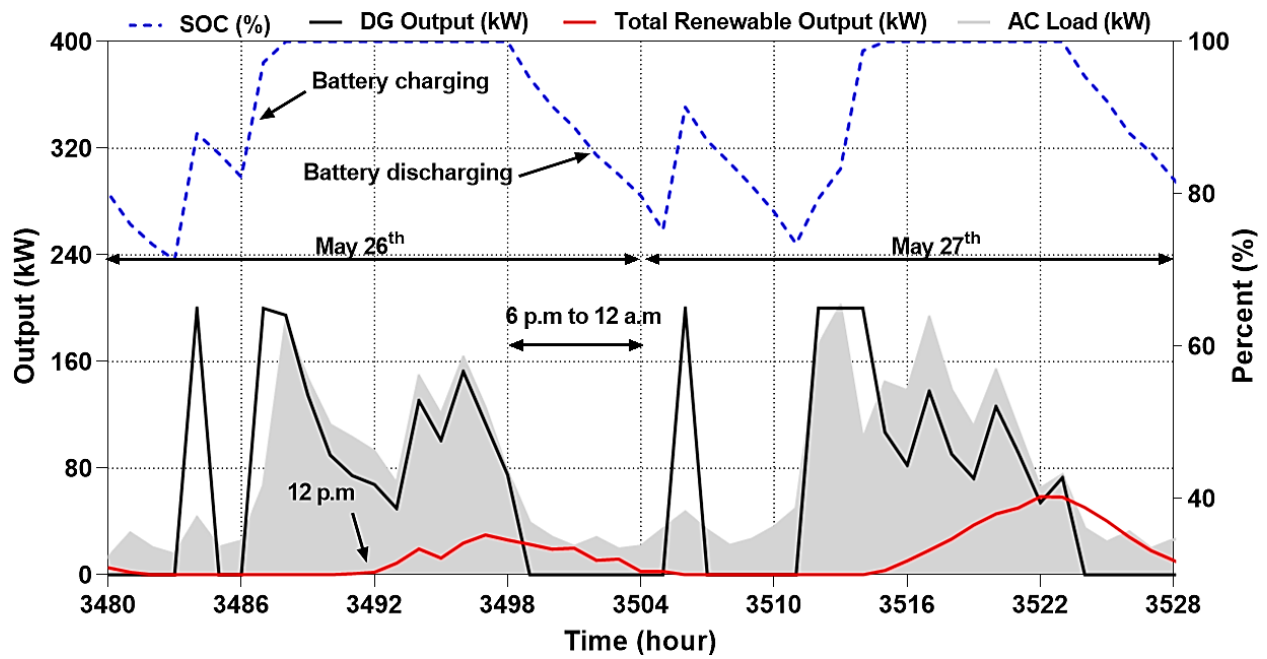
Fig. 2.11. Sample hourly simulation under the scheme (a) in scenario II on May 26th and 27th
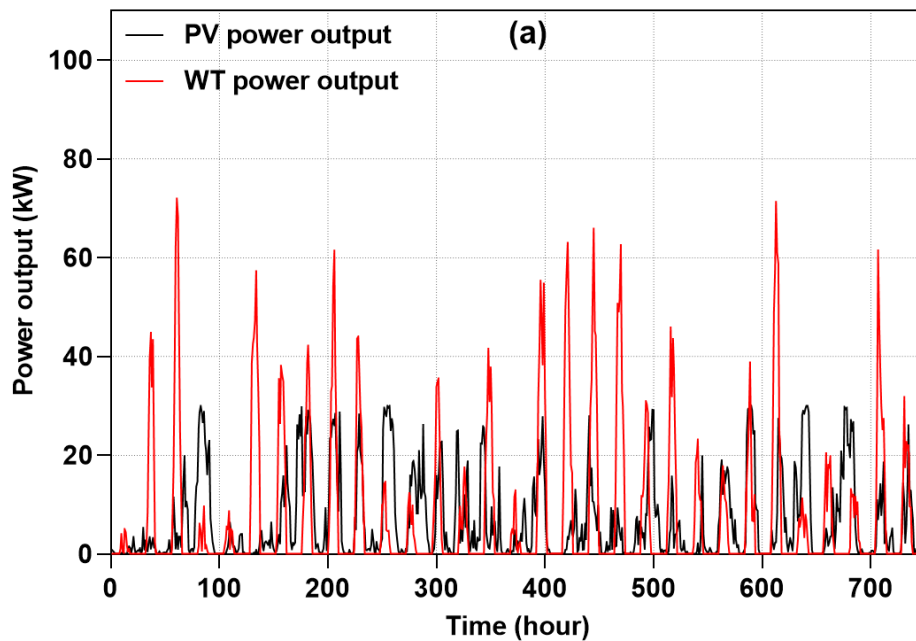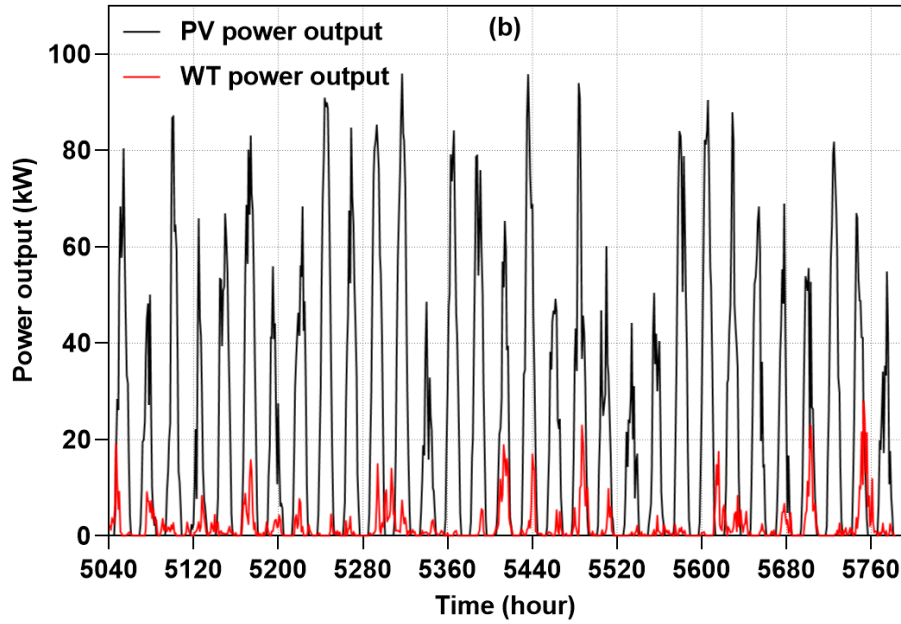
Fig. 2.12. Sample hourly simulation under scheme (b) under scenario II in Jan.(a) and Jul.(b)

2.5.5. Effects of the ambient temperature and temperature coefficient under optimal scheme

PV panels typically convert 13% to 20% of the sun's energy into electricity, while the remainder tends to heat the cells. Fig. 2.13 is provided to specify the impacts of air temperature variation on PV cell electricity production when the average environmental temperature is 10 °C. Initially, due to the temperature coefficient (-0.5 %/°C) of the PV panels specified in Table 2, the power output from the PV system drops by half a percent for every degree the temperature rises. Next, the PV cell temperature can exceed the ambient temperature by up to 15 °C. Increases in the ambient temperature enhance the generation of electron-hole pairs in the solar cell, leading to an increment in the mobility within the p-n junction and larger photocurrent. Hence, it causes an increase in PV output since PV power output has a positive correlation with the circuit's current and voltage. If we take ambient temperature from -3.8 °C to 22.3 °C as an example, the PV output grows by about 8 kW to 30 kW.
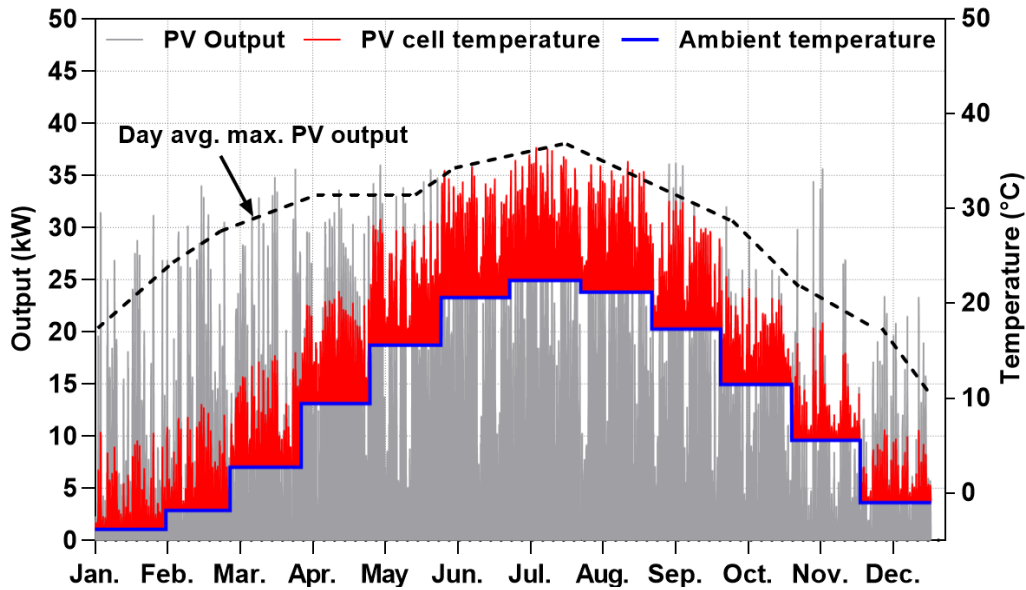
Fig 2.13. Variation of solar PV generation versus ambient temperature and PV temperature during a year under scheme (a) in scenario II

2.5.6. Operating characteristics of the battery bank under the optimal scheme

The proposed battery chemistries have vast disparities in response to various operating conditions involving temperature and depth of cycling [49]. Fig. 2.14(a) and (b) depict the hourly battery SOC for the stand-alone system under the optimal scheme. Assuming that the battery bank discharges from a full charge (100%) at 0:00 a.m. on January 1st, It is observed that the yearly SOC for winning case mostly ranges between 40% to 100% in about 99% of the annual time. The battery bank is found in a "shallow" discharge state most of the time. Further, deep discharges occur mainly late at night till the morning (12 a.m to 8 a.m). The lowest SOC range (20% to 40%) is seen about 1% of the time during a year, primarily in hours of 3000 and 4000, which are April and May, respectively. It is likely owing to the unstable climatic conditions and insufficient solar irradiance of that particular time.

28
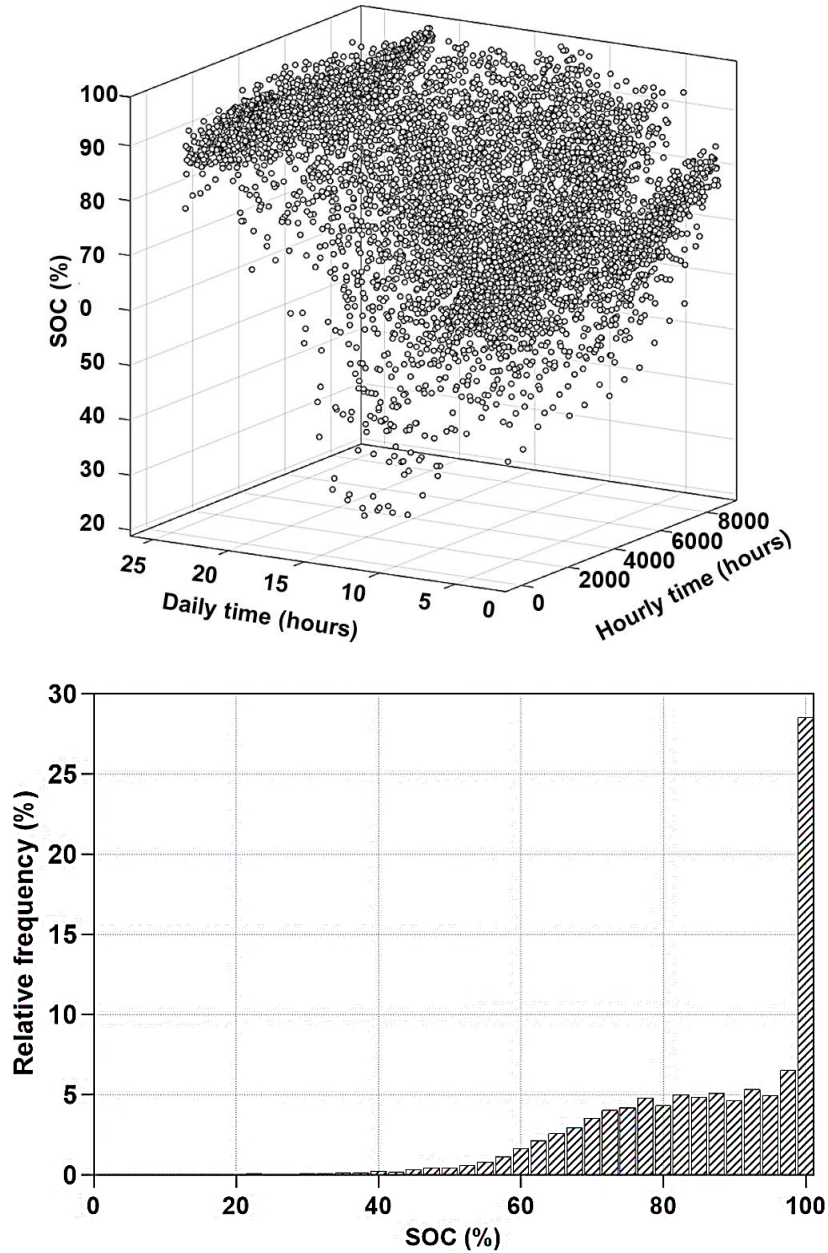
Fig 2.14. Hourly plot (a) and relative frequency(b) of SOC for the battery bank under optimal scheme

2.5.7. Comparison of nominal cash flow of optimal schemes of each scenario

Comparison of nominal cash flows with each scenario's optimal scheme over the 25-year project lifetime is shown in Fig. 2.15. Apart from the salvage cost specified at the end of the project, cash flow from the first year becomes consistently negative. This is due to the associated expenditures defined as the system's initial cost that contains replacement, resource-related, and operating costs. Although scenario III, II, IV, and I, respectively, were estimated to have the highest to lowest

29

initial cost, scenario II will obtain the lowest net present cost on account of the lower replacement and fuel costs during the project's lifetime. As such, each scenario's primary share of the annual funding is allocated to fuel costs that vary between $165k and $185k. Compared to scenarios II and III, scenarios I and IV have $20k lower fuel costs over a year. Furthermore, utilizing the LA battery in scenario, I is followed by a replacement cost of about $330k every 10 years. However, 1 kW and 100 kW Li-Ion batteries show higher profitability as for being replaced once in a project lifetime at $560k.
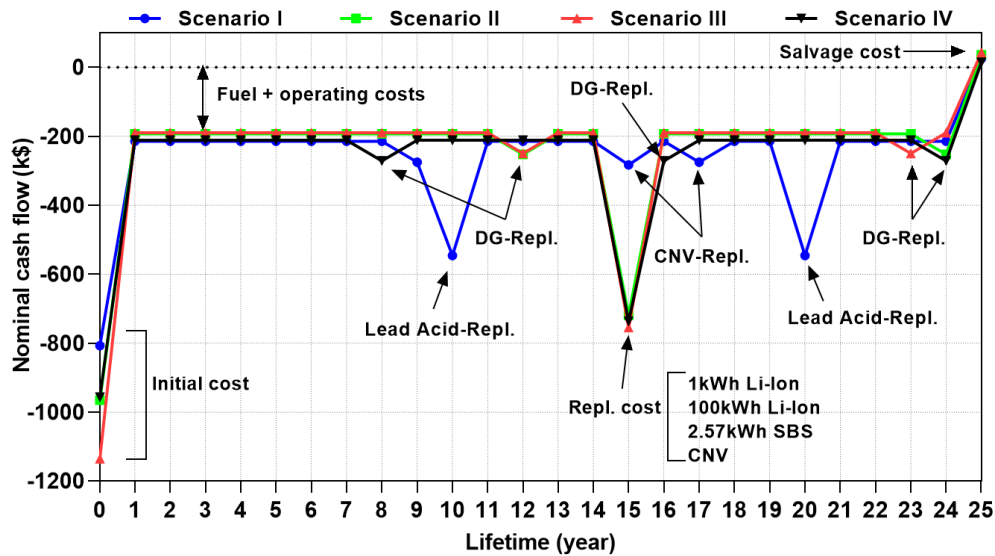
Fig. 2.15. Comparison of nominal cash flow of optimal scheme of each scenario over the project lifetime

References

[1]   M. GRANOVSKII, I. DINCER, and M. ROSEN, "Greenhouse gas emissions reduction by use of wind and solar energies for hydrogen and electricity production: Economic factors," *Int. J. Hydrogen Energy*, vol. 32, no. 8, pp. 927–931, Jun. 2007, doi: 10.1016/j.ijhydene.2006.09.029.

[2]   H. El-houari, A. Allouhi, S. Rehman, and M. S. Buker, "Design, Simulation, and Economic Optimization of an O ff -Grid Photovoltaic System for Rural Electrification."

[3]   M. Shabani and J. Mahmoudimehr, "Techno-economic role of PV tracking technology in a hybrid PV-hydroelectric standalone power system," *Appl. Energy*, vol. 212, pp. 84–108, Feb. 2018, doi: 10.1016/j.apenergy.2017.12.030.

[4]   K. Karanasios and P. Parker, "Recent Developments in Renewable Energy in Remote AboriginalKaranasios, K., & Parker, P. (n.d.). Recent Developments in Renewable Energy in Remote Aboriginal Communities, Ontario, Canada. PCED (Vol. 16). Retrieved from http://www.hydroone.com/OurCommitmen," *Pap. Can. Econ. Dev.*, vol. 16, pp. 82–97, 2016.

[5]   F. Diab, H. Lan, L. Zhang, and S. Ali, "An environmentally friendly factory in Egypt based on hybrid photovoltaic/wind/diesel/battery system," *J. Clean. Prod.*, vol. 112, pp.

3884–3894, 2016, doi: 10.1016/j.jclepro.2015.07.008.

[6] T. Jamal, T. Urmee, M. Calais, G. M. Shafiullah, and C. Carter, "Technical challenges of PV deployment into remote Australian electricity networks: A review," *Renew. Sustain. Energy Rev.*, vol. 77, no. xxxx, pp. 1309–1325, 2017, doi: 10.1016/j.rser.2017.02.080.

[7] L. C. Buildings, "Carbon intensity and the Ontario electrical grid," *Arborus consulting*, 2016. [Online]. Available: http://arborus.ca/2016/05/carbon-intensity-and-the-ontario-electrical-grid/#:~:text=However%2C grid-delivered electricity in,generate most of Ontario's electricity.

[8] J. Thornton, "The Future of Ontario's Electricity Grid. Charging Forward," *Environ. Def. Canada*, 2020, doi: 10.1115/1.2012-aug-2.

[9] "Ontario Ministry of Energy, Northern Development and Mines (2017). The End of Coal," 2017. [Online]. Available: https://www.ontario.ca/page/end-coal.

[10] A. Harvie, M. Collett, G. Smeijers, and Mélissa Devost, "Canada to increase carbon taxes by 566%," *Norton Rose Fulbright*, 2020. [Online]. Available: https://www.nortonrosefulbright.com/en/knowledge/publications/d58ef644/canada-to-increase-carbon-taxes-by-566.

[11] IRENA, *Global Renewables Outlook: Energy transformation 2050*. 2020.

[12] M. Momeni, M. Soltani, M. Hosseinpour, and J. Nathwani, "A comprehensive analysis of a power-to-gas energy storage unit utilizing captured carbon dioxide as a raw material in a large-scale power plant," *Energy Convers. Manag.*, vol. 227, no. July 2020, p. 113613, 2021, doi: 10.1016/j.enconman.2020.113613.

[13] A. Castillo and D. F. Gayme, "Grid-scale energy storage applications in renewable energy integration: A survey," *Energy Convers. Manag.*, vol. 87, pp. 885–894, Nov. 2014, doi: 10.1016/j.enconman.2014.07.063.

[14] S. Dhundhara, Y. P. Verma, and A. Williams, "Techno-economic analysis of the lithium-ion and lead-acid battery in microgrid systems," *Energy Convers. Manag.*, vol. 177, no. May, pp. 122–142, 2018, doi: 10.1016/j.enconman.2018.09.030.

[15] A. M. Patel and S. K. Singal, "Optimal component selection of integrated renewable energy system for power generation in stand-alone applications," *Energy*, vol. 175, pp. 481–504, May 2019, doi: 10.1016/j.energy.2019.03.055.

[16] S. M. Shaahid and M. A. Elhadidy, "Optimal sizing of battery storage for stand-alone hybrid (photo-voltaic + diesel) power systems," *Int. J. Sustain. Energy*, vol. 24, no. 3, pp. 155–166, Sep. 2005, doi: 10.1080/14786450500292188.

[17] L. M. Halabi, S. Mekhilef, L. Olatomiwa, and J. Hazelton, "Performance analysis of hybrid PV/diesel/battery system using HOMER: A case study Sabah, Malaysia," *Energy Convers. Manag.*, vol. 144, pp. 322–339, Jul. 2017, doi: 10.1016/j.enconman.2017.04.070.

[18] C. Li *et al.*, "Techno-economic feasibility study of autonomous hybrid wind/PV/battery power system for a household in Urumqi, China," *Energy*, vol. 55, pp. 263–272, Jun. 2013, doi: 10.1016/j.energy.2013.03.084.

[19] U. Suresh Kumar and P. S. Manoharan, "Economic analysis of hybrid power systems (PV/diesel) in different climatic zones of Tamil Nadu," *Energy Convers. Manag.*, vol. 80, pp. 469–476, Apr. 2014, doi: 10.1016/j.enconman.2014.01.046.

[20] N.-K. C. Nair and N. Garimella, "Battery energy storage systems: Assessment for small-scale renewable energy integration," *Energy Build.*, vol. 42, no. 11, pp. 2124–2130, Nov. 2010, doi: 10.1016/j.enbuild.2010.07.002.

[21] A. Testa, S. De Caro, R. La Torre, and T. Scimone, "Optimal design of energy storage

systems for stand-alone hybrid wind/PV generators," in *SPEEDAM 2010*, 2010, pp. 1291–1296, doi: 10.1109/SPEEDAM.2010.5542078.

[22] G. Kear, A. A. Shah, and F. C. Walsh, "Development of the all-vanadium redox flow battery for energy storage: a review of technological, financial and policy aspects," *Int. J. Energy Res.*, vol. 36, no. 11, pp. 1105–1120, Sep. 2012, doi: 10.1002/er.1863.

[23] C. Fabjan *et al.*, "The vanadium redox-battery: an efficient storage unit for photovoltaic systems," *Electrochim. Acta*, vol. 47, no. 5, pp. 825–831, Dec. 2001, doi: 10.1016/S0013-4686(01)00763-0.

[24] Y. Chang, X. Mao, Y. Zhao, S. Feng, H. Chen, and D. Finlow, "Lead-acid battery use in the development of renewable energy systems in China," *J. Power Sources*, vol. 191, no. 1, pp. 176–183, Jun. 2009, doi: 10.1016/j.jpowsour.2009.02.030.

[25] Z. Sun *et al.*, "Spent lead-acid battery recycling in China – A review and sustainable analyses on mass flow of lead," *Waste Manag.*, vol. 64, no. 1, pp. 190–201, 2017, doi: 10.1016/j.wasman.2017.03.007.

[26] H. Y. Chen, A. J. Li, and D. E. Finlow, "The lead and lead-acid battery industries during 2002 and 2007 in China," *J. Power Sources*, vol. 191, no. 1, pp. 22–27, Jun. 2009, doi: 10.1016/j.jpowsour.2008.12.140.

[27] X. Tian *et al.*, "Environmental impact and economic assessment of secondary lead production: Comparison of main spent lead-acid battery recycling processes in China," *J. Clean. Prod.*, vol. 144, pp. 142–148, 2017, doi: 10.1016/j.jclepro.2016.12.171.

[28] F. Schipper, E. M. Erickson, C. Erk, J.-Y. Shin, F. F. Chesneau, and D. Aurbach, "Review—Recent Advances and Remaining Challenges for Lithium Ion Battery Cathodes," *J. Electrochem. Soc.*, vol. 164, no. 1, pp. A6220–A6228, 2017, doi: 10.1149/2.0351701jes.

[29] G. Zubi, R. Dufo-López, M. Carvalho, and G. Pasaoglu, "The lithium-ion battery: State of the art and future perspectives," *Renew. Sustain. Energy Rev.*, vol. 89, no. April 2017, pp. 292–308, 2018, doi: 10.1016/j.rser.2018.03.002.

[30] M. T. Yeshalem and B. Khan, "Design of an off-grid hybrid PV/wind power system for remote mobile base station: A case study," *AIMS Energy*, vol. 5, no. 1, pp. 96–112, 2017, doi: 10.3934/energy.2017.1.96.

[31] PowerSys, "SBS Performance," 2020. [Online]. Available: https://www.enersys.com/en/solutions/batteries/?page=1&capacity=0&categories=&range s=PowerSafe&industries=&applications=&technologies=&designs=&communicationcapa bilities=&voltages=0,30.

[32] J. Li, P. Liu, and Z. Li, "Optimal design and techno-economic analysis of a solar-wind-biomass off-grid hybrid power system for remote rural electrification: A case study of west China," *Energy*, vol. 208, p. 118387, 2020, doi: 10.1016/j.energy.2020.118387.

[33] B. U. Kansara, B. R. Parekh, and I. Introduction, "Dispatch , Control Strategies and Emissions for Isolated Wind-Diesel Hybrid Power System," *Int. J. Innov. Technol. Explor. Eng.*, vol. 2, no. 6, pp. 152–156, 2013.

[34] A. S. Aziz, M. F. N. Tajuddin, M. R. Adzman, M. A. M. Ramli, and S. Mekhilef, "Energy management and optimization of a PV/diesel/battery hybrid energy system using a combined dispatch strategy," *Sustain.*, vol. 11, no. 3, 2019, doi: 10.3390/su11030683.

[35] R. Durocher, "Township of Pelee," 2020. [Online]. Available: https://www.pelee.org/.

[36] D. Methodology, "NASA, Surface meteorology and Solar Energy." [Online]. Available: https://power.larc.nasa.gov/.

[37] M. Jahangiri, A. Haghani, A. Mostafaeipour, A. Khosravi, and H. A. Raeisi, "Assessment of solar-wind power plants in Afghanistan: A review," *Renew. Sustain. Energy Rev.*, vol. 99, no. April 2017, pp. 169–190, 2019, doi: 10.1016/j.rser.2018.10.003.

[38] A. H. Mondal and M. Denich, "Hybrid systems for decentralized power generation in Bangladesh," *Energy Sustain. Dev.*, vol. 14, no. 1, pp. 48–55, 2010, doi: 10.1016/j.esd.2010.01.001.

[39] S. Kucukali and C. Dinçkal, "Wind energy resource assessment of Izmit in the West Black Sea Coastal Region of Turkey," *Renew. Sustain. Energy Rev.*, vol. 30, no. May 2005, pp. 790–795, 2014, doi: 10.1016/j.rser.2013.11.018.

[40] U. S. F. T. Framework, "UNCTAD FRAMEWORK FOR SUSTAINABLE FREIGHT TRANSPORT (UNCTAD SFT Framework)," 2017.

[41] P. Arévalo, D. Benavides, J. Lata-García, and F. Jurado, "Energy control and size optimization of a hybrid system (photovoltaic-hidrokinetic) using various storage technologies," *Sustain. Cities Soc.*, vol. 52, no. August 2019, p. 101773, 2020, doi: 10.1016/j.scs.2019.101773.

[42] F. Rinaldi, F. Moghaddampoor, B. Najafi, and R. Marchesi, "Economic feasibility analysis and optimization of hybrid renewable energy systems for rural electrification in Peru," *Clean Technol. Environ. Policy*, no. 0123456789, 2020, doi: 10.1007/s10098-020-01906-y.

[43] M. H. Jahangir, S. A. Mousavi, and M. A. Vaziri Rad, "A techno-economic comparison of a photovoltaic/thermal organic Rankine cycle with several renewable hybrid systems for a residential area in Rayen, Iran," *Energy Convers. Manag.*, vol. 195, no. April, pp. 244–261, 2019, doi: 10.1016/j.enconman.2019.05.010.

[44] M. Hossain, S. Mekhilef, and L. Olatomiwa, "Performance evaluation of a stand-alone PV-wind-diesel-battery hybrid system feasible for a large resort center in South China Sea, Malaysia," *Sustain. Cities Soc.*, vol. 28, pp. 358–366, 2017, doi: 10.1016/j.scs.2016.10.008.

[45] A. Cano, P. Arévalo, and F. Jurado, "Energy analysis and techno-economic assessment of a hybrid PV/HKT/BAT system using biomass gasifier: Cuenca-Ecuador case study," *Energy*, vol. 202, 2020, doi: 10.1016/j.energy.2020.117727.

[46] M. H. Jahangir, S. A. Mousavi, and M. A. Vaziri Rad, "A techno-economic comparison of a photovoltaic/thermal organic Rankine cycle with several renewable hybrid systems for a residential area in Rayen, Iran," *Energy Convers. Manag.*, vol. 195, pp. 244–261, Sep. 2019, doi: 10.1016/j.enconman.2019.05.010.

[47] S. K. Singal, Varun, and R. P. Singh, "Rural electrification of a remote island by renewable energy sources," *Renew. Energy*, vol. 32, no. 15, pp. 2491–2501, 2007, doi: 10.1016/j.renene.2006.12.013.

[48] A. S. Aziz, M. F. N. Tajuddin, M. R. Adzman, M. F. Mohammed, and M. A. M. Ramli, "Feasibility analysis of grid-connected and islanded operation of a solar PV microgrid system: A case study of Iraq," *Energy*, vol. 191, p. 116591, Jan. 2020, doi: 10.1016/j.energy.2019.116591.

[49] R. E. Ciez and J. F. Whitacre, "Comparative techno-economic analysis of hybrid micro-grid systems utilizing different battery types," *Energy Convers. Manag.*, vol. 112, pp. 435–444, 2016, doi: 10.1016/j.enconman.2016.01.014.

Dispatch strategies-based feasibility analysis of grid-connected hybrid energy systems using sun-tracking PV modules

3.1. Introduction

The employment of renewable power is necessary to respond to ever-increasing global energy consumption and emission production worldwide. Driven by economies of scale, solar energy has shown significant advancement and maturity in power generation amongst other renewable energy options [1], [2]. Among these technologies, the solar photovoltaic (PV) option is among the fastest-growing solar energy technologies worldwide.

While PV has established itself as cost-competitive, the optimization of the solar energy harvesting process continues to evolve. Several techniques integrated into PV systems have been used to maximize the energy obtained from solar photovoltaic modules [3]. One of these is the solar tracking method adopted to track the sun's trajectory during the day. It assists the PV system by maintaining the optimum position of the solar collector during daylight hours [4]. The tracking motion can be around one axis (single-axis tracker) or two axes (dual-axis tracker). Dual-axis solar trackers have higher efficiency than single-axis tracking systems. However, this advantage results in increased expense and complexity [3], [5].

Since finding the optimal movement of the PV trackers can assist in enhancing production, analyzing panel conditions during a day can be of the utmost priority. Fig. 3.1 shows the panel conditions toward the sun. The tilt angle here is the angle formed by the horizontal plane and the surface of the solar panel (If the PV site is in the northern hemisphere, it is usually to the south.). The azimuth angle is the horizontal divergence between the surface and the south direction. The ratio of reflected radiation to the total radiation incident on the ground is known as ground reflectance or albedo (not shown in the figure). The ground albedo varies during a day from place to place in the spot due to diverse properties of ground surface material, sun position, cloud cover, snow cover, and ground vegetation. The spectral distribution of incident radiation on solar modules is influenced by albedo radiation, and hence the PV system's performance is affected [6].
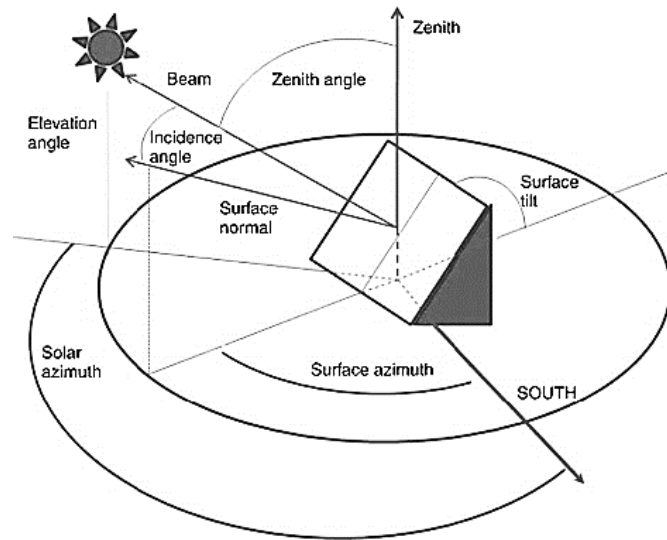
Fig. 3.1. Illustration of solar and PV module characteristic angles [7]

Utilization of PV system as the sole energy production option has some drawbacks such as intermittent availability and higher cost of energy (COE) and/or net present cost (NPC). Two different strategies can be employed to address these disadvantages. The first is to use suitable storage technology to balance the mismatch between energy supply and demand fluctuations. The second strategy is to integrate solar energy with other renewable energy components such as diesel generation, bio gasification, or centralized grid systems so that they complement each other and lower NPC or COE [8]. Additionally, the use of hybrid energy systems can potentially increase central grid dynamism, reduce network distribution losses, notably boost the renewable energy portion of the supply portfolio – thereby reducing emissions (such as CO_2) into the atmosphere [9]. Grid integrated BG and DG can also limit the operating hours, running costs, and fuel consumption of DG and BG [10].

Design optimizations of such systems start at the component level – but must maintain a holistic lens [11]. Proper system design and management will boost stability, ensure the continuity of supply, lowers the energy cost (COE), and protects equipment against damage due to overloads. Appropriate management is particularly vital in grid-integrated systems where the energy is metered as it flows to and from the grid [12], [13]. Considering various hybrid energy solutions (HES), various dispatch strategies are introduced based on economic and technical criteria. Dispatch strategies are control algorithms that manage battery units and DG/BG to satisfy a 24-hour load with the energy resources available. The most common dispatch controllers to manage a system like this are cycle charging (CC) and load following (LF). Under the CC dispatch strategy, the DG/BG works at its full-rated power to serve the required load, and any surplus electrical generation goes toward the lower-priority objectives such as charging the storage bank. Under the LF dispatch strategy, DG/BG operates to generate merely enough energy to satisfy the primary load. The lower-priority objectives, such as batteries, are remained to be charged by renewable energy sources [14], [15].

35

This study examines hybrid systems connected to the gasifier and generator simultaneously to enhance the reliability and environmentally friendly system aspects and considers a realistic maintenance program to improve the real-world accuracy of true costs. This would be the first study that introduces a grid-connected hybrid system as a possible alternative for Pelee Island. The key objectives of this Pelee Island study are to: (i) Produce reliable and cost-effective designs of a grid-integrated, hybrid PV tracker-based, renewable energy system; (ii) Evaluate the results of the optimal case under both CC and LF dispatch strategies; (iii) Conduct sensitivity analysis to analyze the impacts of critical financial variables (capital cost multiplier of trackers) and technical characteristics (SOC_{min}, load demand, and albedo) on system economic viability.

This target area is one of Canada's southernmost communities, Pelee Island. Located in Essex County, Ontario, this area has singular biological significance to Canada's national heritage. Pelee residents are currently reliant on a 26-kilometer underwater cable that fails when they need it the most, especially during tourist season. Also, although three-phase power is the standard in Canada's business and agricultural sectors, the cable only delivers single-phase power. A reliable hybrid energy solution can serve as an intriguing non-wires alternative to upgrading the compromised underwater cable. This study considers the western side of Pelee Island as it is home to the Island's essential loads, which are the backbone of this small community.

3.2. Methods and materials

The commercially available HOMER software is used in this analysis. Its modeling principles are primarily based on cost minimization. Fixed cost ($\hour) and a marginal cost of energy ($\kWh) are central to our cost analysis. The model weighs possible options based on operational requirements and the minimum expense. It is worth emphasizing that meeting the required load and reserve is here set as a mandatory condition and thus will be met at any cost. Fig. 3.2 Illustrates the methodology used to ascertain the optimal hybrid energy design. The feasible solutions that can satisfy the intended load based on the hourly renewable resources are identified under the CC and LF dispatch strategies. Then the cost-effective and reliable components will be sorted based on their net present cost(NPC). The system with the lowest NPC is considered to be the winning option of the area. Sensitivity analysis then examines how financial variables (capital cost multiplier of trackers) and technical characteristics (SOC_{min}, load demand, and albedo) impact system economic viability of the winning solution. Finally, the accuracy of the present findings will be compared with other studies worldwide based on the NPC and winning tracking systems.
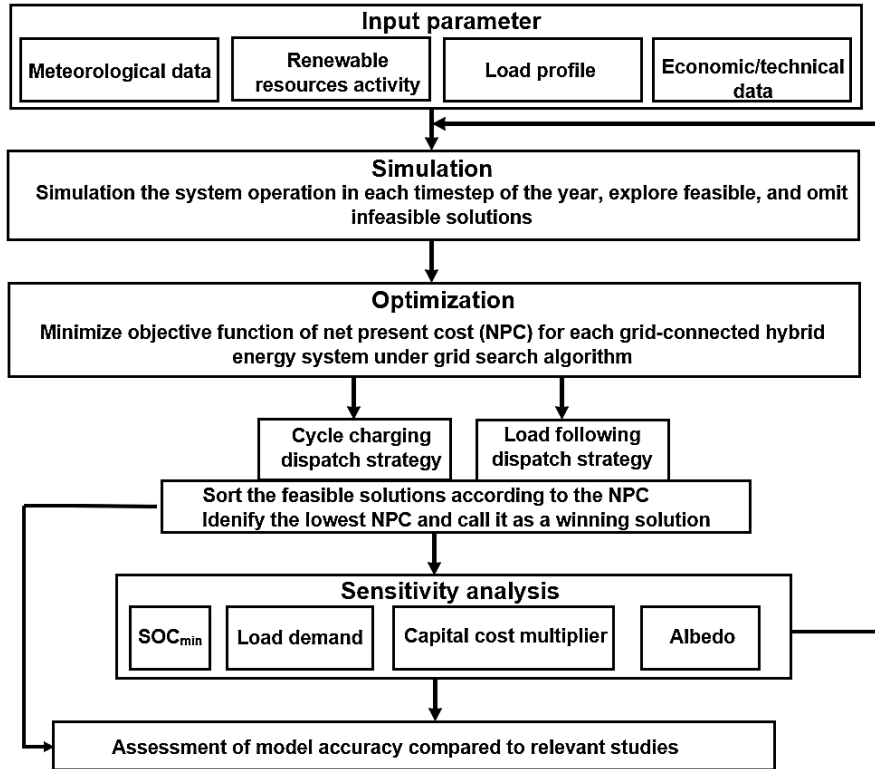
Fig. 3.2. Flow chart of the main objectives of this study

3.2.1. Control strategy

A dispatch control strategy includes a set of rules used to operate the diesel generators and storage batteries when there is insufficient renewable energy to satisfy the load demand [16]. This paper conducts a comparative analysis with LF and CC dispatch control strategies for a grid-connected HES made up of cheaper and more reliable components than previous research. In the cycle charging (CC) strategy, whenever the power supplied by renewable resources and the stored energy is not adequate to meet demand, the DG is used to satisfy the electrical load at its maximum range of operation. Any excess electricity from renewable resources then charges the storage units. In a LF strategy, the DG is utilized to satisfy demand when the renewables are insufficient.

3.2.2. Electric load data

The load demand for residential households and surrounding areas in Pelee Island mostly contains lights, fan, TV, refrigerator, washing machine, and miscellaneous. The annual load profile is shown in Fig. 3.3. The total annual average load is estimated to be 2426.4 kWh/day with the day-to-day variability and time-step variability of 10% and 20%, respectively. Further, the peak load occurs during the summer reaching up to 400 kW when seasonal residents and tourists visit this island. During the fall and winter, the electricity consumption reaches its lowest values.
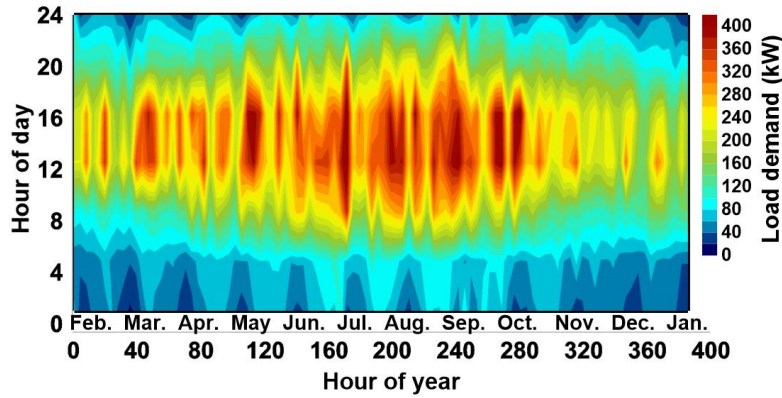
Fig. 3.3 Electric load profile in western Pelee Island

3.2.3. Available renewable resources

Table 3.3 depicts the monthly averaged metrological resources of the site. The clearness index indicates the fraction of the solar irradiance that strikes the Earth's surface. This is a dimensionless number of ranges between 0 and 1. The solar intensity and ambient temperature are the two parameters with the most profound impacts on the PV solar system. Relative humidity and precipitation also impact the ability of the PV panels to receive irradiance from the sun. January and July, due to their irradiance values, are expected to have the highest and lowest energy production from the PV modules, respectively. Fig. 3.4 and 3.5 demonstrate the monthly average and frequency of solar irradiance during a year, respectively. The highest irradiance is observed from 5 to 6 kWh/m^2/day, from May to August. While from November to January, the solar irradiance varies below 2 kWh/m^2/day. Moreover, the irradiance below 3 kWh/m^2/day is likely to be seen more than 70% of the time over the annual period.

Table 3.1. Meteorological data of Pelee Island

Month	Ambient temperature (°C)	Clearness index	Relative humidity (%)	Precipitation (mm)
Jan.	-2.6	0.457	0.721	49.9
Feb.	-1.7	0.488	0.712	45.9
Mar.	1.6	0.467	0.689	59.2
Apr.	6.7	0.474	0.694	73.8
May	13.5	0.481	0.714	83.7
Jun.	19.5	0.508	0.747	83.4
Jul.	22.4	0.533	0.72	86.8
Aug.	21.9	0.527	0.715	82.1
Sep.	18.2	0.529	0.67	79.5
Oct.	12.3	0.491	0.652	69.4
Nov.	5.5	0.417	0.68	67.5
Dec.	0.1	0.410	0.702	62.0
Average	9.8	0.481	0.70	70.2
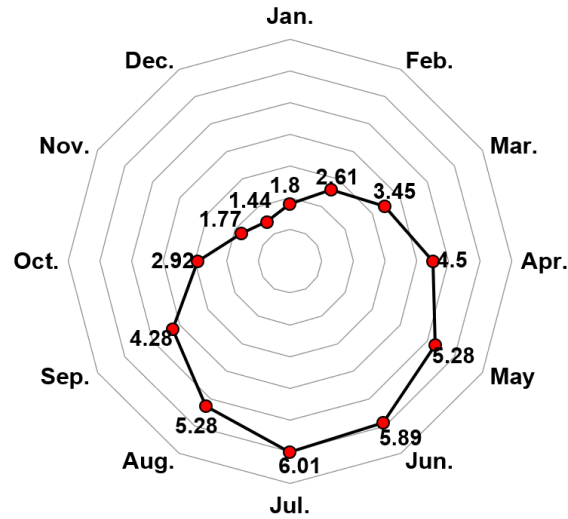
Fig. 3.4. Profile of monthly solar irradiance of Pelee Island
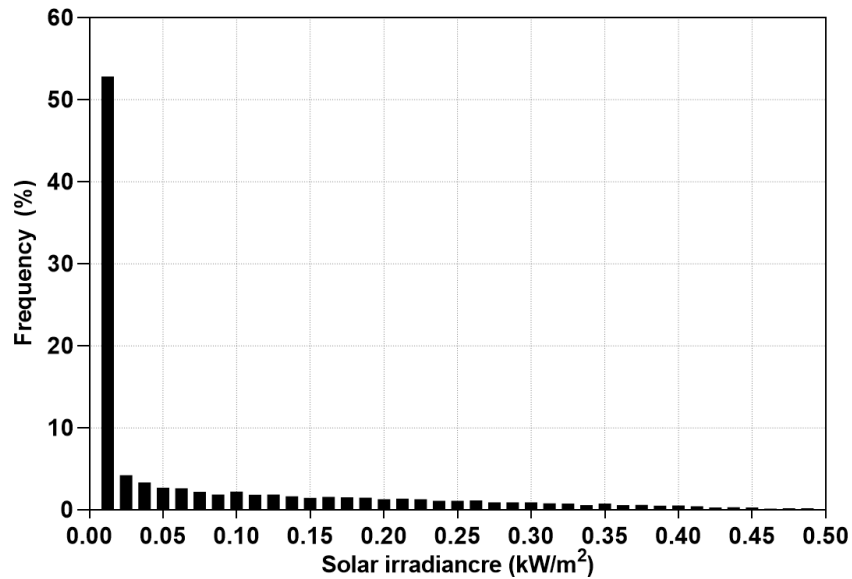
Fig. 3.5. Frequency of average solar irradiance

3.2.4. Configuration of the hybrid energy system

Fig. 3.6 provides a schematic of the proposed hybrid energy system (HES) based on the 2426 kWh/day average load of the site. The intended configuration is equipped with a diesel generator and a bio gasifier, a converter, a 1kWh Li-Ion and sun-tracking PV systems. Each component's technical and economic characteristics are shown in Tables 3.4 and 3.5, respectively. A lithium storage system is used for the proposed HES. Based on the local survey, the energy sold to/purchased from Ontario's grid system is $0.15 /kWh and $0.30/kWh, respectively.
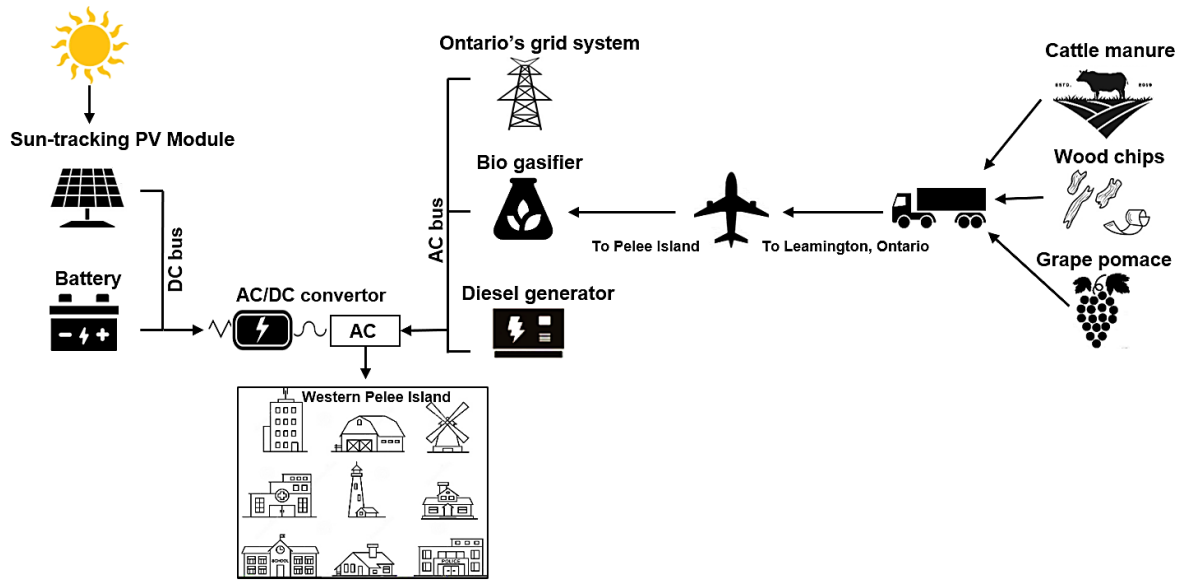
Fig. 3.6. Schematic diagram of system configuration

Table 3.2. Technical details of the components

Equipment	Parameter	Value
PV system	Temperature coefficient(%/°C)	-0.4
	Efficiency (%)	19.1
	Derating factor(%)	80
	Lifetime(years)	30
Diesel generator	Fuel price ($/L)	0.7
	Minimum load ratio (%)	25
	LHV (MJ/kg)	43.2
	Minimum load ratio (%)	0.25
	Lifetime (hours)	15,000
Biomass gasifier	LHV(MJ/kg)	5.5
	Density (kg/m^3)	0.72
	Lifetime(hours)	20,000
Battery storage	Nominal voltage (V)	6
	Nominal capacity (kWh)	1
	Lifetime (years)	15
	Maximum charge-discharge current (A)	167-500
	Minimum SOC (%)	40
Converter	Inverter lifetime(years)	15
	Inverter efficiency(%)	95
	Rectifier efficiency(%)	95

Table 3.3. Economic characteristics of the components

Equipment	Capital cost ($/kW)	Replacement cost ($/kW)	O&M ($/year)
PV	650	650	20
BG	1000	1000	0.10 $/op.hr
DG	17,000 $/50 kW	17,000 $/50 kW	1 $/op.hr
Battery	550	550	10
Converter	300	300	10
	Power price ($/kWh)	Sellback price ($/kWh)	
Grid	0.15	0.30	

3.2.5. Grid modelling

HOMER Pro allows users to simulate an unreliable grid by considering frequent power outages during a year. An unstable grid modelling of Pelee Island with unplanned power outages was examined for this analysis. Since no data has been announced about the grid's failure timing or maintenance schedule in Pelee Island, average mean failure frequency, mean repair time, and variability in repair time are used as inputs to simulate the grid with the unexpected outage. Random outages were simulated by the software based on the provided input and by picking a pseudo-random time step from a full-year simulation period. Fig. 3.7 illustrates the profile of grid outages over a year. The black and green spots represent a random outage and normal grid functioning, respectively, throughout the year. In these power outages, load demand will be satisfied by PV/DG/BG system.
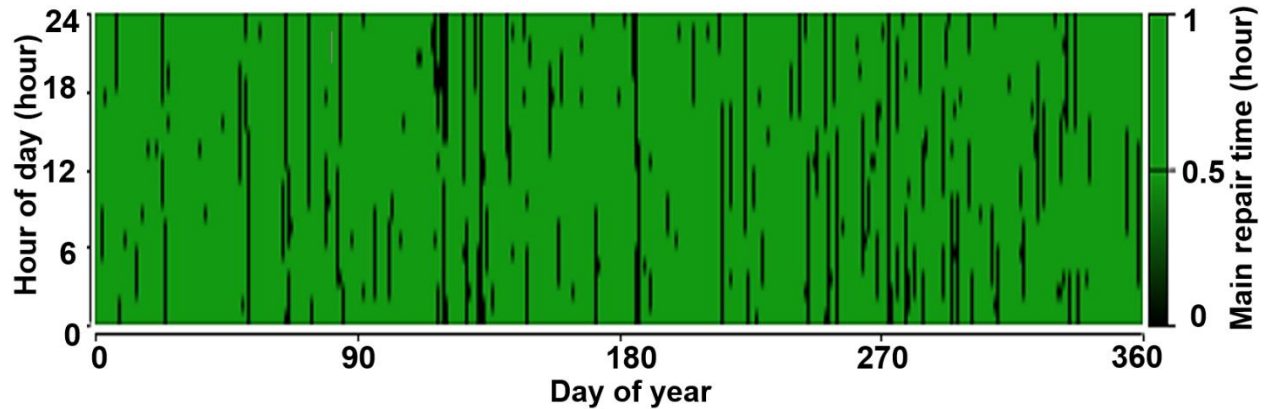
Fig. 3.7. Profile of grid outage during a year

3.2.6. PV system equipped with tracking modules

The PV module harvests DC electricity in direct proportion to the solar irradiance incident upon it. The derating factor represents the reduced output in real-world operating conditions as a result of dust accumulation, shading snow cover, wiring losses, and ageing [17]. Since Pelee Island has

a relatively high precipitation rate and climate variability, the derating factor was assumed to be 80%. The power output of a solar panel can be calculated using the following equation [62]:

$$p_{PV} = W_{PV} f_{PV} \frac{G_T}{G_S} [1 + \alpha_p (T_C - T_S)]$$

(3.1)

where W_{pv} is the peak power output of PV array (kW), f_{pv} is the PV derating factor (%), G_T is the solar radiation incident in the current hour (kW/m^2), G_S is the incident radiation at standard test conditions(1 kW/m^2), α_p is the temperature coefficient (%/°C), T_C is the PV module temperature in the current time step (°C), and T_S is the PV module temperature in standard test condition(25 °C). The number of solar PV panels is assumed to be variable, with each 1 kW generic flat plate with specifications presented in Table 4.

Moreover, PV tracking mechanisms are utilized here to adjust the PV modules to enhance their productivity. In most cases, fixed-tilt solar PV modules use manually adjustable slopes to suit simplicity and cost-effectiveness. Since the sun moves during the day and shifts its orbit seasonally, the PV system is installed at a fixed slope, and thus the azimuth will see a notable drop in received solar irradiance [1]. The major PV tracking techniques utilized in this analysis are:

- **Horizontal-axis monthly adjustment (HMA):** the rotation axis is around the horizontal (east-west) axis, while the tilt angle is adjusted each month to have a close-to-perpendicular angle between sun rays and panels at noontime.
- **Horizontal-axis continuous adjustment (HCA):** the rotation is around the horizontal, whereas the tilt angle is continuously adjusted.
- **Vertical-Axis continuous adjustment (VCA):** the PV array rotates continuously around the vertical (north-south) axis, whereas the tilt is constant.
- **Dual-axis-tracker (DAT):** the PV arrays rotate in both axes (horizontal and vertical) continuously to maintain the perpendicular angle between PV panels and sun rays.

Whether single-axis or two-axis, PV trackers require auxiliary accessories such as motors, gears, control units, and sensors that make them more expensive. Table 3.6 depicts the market costs of sun-tracking PV technology of horizontal, vertical and dual-axis trackers involved in this study, excluding the PV module cost. Four cases are shown; Scenario I: Horizontal axis with monthly adjustment (HMA), Scenario II: Horizontal axis continuous adjustment (HCA), Scenario III: Vertical Axis continuous adjustment (VCA), and Scenario IV: Two-Axis (DTA) tracking. Such PV tracking systems are categorized according to their number of rotation axes, as are illustrated in Fig. 3.8.

Table 3.4. Description of the studied scenario [1]

Scenario	Name	Technologies involved	Capital cost ($/kWh)
I	HMA	Horizontal axis with monthly adjustment	563
II	HCA	Horizontal axis continuous adjustment	870
III	VCA	Vertical Axis continuous adjustment	255

IV	DAT	Dual-axis tracker	1000
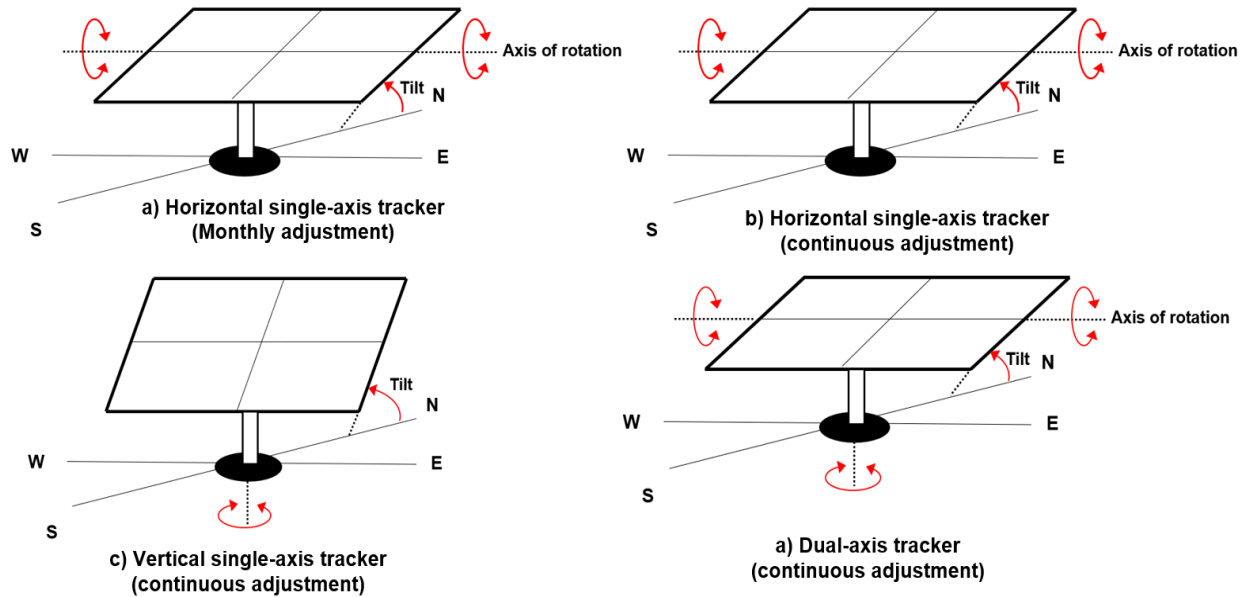
Fig. 3.8. Illustration of tracking systems studied in this analysis

3.2.7. Biogasifier/Diesel generator

Given PV's daylight dependency, a biogas gasifier and diesel generator were selected to firm up system power delivery. Biomass is typically composed of organic matter, including crop residues, wood, animal and human waste [18]. The utilization of biomass to produce energy has gained some momentum in the region and is readily available in Pelee Island and southern Ontario at large.

The following equation defines the diesel generator efficiency:

$$\eta_g = \frac{3600 \, P_e}{\rho_f (P_{gen} F_0 + P_e F_1)} \tag{3.2}$$

Where η_g is the generator efficiency(%), P_e is the output power(kW), ρ_f is the fuel density (kg/m^3), P_{gen} is the rated generator power(kW), F_0 is the generator fuel curve intercept co-efficient(L/h/rated kW or m^3/h/rated kW), and F_1 is the fuel curve slope(L/h/ output kW or, m^3/h/output kW). HOMER assumes that the fuel curve is a straight line. The following relation calculates the real generator's fuel consumption in L/h [19]:

$$\dot{m}_{fuel} = F_0 Y_{gen} + F_1 P_{gen} \tag{3.3}$$

where Y_{gen} is the rated capacity of the generator (kW)

The energy output will not be the same for different types of biomass wastes. In this study, these wastes are mixed to ensure effective anaerobic co-digestion for enhancing biogas production capability as well as process efficiency [20]

43

$$P_E = \frac{W\,B_{kw}}{B_{kw}} \tag{3.4}$$

In the above equation, W, BW, and B_{kw} represent total waste in kg, biogas production per kg of waste and biogas required for 1 kW electricity generation, respectively.

Table 3.7 sheds light on the cost-effective accessibility of quality bioresources collected from onsite and neighboring regions over a year. Further, since Pelee Island per see is home to more than 700-acres of Canada's warmest grape-growing region, grape pomace biomass will be readily available [21]. The average price of biomass plus Pelee Island's collection and transportation cost has been estimated at 340 $/tonne. Table 3.8 represents the characteristics of each type of biomass and the measured parameters. The performance of the gasifier is critical to the efficiency of biomass utilization; it is discussed next.

Table 3.5. Estimation for cost breakdowns of biomass resources in Pelee Island

Fuel type	Purchase cost ($)	Transport cost ($)	
		Factory to Leamington ($) (10-45 $/tonne)	Leamington to Pelee Island (0.14 $/Ib) [22]
Wood residue	650 [23]	90 [24]	618
Grape pomace/Winery waste	-	584	22,531
Cattle manure	450 [25]	150 [26]	4,630
Total (3% additional cost)	1,133	848	28,612

Table 3.6. Characteristic of the type of biomass used

Fuel type	Scaled annual average (t/day)	LHV biomass (MJ/kg)	Carbon content (%)
Wood residue	6	19	43–51% [27]
Grape pomace	9	14.60 -17.75 [28]	51.1 [29], [30]
Cattle manure	45	<5.8 [31]	52.2 [32]

3.2.7.1. Gasifier configuration

The diesel generator operates with a fuel price of 0.7 $/L. The gasifier burns wood residue, grape pomace, and cattle manure at an average of 340 $/tonne. Fig. 3.9 illustrates a proposed digester technology constructed of concrete with a steel skeleton. Their sizes vary between 500 and 3,000 m³. In most cases, the biogas digesters typically have a cylindrical shape standing upright. Inside, the digester tank is designed with insulation and a system to regulate heat dissipation. As such, digesters also are equipped to stir the digesting slurry (not shown here). Instead, in our case, the slurry is agitated by pressurized biogas. A premixing pit is attached to the system in which other

feedstock can be added to the slurry. However, an extra input system is typically considered when a very large feedstock is used [33].
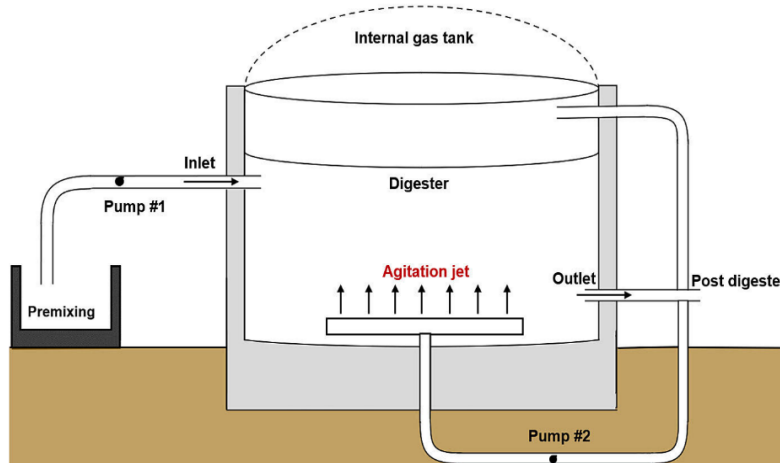
Fig. 3.9. Intended configuration of gasifier technology

3.2.7.2. Weekly schedule of biogas and diesel generator

As depicted in Fig. 3.10(a) and (b), the diesel generator and biogas gasifier are scheduled to be off for two hours each weekend (from 7:00 a.m to 9:00 a.m and 9:00 a.m to 11:00 a.m, respectively) for maintenance operations. It is here assumed that during each hour that the biogas gasifier or diesel generator is taken offline, its counterpart goes online to compensate. Both gasifier and generator are set to work in an optimized mode for the rest of the weekdays.
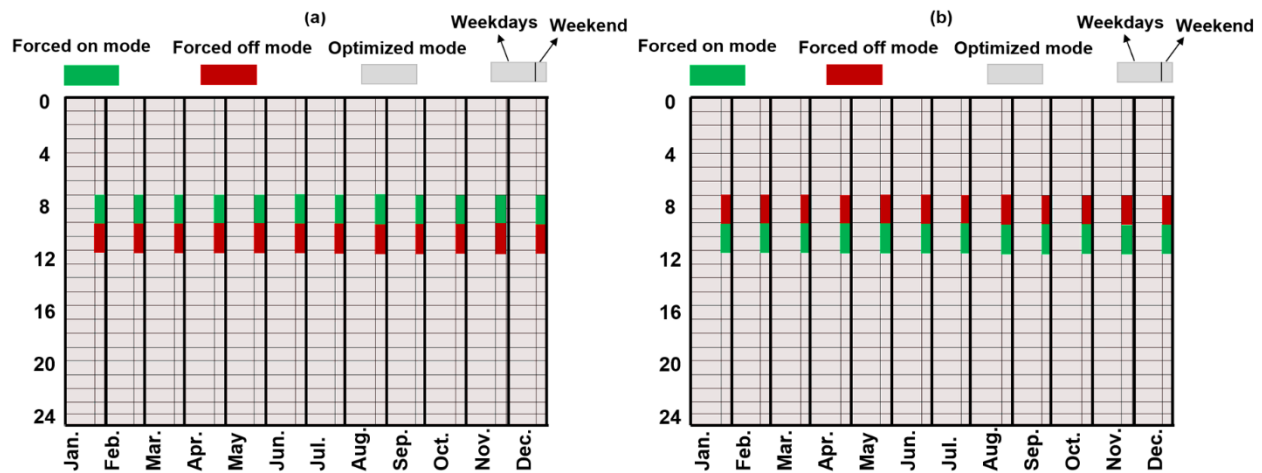
Fig. 3.10. Maintenance weekly schedule of (a) diesel generator and (b) bio gasifier

3.2.8. Battery Storage

The battery stores electricity in a chemical form, and subsequently, this stored energy can be recharged and reused to supply continuous operation as required. For the longevity of the battery

bank, the maintenance of the battery charge within 20% is very necessary [34]. The following equation shows how values of battery energy can be estimated [35].

$$Q_{battery} = Q_{battery,0} + \int_0^\tau V_{battery} I_{battery} \, dt \tag{3.5}$$

$Q_{battery,0}$(kWh) is the initial battery charge, $V_{battery}$(V) is the battery voltage and $I_{battery}$(A) is the battery current

The state of battery charge is expressed by the equation (3.6).

$$B_{soc} = \frac{Q_{battery}}{Q_{battery,max}} \times 100(\%) \tag{3.6}$$

3.2.9. Converter

The converter maintains the flow of energy between DC and AC, here equivalent to either an inverter or rectifier. The converter converts DC power from the PV module and battery output into AC. In the case of excess wind energy generation, a rectifier converts AC power to DC to be stored in the battery storage system [36]. The power rating of the converters can be obtained from the following equation [37]:

$$P_{inv} = \frac{P_{peak}}{\eta_{inv}} \tag{3.7}$$

3.3. Results and discussion

In order to present a performance analysis of CC-based and LF-based systems with the tracking configurations, the techno-econo-environmental parameters of each are discussed here. First, we highlight characteristics of optimal hybrid energy solutions. Then we illustrate characteristics of the best case are illustrated in surface plots. Then, cost breakdown and energy distribution in both the CC and LF dispatch strategies are compared. Next, a sensitivity analysis is carried out to compare the impacts of load growth, SOC_min, tracking cost multiplier, and albedo on each tracker's economic and technical parameters. Finally, the impact of the utilization of optimal trackers is compared with the relevant studies.

3.3.1. Optimization results

Several possible solutions with different PV trackers under LF and CC were considered. A potential energy solution is one that can satisfy the load demands of the area based on available resources. In this simulation, the infeasible systems were omitted, and feasible ones are classified based on their NPC. Table 3.9 depicts each optimal component capacity and the proposed properties based on the tracking device and dispatch strategy. Given the noted capacity, performance, and reliability limitations of the central grid option for the island, the proposed hybrid options depend more on the PV/DG/BG system for energy generation. The table indicates that the best or winning case is the CC-controlled configuration that uses 776 kW PV modules

with a VCA tracker, 50 kW gasifier, 120 kW DG, 583 kW converter and 73 units of 1 kWh Li-Ion. The optimal case has an NPC, COE, and a renewable fraction of $1.60M, $0.083/kWh, and 78.7%, respectively. This system also has ~$0.02M, ~$0.002/kWh and 7.6% lower NPC, COE and RF, respectively, than the same case (scenario III) in the LF controller. The highest renewable fraction (86.3%) is observed in the VCA-based solution (scenario III) operating with an LF controller. The cleanest configuration is also the HMA-based option (Scenario III) under CC controller, having 21.6 t emissions per year. Table 3.10 presents the share of energy generation by component under each tracker technology. The CC-based solutions, on average, have ~0.5% lower use of PV and DG capacity as compared to LF-based systems. While the contribution of LF-based options in the total generation of BG and central grid, respectively, is ~0.1% and ~0.8% higher than the CC-based system.

Table 3.7. Optimization solutions of tracker-based configurations in two dispatch strategies

Parameter	Unit	CC controller				LF controller			
		I	II	III	IV	I	II	III	IV
PV	kW	635	611	776	506	640	623	829	510
BG	kW	50	50	50	50	50	50	50	50
DG	kW	120	120	120	120	160	200	160	200
CNV	kW	480	499	583	434	478	440	605	430
BT	No.	93	99	73	113	91	17	42	40
Grid purchased	MWh	349.3	345.1	295.3	355.2	345.0	338.2	285.4	350.3
Grid sold	MWh	290.4	288.2	590.6	300.1	292.4	286.6	651.6	305.0
COE	$/kWh	0.132	0.142	0.083	0.125	0.134	0.144	0.0815	0.130
NPC	M$	2.0	2.15	1.60	1.96	2.04	2.18	1.62	2.00
RF	%	68.5	68.8	78.7	68.2	68.7	68.4	86.3	68
CO_2 emission	t/yr	21.6	44.8	39.8	45.7	48.3	54.9	43.3	55.2
Diesel consumption	L/yr	7,101	7,033	6,539	7,016	8,326	1,1026	8,175	10,811
Biomass consumption	t/yr	10.4	10.2	10.3	10.1	9.12	9.7	9.60	9.38

Table 3.8. Share of energy generation for the optimal solutions

Component	Unit	CC				LF			
		I	II	III	IV	I	II	III	IV
PV	(%)	69.6	69.7	79.8	69.2	69.9	70	81.1	69.1
BG	(%)	0.91	0.90	0.70	0.88	0.78	0.83	0.61	0.80
DG	(%)	1.72	1.72	1.22	1.71	1.92	2.51	1.39	2.46
Grid	(%)	27.8	27.7	18.3	28.2	27.4	26.7	16.9	27.6

3.3.2. Surface plot of electricity to/from the central grid under optimal solution

In this analysis, the energy production components (BG/DG/PV) are able to sell energy to the grid during the daylight in winter at the maximum rate and a longer period in the summer. Fig. 3.11 (a)

and (b) demonstrate the fluctuation of hourly energy flow from/to the grid during a year. Electricity purchases from the grid are needed at a rate higher than 100 kW in December when solar availability is low. Most of the load requirement in the spring and summer is supplied by the PV system, and thus grid purchase reaches its minimum values. As is observable in Fig. 11(b), the Pelee residents can expect the highest amount of energy sold to the grid during the daytime, mainly in the summer, at a rate higher than 200 kW.
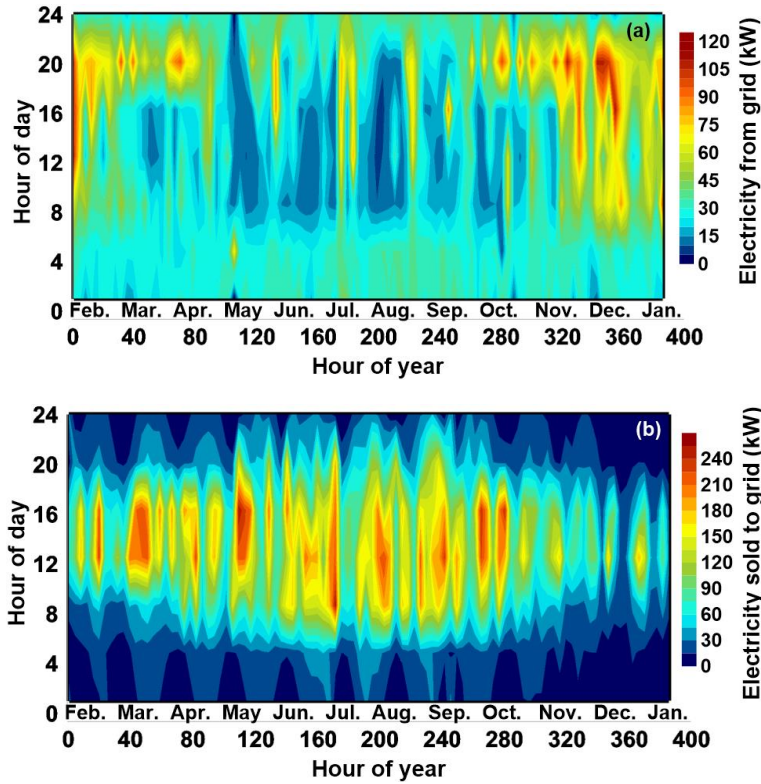
Fig. 3.11. Annual surface plot of (a) energy purchased (b) energy sales to the grid under optimal scenario

3.3.3. Surface plot of solar angles under optimal solution

The solar azimuth angle is the azimuth angle of the Sun's position. This horizontal coordinate defines the Sun's relative direction along the local horizon. Here we use a convention where displacements east of a due south line are negative, and west of a due south line is positive; the solar azimuth angle ranges ±180 degrees [38]. Further, the incident angle refers to the angle between the sun's rays impact direction and a solid surface. The solar incidence angle, θ, is the angle between the sun's rays and a normal surface. Fig. 3.12 (a) and (b) display the annual fluctuation of solar azimuth and incident angle, respectively. The lower the azimuth angle the more electricity generated by the panels. The higher PV electricity generation normally occurs at noon, wherein the optimum azimuth angle varies ±20 degrees. Also, the incident angle varies from 0 to 40 degrees during the peak periods and reaches higher than 70 degrees when the panels are inactive.
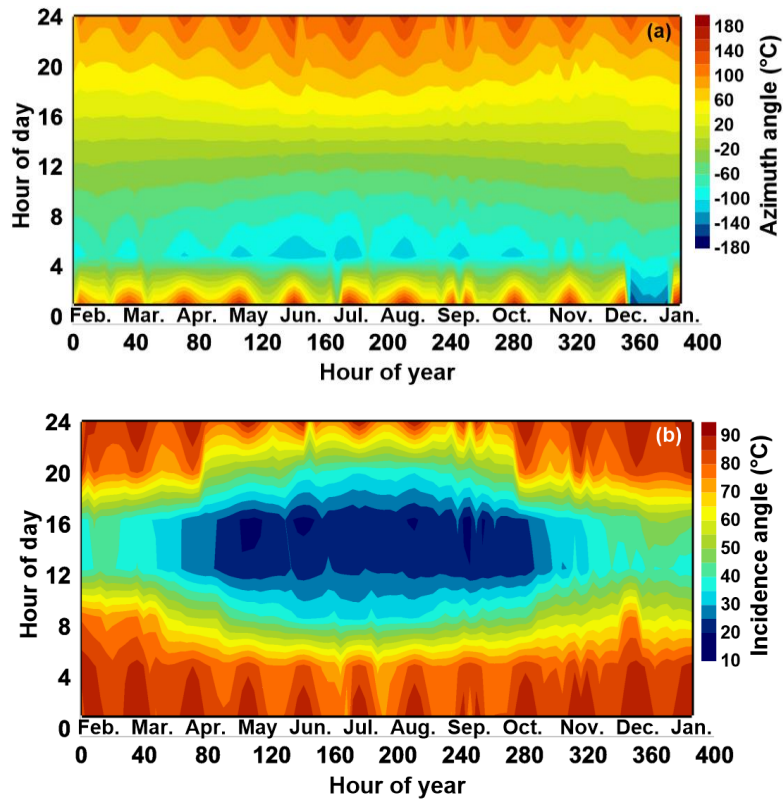
Fig. 3.12. Annual surface plot of (a) solar azimuth and (b) incidence angle under optimal scenario

3.3.4. Sample of system performance under optimal case

This subsection illustrates how the winning solution works over a particular period. With respect to the hourly variation of load demand at various months, each component acts differently to satisfy the required load. Fig. 3.13 (a) and (b) depict a sample of energy balance for the optimal case on the weekday and weekend, respectively. Based on the meteorological charts, since May has a mild climate distinction during a year, the comparison of component outputs in this month is considered in Fig. 12(a). This Figure reveals that the PV arrays can provide nearly six times more electricity than the central grid. Also, once demand increases, the system selects PV arrays to satisfy the load, and the central grid does not contribute to power generation. Further, the sum of PV and the grid power moves in the same direction, and the sum of outputs is equivalent to the amount of total electrical load served, implying that the system will deliver the right amount of power with trivial unmet power demand. Fig. 3.13 (b) shows how energy generation is divided into the scheduled gasifier and diesel generator on the weekend and how batteries respond to this. Since solar PV modules cannot perform at their maximum energy production in January, the operation of scheduled backups (gasifier and diesel generator) is plotted for this month. As scheduled, DG and BG have to operate from 7-9 a.m. and 9-11 a.m., respectively, on the weekend. The production of DG and GB is at least ten times lower than the production from the PV's. The batteries discharge their power on Jan. 7th at midnight and early morning to meet the load with the bio-gasifier since no solar irradiation is available to supply the PV arrays.

49
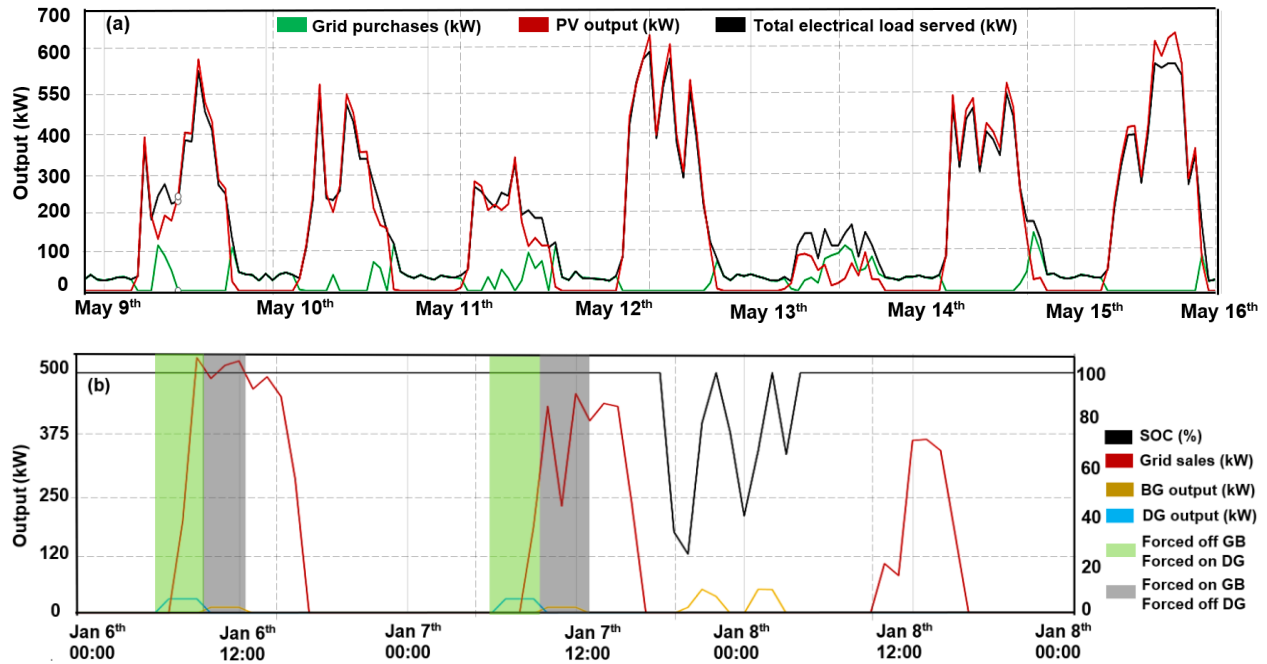
Fig. 3.13. Sample of power outputs of the components for the optimal system under LF strategy on (a) weekdays and (b) weekend

3.3.5. Comparison of the optimal cases under CC and LF dispatch strategies

Fig. 3.14 illustrates how the total system investment is distributed between HES components under LF and CC controllers. The proportion of DG cost, which is primarily due to the O&M cost, is around 10% and 13% in LF-based and CC systems, respectively. The biggest portion of the cost is allocated to CC-based PV arrays that are 5% higher than the CC-based options. The battery units and BG have the smallest costs during the project lifetime. The funnel in Fig. 3.15 summarizes the energy distribution of the optimal cases in LF and CC dispatch strategies. Unmet load under both cases is zero, meaning that both proposed systems have proper reliability to satisfy the load demand. Total energy production and consumed energy under the LF-based hybrid option, respectively, is ~80 MW and ~64 MW higher than the CC-based systems.
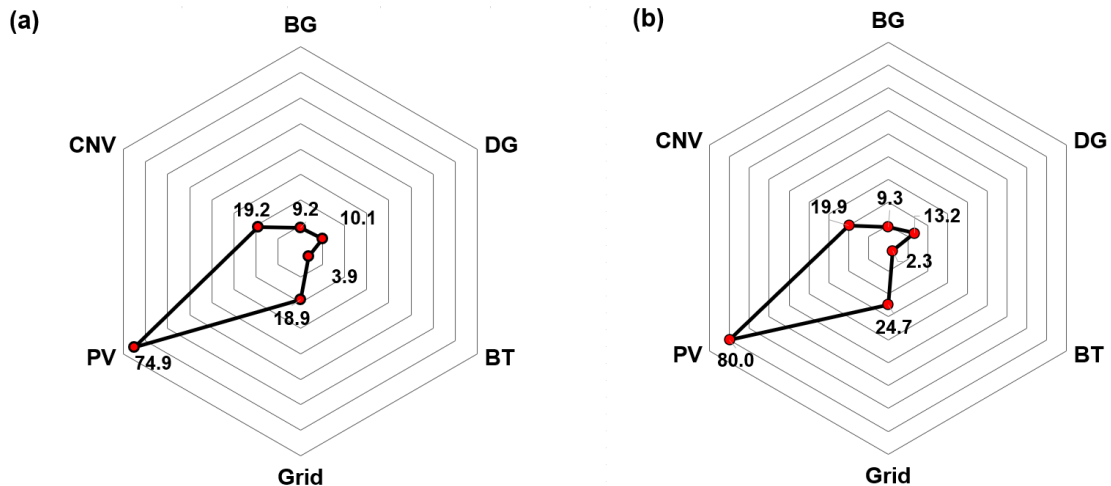
Fig. 3.14. Cost breakdown of the optimal solutions of (a) LF and (b) CC dispatch strategies
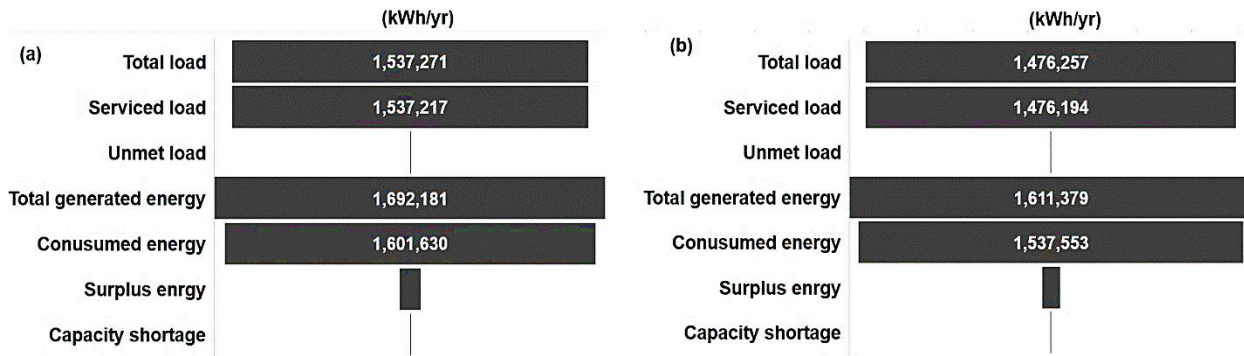
Fig. 3.15. Energy contribution of the optimal systems under (a) LF and (b) CC dispatch strategy

3.4. Sensitivity analysis

This section considers how technical performance factors influence the cost factors of each tracker-based system for both dispatch strategies. The sensitivity analysis illustrates how the uncertainty in simulation and mathematical modeling can potentially impact the output parameters.

3.4.1. Sensitivity analysis on SOC_{min} variation

Minimum state of charge (SOC_{min}) is expressed as the lowest acceptable level of battery charge. The battery level cannot be drawn lower than the SOC_{min}, given as a percentage of the total capacity. The SOC_{min} range is typically selected to be between 20% to 50% to avoid averse impacts on battery service life. In this study, the SOC_{min} variable was set at 20%. Fig. 3.16 (a) and (b) compare the impacts of SOC_{min} fluctuation on the economic variables of the tracker-based systems operating under CC and LF controlling strategies. Plus or minus 50% increase in SOC_{min} values increases the NPC of systems operating with CC and LF controllers. Because of the lower capacity of the battery units (higher SOC_{min}), the system would have to utilize more energy produced from BG, DG and PV. Hence, the system increases fuel, operating, and replacement costs resulting in an increment of NPC. The NPC of the HMA-based hybrid option under the CC controller is more sensitive to SOC_{min} variation, while the DA-based hybrid option changes less than other cases in this variation. The energy cost in HVA-based systems with the CC controllers has the highest dependence on SOC_{min}, and the DA-based systems with LF controllers have the lowest.

51
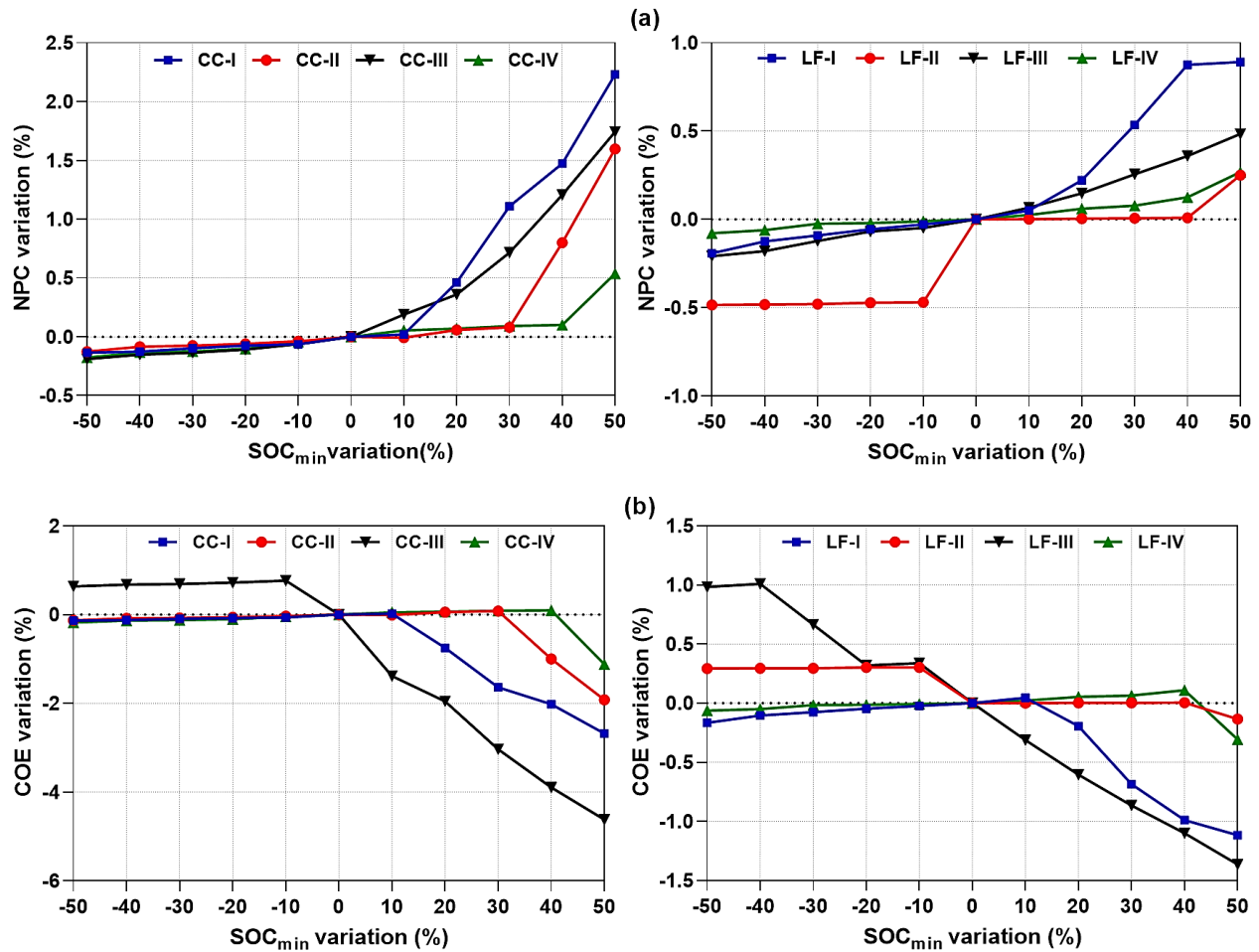
Fig. 3.16. Impact of SOC_{min} on (a) NPC and (b) COE of optimal cases in both dispatch strategies

3.4.2. Sensitivity analysis on load variation

The yearly load profile of the site plays a key role in estimating the NPC and COE of the proposed autonomous hybrid energy options. Fig. 3.17 (a) and (b) display the impacts of load variation versus NPC and COE for both control approaches. The higher load leads to increased NPC since more load requires a larger storage bank size, an increased O&M cost of grid, an increase in PV size, and an increase in the operation time of gasifier and diesel generator. Although it does reduce the energy costs in both controllers. Further to this, load variation has a greater effect on economic indicators compared to SOC_{min}. Over ±50% load variation, the highest NPC volatility is found in the HMA-based system working with the CC dispatch strategy. The largest and lowest decrement of COE is observed in HVA-based and DA-based systems of CC dispatch strategy, respectively.
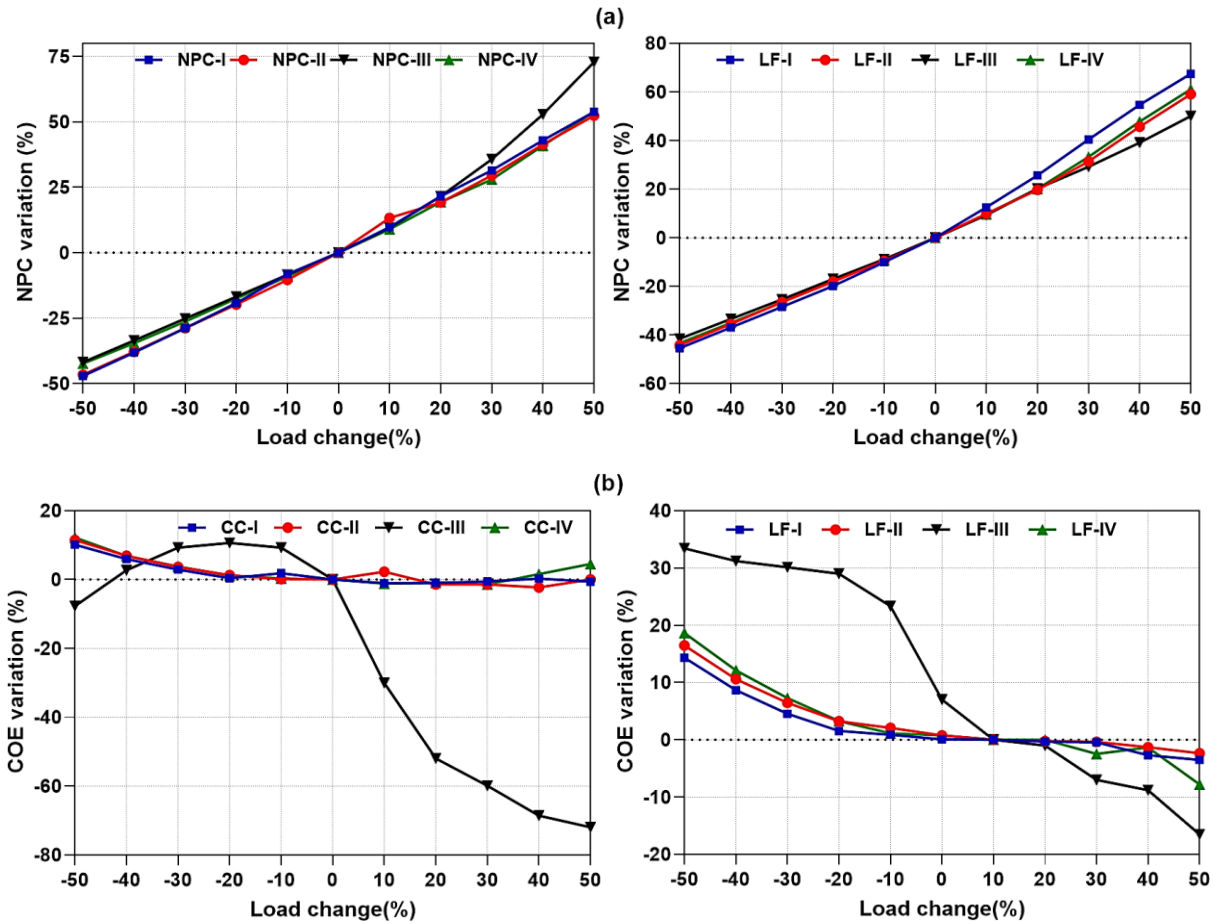
Fig. 3.17. Impact of load growth on (a) NPC and (b) COE of winning systems

3.4.3. Sensitivity analysis on capital cost multiplier of each tracking system

Fig. 3.18 displays how the COE of the system with each dispatch strategy shifts when the capital cost of the PV tracking system fluctuates. An increase in tracking technology cost obviously raises the energy cost of the system. The COE result for each capital cost multiplier in both CC-based and LF-based is approximately similar. Moreover, the cost of the DA tracking option (scenario IV) in the CC-based and LF-based systems has to be minimized by at least ~41% and ~43%, respectively, in order for the resultant to be comparable to that of a VCA tracker (scenario III) with the original initial value.
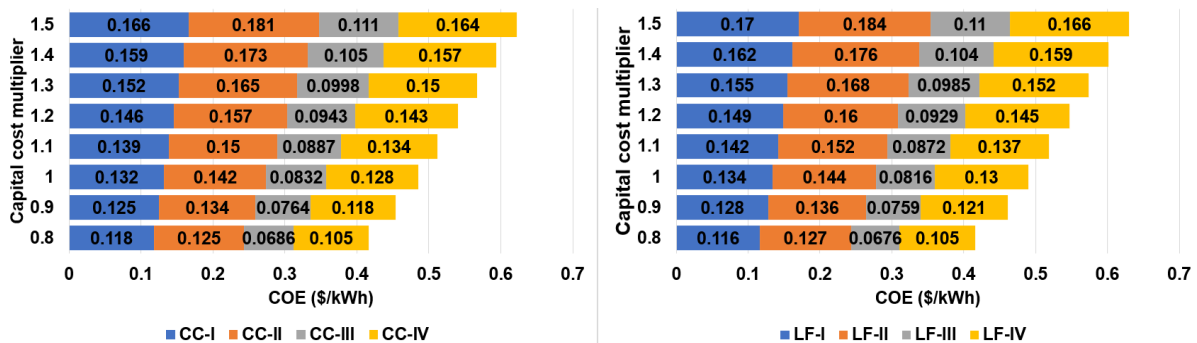
Fig. 3.18. Variation of COE upon tracking system initial costs under two dispatch strategies

3.4.4. Sensitivity analysis on albedo

According to Pelee Island meteorological conditions, the ground cover tends to be grass in summer and snow in winter. Although both are occasionally available in the same place and at the same time. As a result, different ground reflectance values are investigated in this study to explore the effects of albedo volatility on PV efficiency and cost. The term "albedo" refers to an object's capacity to reflect light from sources such as the sun. Fig. 19 (a) and (b) illustrate the variation of ground reflectance against PV capacity and the renewable fraction of each tracker-based system under the CC and LF control modes. For higher albedo, solar irradiation on the PV arrays increases and thus, the output produced will be higher. This leads to a reduction of required PV capacity and renewable fraction in both dispatch strategies. LF-based optimal solutions show more volatility toward albedo variation than CC-based systems. The highest decrease in PV capacity and RF values are observed under LF-based HVA and HMA tracking systems, respectively. Fig. 3.20(a) and (b) show the fluctuation of albedo against the NPC and LCOE of each tracker-based hybrid solution for both controllers. Since increasing albedo resulted in a decrease in PV capacity, the NPC and energy cost of the system will be reduced accordingly. Economic indicators are more sensitive in the DA-based hybrid options (scenario IV) due to its highest capital cost. The highest decrease of energy and present cost, respectively, is found for the DA-based system in the CC and LF dispatch strategies. These results also indicate that snow cover surface with a ground reflectance of about 60% obtains the best results compared to all other ground cover types. This is because lighter ground reflects more solar energy back to the solar panels. Although a high albedo is desirable, multiple factors such as damage potential from strong winds and snow must be taken into consideration when determining the optimal size of solar panels.
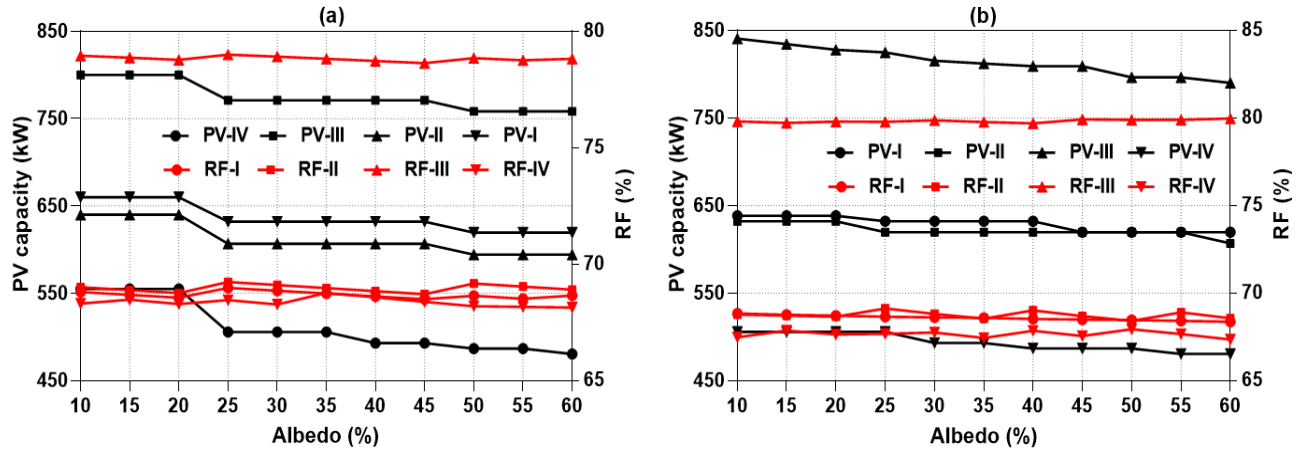
Fig. 3.19. Effect of the albedo versus PV capacity and the renewable fraction of each tracker in (a) CC and (b) LF dispatch strategies
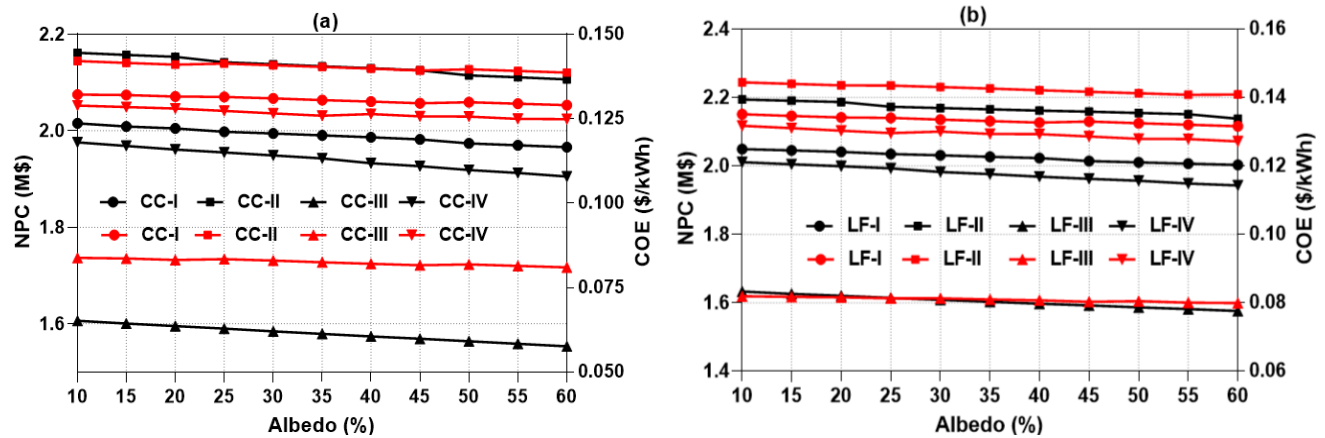
Fig. 3.20. Effect of the albedo versus NPC and COE of each tracker in (a) CC and (b) LF dispatch strategies

References

[1] H. Z. Al Garni, A. Awasthi, and M. A. M. Ramli, "Optimal design and analysis of grid-connected photovoltaic under different tracking systems using HOMER," *Energy Convers. Manag.*, vol. 155, no. July 2017, pp. 42–57, 2018, doi: 10.1016/j.enconman.2017.10.090.

[2] N. Choubineh, H. Jannesari, and A. Kasaeian, "Experimental study of the effect of using phase change materials on the performance of an air-cooled photovoltaic system," *Renew. Sustain. Energy Rev.*, vol. 101, no. April 2018, pp. 103–111, 2019, doi: 10.1016/j.rser.2018.11.001.

[3] V. Sumathi, R. Jayapragash, A. Bakshi, and P. Kumar Akella, "Solar tracking methods to maximize PV system output – A review of the methods adopted in recent decade," *Renew. Sustain. Energy Rev.*, vol. 74, no. December 2016, pp. 130–138, 2017, doi: 10.1016/j.rser.2017.02.013.

[4] M. H. M. Sidek, N. Azis, W. Z. W. Hasan, M. Z. A. Ab Kadir, S. Shafie, and M. A. M. Radzi, "Automated positioning dual-axis solar tracking system with precision elevation and azimuth angle control," *Energy*, vol. 124, pp. 160–170, 2017, doi: 10.1016/j.energy.2017.02.001.

[5] H. S. Akbar, A. ISiddiq, and M. W. Aziz, "Microcontroller Based Dual Axis Sun Tracking System for Maximum Solar Energy Generation," *Am. J. Energy Res.*, vol. 5, no. 1, pp. 23–27, 2017, doi: 10.12691/ajer-5-1-3.

[6] A. S. Aziz, M. Faridun, N. Tajuddin, and S. Padmabaran, "Evaluating the Impacts of Ground and Atmospheric Conditions on the Efficiency of Solar Energy System and Its Economic Analysis," no. June, 2018, doi: 10.20944/preprints201806.0324.v1.

[7] G. S. Campbell and J. M. Norman, *An Introduction to Environmental Biophysics*. New York, NY: Springer New York, 1998.

[8] B. Ming, P. Liu, S. Guo, X. Zhang, M. Feng, and X. Wang, "Optimizing utility-scale photovoltaic power generation for integration into a hydropower reservoir by incorporating long- and short-term operational decisions," *Appl. Energy*, vol. 204, pp. 432–445, 2017, doi: 10.1016/j.apenergy.2017.07.046.

[9] O. Ellabban and A. Alassi, "Integrated Economic Adoption Model for residential grid-connected photovoltaic systems : An Australian case study," *Energy Reports*, vol. 5, pp.

310–326, 2019, doi: 10.1016/j.egyr.2019.02.004.

[10] M. Muselli, G. Notton, and A. Louche, "DESIGN OF HYBRID-PHOTOVOLTAIC POWER GENERATOR , WITH OPTIMIZATION OF ENERGY MANAGEMENT," vol. 65, no. 3, pp. 143–157, 1999.

[11] L. Cheng, W. Wang, S. Wei, H. Lin, and Z. Jia, "An Improved Energy Management Strategy for Hybrid Energy Storage System in Light Rail Vehicles," *Energies*, vol. 11, no. 2, p. 423, Feb. 2018, doi: 10.3390/en11020423.

[12] L. Olatomiwa, S. Mekhilef, M. S. Ismail, and M. Moghavvemi, "Energy management strategies in hybrid renewable energy systems: A review," *Renew. Sustain. Energy Rev.*, vol. 62, pp. 821–835, Sep. 2016, doi: 10.1016/j.rser.2016.05.040.

[13] H. Li, A. T. Eseye, J. Zhang, and D. Zheng, "Optimal energy management for industrial microgrids with high-penetration renewables," *Prot. Control Mod. Power Syst.*, vol. 2, no. 1, pp. 1–14, 2017, doi: 10.1186/s41601-017-0040-6.

[14] Y. Sawle, S. C. Gupta, and A. K. Bohre, "Optimal sizing of standalone PV/Wind/Biomass hybrid energy system using GA and PSO optimization technique," *Energy Procedia*, vol. 117, pp. 690–698, Jun. 2017, doi: 10.1016/j.egypro.2017.05.183.

[15] R. Hosseinalizadeh, G. Hamed Shakouri, M. S. Amalnick, and P. Taghipour, "Corrigendum to 'Economic sizing of a hybrid (PV–WT–FC) renewable energy system (HRES) for stand-alone usages by an optimization-simulation model: Case study of Iran' [Renew. Sustain. Energy Rev. 54 (2016) 139–150]," *Renew. Sustain. Energy Rev.*, vol. 57, p. 1657, May 2016, doi: 10.1016/j.rser.2016.01.119.

[16] M. Ramesh and R. P. Saini, "Dispatch strategies based performance analysis of a hybrid renewable energy system for a remote rural area in India," *J. Clean. Prod.*, vol. 259, p. 120697, 2020, doi: 10.1016/j.jclepro.2020.120697.

[17] A. H. Mondal and M. Denich, "Hybrid systems for decentralized power generation in Bangladesh," *Energy Sustain. Dev.*, vol. 14, no. 1, pp. 48–55, 2010, doi: 10.1016/j.esd.2010.01.001.

[18] M. K. Shahzad, A. Zahid, T. Rashid, M. A. Rehan, M. Ali, and M. Ahmad, "Techno-economic feasibility analysis of a solar-biomass off grid system for the electrification of remote rural areas in Pakistan using HOMER software," *Renew. Energy*, vol. 106, pp. 264–273, 2017, doi: 10.1016/j.renene.2017.01.033.

[19] M. Jahangiri, A. Haghani, A. Mostafaeipour, A. Khosravi, and H. A. Raeisi, "Assessment of solar-wind power plants in Afghanistan: A review," *Renew. Sustain. Energy Rev.*, vol. 99, no. April 2017, pp. 169–190, 2019, doi: 10.1016/j.rser.2018.10.003.

[20] B. Lee, J. Park, W. Shin, B. Kim, B. Byun, and H. Jun, "Maximizing biogas production by pretreatment and by optimizing the mixture ratio of co-digestion with organic wastes," vol. 24, no. 4, pp. 662–669, 2019.

[21] P. I. Winery, "Walter Schmoranz," *Pelee Island*. [Online]. Available: https://www.peleeisland.com/about-us/.

[22] Customer Information Guide, "Pelee Island Winter Air Service," 2020. [Online]. Available: https://www.ontarioferries.com/pelee-island-ferries/pelee-island-winter-air-service/. [Accessed: 01-Jul-2021].

[23] V. Rutter, "Wood fuel supply in Ontario - CRIBE." [Online]. Available: https://cribe.ca/old-assets/2016_BHCP_Workshop/4-_Vince_Rutter_-_Supply_Chain_in_Ontario_-_Mar_8_2016.pdf.

[24] GildaleFarms, "Biomass crops," 2020. [Online]. Available: http://www.gildalefarms.ca/.

[25] A. J. White, D. W. Kirk, and J. W. Graydon, "Analysis of small-scale biogas utilization systems on Ontario cattle farms," *Renew. Energy*, vol. 36, no. 3, pp. 1019–1025, 2011, doi: 10.1016/j.renene.2010.08.034.

[26] Beef Research3, "Beef Cattle Research Council," 2020.

[27] A. Greinert, M. Mrówczyńska, and W. Szefner, "The use of waste biomass from thewood industry and municipal sources for energy production," *Sustain.*, vol. 11, no. 11, 2019, doi: 10.3390/su11113083.

[28] P. Burg *et al.*, "Calorific evaluation and energy potential of grape pomace," *Int. Agrophysics*, vol. 30, no. 2, pp. 261–265, 2016, doi: 10.1515/intag-2015-0082.

[29] A. C. Gowman *et al.*, "Physicochemical analysis of Apple and Grape Pomaces," *BioResources*, vol. 14, no. 2, pp. 3210–3230, 2019, doi: 10.15376/biores.14.2.3210-3230.

[30] T. Botelho, M. Costa, M. Wilk, and A. Magdziarz, "Evaluation of the combustion characteristics of raw and torrefied grape pomace in a thermogravimetric analyzer and in a drop tube furnace," *Fuel*, vol. 212, no. August 2017, pp. 95–100, 2018, doi: 10.1016/j.fuel.2017.09.118.

[31] L. Ladmin, "Livestock and Poultry Environmental Learning," 2019. [Online]. Available: https://lpelc.org/what-is-the-energy-value-btu-lb-of-livestock-manure-our-manure-source-is-dairy-solids-that-are-separated-from-the-slurry-at-about-60-moisture-we-want-to-reduce-that-moisture-further-and-burn-the-f/#:~:text=LHV values for livestock biomas.

[32] F. J. Larney, B. H. Ellert, and A. F. Olson, "Carbon, ash and organic matter relationships for feedlot manures and composts," *Can. J. Soil Sci.*, vol. 85, no. 2, pp. 261–264, 2005, doi: 10.4141/S04-060.

[33] M. Plochl and M. Heiermann, "Biogas Farming in Central and Northern Europe: A Strategy for Developing Countries? Invited Overview," *ecommons*, no. January 2006, 2006.

[34] U. S. F. T. Framework, "UNCTAD FRAMEWORK FOR SUSTAINABLE FREIGHT TRANSPORT (UNCTAD SFT Framework)," 2017.

[35] C. Li *et al.*, "Techno-economic feasibility study of autonomous hybrid wind/PV/battery power system for a household in Urumqi, China," *Energy*, vol. 55, pp. 263–272, Jun. 2013, doi: 10.1016/j.energy.2013.03.084.

[36] F. Rinaldi, F. Moghaddampoor, B. Najafi, and R. Marchesi, "Economic feasibility analysis and optimization of hybrid renewable energy systems for rural electrification in Peru," *Clean Technol. Environ. Policy*, no. 0123456789, 2020, doi: 10.1007/s10098-020-01906-y.

[37] M. H. Jahangir, S. A. Mousavi, and M. A. Vaziri Rad, "A techno-economic comparison of a photovoltaic/thermal organic Rankine cycle with several renewable hybrid systems for a residential area in Rayen, Iran," *Energy Convers. Manag.*, vol. 195, no. April, pp. 244–261, 2019, doi: 10.1016/j.enconman.2019.05.010.

[38] A. Senpinar, "Optimization of Slope Angles of Photovoltaic Arrays for Different Seasons," in *Exergetic, Energetic and Environmental Dimensions*, Elsevier, 2018, pp. 507–521.

Optimal Planning of Off-grid Hybrid Renewable Microgrids Using Sustainable Hydrogen Production

4.1. Introduction

Electricity access is a significant component of human society and economic progress. The electricity production and energy demand are mainly met from fossil fuels such as coal, oil and natural gas worldwide [1]. However, about 940 million (13% of the world) people are deprived of electricity [2]. About 2.4 billion people are also endowed with limited or unreliable energy [3]. The minority of these people live in remote localities of developed countries, lacking electricity due to the high distance from the nearest city or grid infrastructure, old equipment, or huge sea lane. To address this challenge, the hybridization of renewable energy systems has become a national purpose for worldwide countries towards green development and a cleaner future.

The integration of renewable components to generate energy called the hybrid energy system is getting much attention due to enhancing reliability, flexibility, reducing power fluctuations, and retaining electricity produced [4]. The connectivity status of hybrid systems distance is affected by uneven terrain and vast investment, high distance from grid infrastructure and inefficient power delivery. The rapid advancement of decentralized renewable energy generation technology offers cost-effective grid-isolated cases.

In addition to electrification purposes, renewable energy components can be promising options for supporting green transportation due to introducing new vehicle concepts and refuelling technologies based on hybrid renewable energy sources. However, the main obstacle of hybrid energy systems into conventional energy systems is the vital necessity for large-scale energy storage systems to overcome the variability and uncertainties of renewable resources [5], [6]. In fact, the intermittent nature and load dynamics of the hybrid renewable microgrids are considered as a significant impediment hurdling the transition towards 100% of clean energy fraction into the hybrid energy systems [7]. Hence, the hybrid energy systems require axillary equipment to store and move the electricity produced on various time scales, i.e., hourly, daily, and seasonally [8]. The common energy storage technologies are introduced as mechanical, batteries, pumped-hydro, etc., with technical limitations such as additional cost and infrastructure, complexity and space

requirements [9]. Therefore, the novel approach of storing power in a transportable, storable and utilizable energy carrier such as hydrogen has recently piqued global interest [6], [10].

Hydrogen can be produced in various ways; the most environmentally friendly option is recognized with water electrolysis fueled by renewables. Water electrolysis is expressed as the process of dividing water into oxygen and hydrogen gas with a direct electric current [11]. The solar/wind renewable options combined with water electrolysis topologies are among the most established hybrid systems to produce hydrogen [12]. In this regard, various communities explored using hydrogen for mobility via the research on fuel cell electric vehicles (FCEV) and H_2 refuelling processes.

The transportation sector has been a key focus for different policy measures across Canada, being the second greatest contributor to GHG emissions, accounting for over 25% of emissions in 2016 [13]. In line with this, federal and provincial governments have commended to adopt a variety of legislative initiatives, including electric vehicle purchase and private charger incentive programs. It has tremendous potential for renewable energy resources that can provide a year-round supply.

Wind and solar energy technologies are currently mature enough in Canada to provide various technical and financial advantages for the hydrogen production for remote communities, such as no risk of depletion or price increases like fossil fuels, simple to install and operate, feasible to compete with today's power plants, and financial incentives from the government [14]. Furthermore, a new market for hydrogen-powered light cars is already forming in Canada. Hence, it is crucial to promote practical refuelling options to foster the expansion of this hydrogen transportation in Canadian provinces. To date, there were few studies focusing on the optimal sizing of techno-economic feasibility analysis for hydrogen and electrification purposes simultaneously. Moreover, the residual value of the renewable components grows as the project lifetime lowers, which is a crucial consideration in the economic analysis of hydrogen-based hybrid systems. However, the project lifetime in many studies was assumed to be long-term (≥ 20 years), and the impact of shortening the project duration has not been explored.

In this research, three energy-poor islands in Canada are evaluated: Pelee, Saint Pierre, and Wolfe Island, all of which are located in separate directions in Eastern Canada. The optimal sizing for the electric load of 50 residential households and hydrogen for 50 fuel cell electric cars will be conducted in each location. The study's main contributions are arranged as follows:(i) compare a

hybrid system based on the financial, reliability, sustainability, and technical perspectives for satisfying both electric and hydrogen demand, (ii) examine profiles of electricity and hydrogen production, and (iv) sensitivity analysis on project lifetime, capital cost multiplier of each component, and also salvage ratios for optimal cases.

4.2. Methods and data

A procedural methodology of renewable modeling and optimization for autonomous hydrogen-based power options is studied in this research. The flowchart of the proposed optimization procedure utilizing HOMER Pro is demonstrated in Fig. 4.1. Initially, a comprehensive pre-feasibility evaluation is conducted to obtain the following indicators in each island: the project location and lifetime, available renewable resources in the site, and electric/hydrogen loads. The system challenges contain battery constraints such as SOC_{min}, resource availability such as no access to solar irradiation at night, etc. Before beginning the optimization process, all of these data are provided to HOMER as key input parameters affecting the obtained results. All feasible hybrid solutions are studied, in which techno-socio-economic assessment is performed based on the hourly-based calculations over 8760 h for each scenario. The optimization tends to stop once the NPC accuracy convergence criteria are met, and a list of feasible options is ranked based on the optimization objective(NPC reduction). The winning system is one that has the lowest NPC.
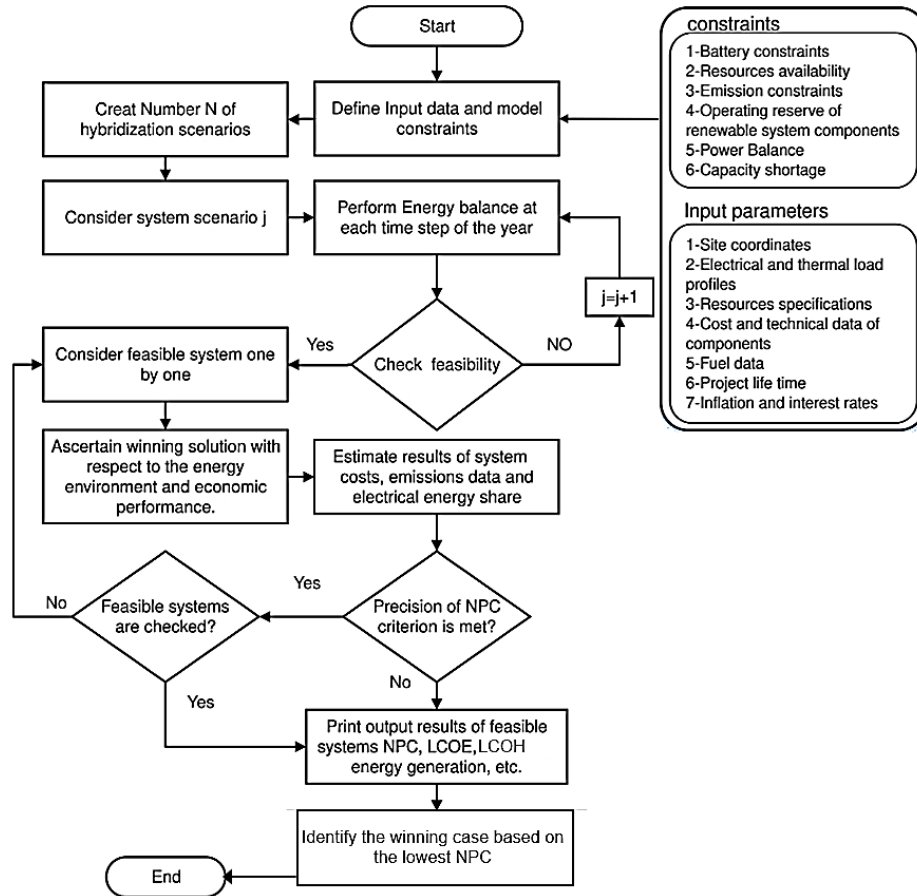
Fig. 4.1. Schematic representation of the implemented method

4.2.1. Climate and demographic data

In this study, three residential places in energy-poor islands are assumed: Pelee, Saint Pierre and Wolfe Island, located in various directions in Eastern Canada. Fig. 4.2 illustrates the geographical locations of these islands. The general information regarding analyzed areas is depicted in Table 4.1. Pelee and Wolfe islands are territories belonging to Ontario, while Saint Pierre is ruled by Newfoundland. The total area of Wolfe Island is about three and five times higher than Pelee and Saint Pierre Island, respectively. The studied areas have a similar climate distinction, although hourly renewable resources are completely different during a year. The average data for ambient temperature, solar irradiation, clearness index, and wind speed collected from NASA's meteorological resource data centre (NASA) for each area is shown in Fig. 4.3 [15]. Among the target islands, Pelee Island has the highest average annual average solar radiation, clearness index and ambient temperature among the other places, with values equal to 3.77 kWh/m^2/day, 0.481

and 9.5°C, respectively. Saint Pierre Island has the lowest yearly clearness index and solar irradiation due to the higher number of cloudy or rainy days. Saint Pierre Island is the windiest area with 2.7 m/s and 3.6 m/s higher wind speed compared to Pelee and Wolfe Islands, respectively. The islands' overall average solar irradiation, clearness index, and wind speed are 3.6 kWh/m^2/day, 0.47, 6.3 m/s, and 7.8 °C, respectively.
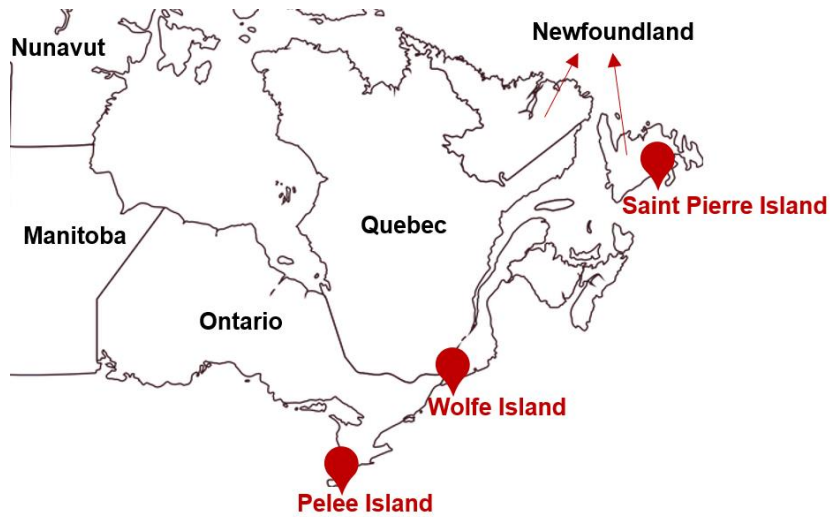
Fig. 4.2. Map of selected islands in eastern Canada

Table 4.1. General description of the selected islands

Island name	Direction in Canada	Area (km^2)	Coordinate	Climate type
Pelee	Southern Ontario	42	41.77° N, 82.65° W	Cool-humid
Saint Pierre	Eastern Newfoundland	25	46.77° N, 56.18° W	Cold-humid
Wolfe	Eastern Ontario	124	44.17° N, 76.39° W	Cold-humid
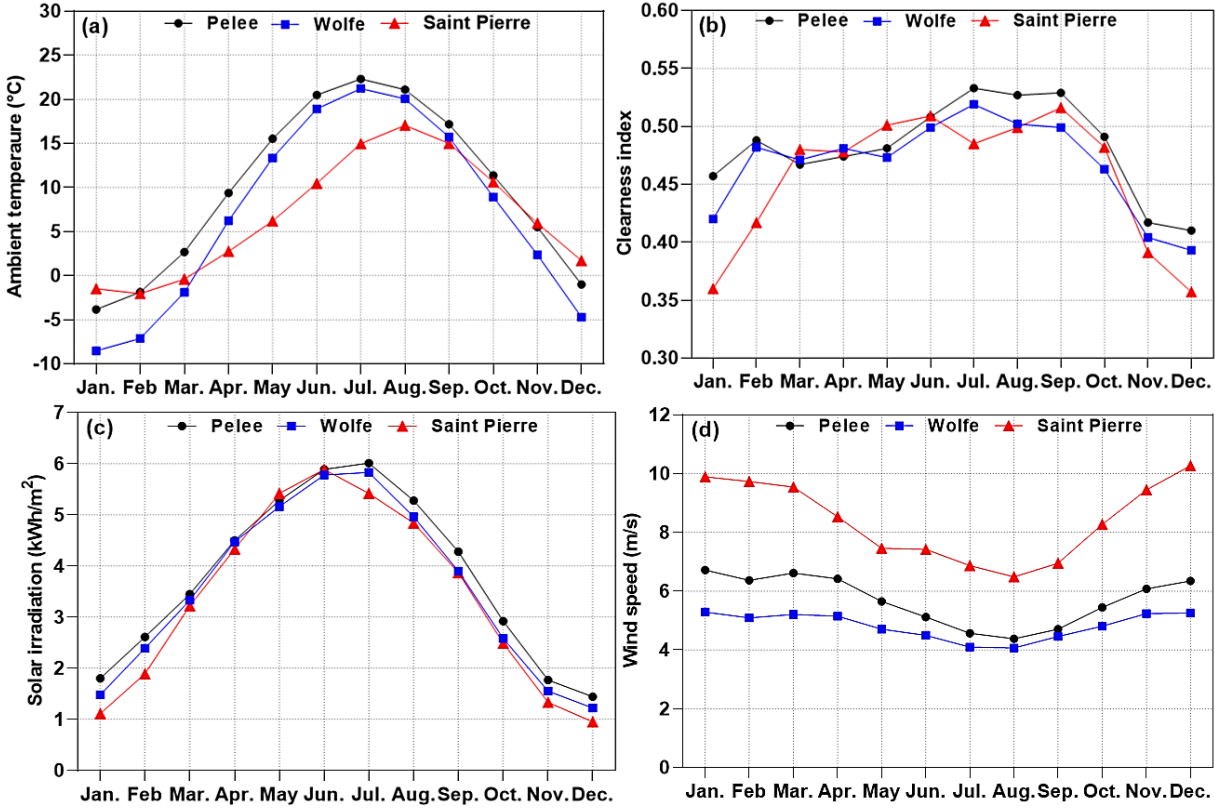
Fig. 4.3 Monthly average data of (a)ambient temperature, (b) clearness index, (c) solar irradiation, and (d) wind speed

4.2.2. Electric/Hydrogen load data

The residential electricity in these small communities is mainly used to supply the lights, radio, TV, iron, kettle, fan etc. This study examines the electrification of 50 residential households in the three islands [16]–[18]. The hourly load demands of each area are different from another. Table 4.2 presents the load profile and load details considered in the selected regions. The typical highest load occurs mostly from 6 to 8 p.m when there is a high possibility that all the households' appliances are connected simultaneously. Moreover, the average load demand per day and peak load is observed higher in Saint Pierre island. A load factor is a dimensionless number equal to the average load divided by the peak load. The load factor is calculated to be lower than 0.2 in these areas. Further to this, daily hydrogen demands are assumed to be similar for the hypothetical refuelling stations in the target islands. This load would be designed to meet a hydrogen demand of 125 kg/day, which is sufficient to refuel 25 vehicles having a hydrogen tank of 5 kg of capacity on a day [19]. In this simulation, hourly hydrogen loads become satisfied based on the most

effective electrolyzers operation hours, with PV and wind turbines operating based on renewable resources.

Table 4.2. Hydrogen and electrical load requirements in the target areas

	Electrical load	Hydrogen demand
Pelee Island	Average load: 54.8 kW,Peak load: 308.8 kW, Load factor: 0.18	
Wolfe Island	Average load: 61.7 kW,Peak load: 318.7 kW Load factor: 0.19	Average load: 5.2 kg/hr,Average peak load: 21.5 kg/hr, Load factor: 0.24
Saint Pierre island	Average load: 109.8 kW,Peak load: 595.6 kW, Load factor: 0.18	
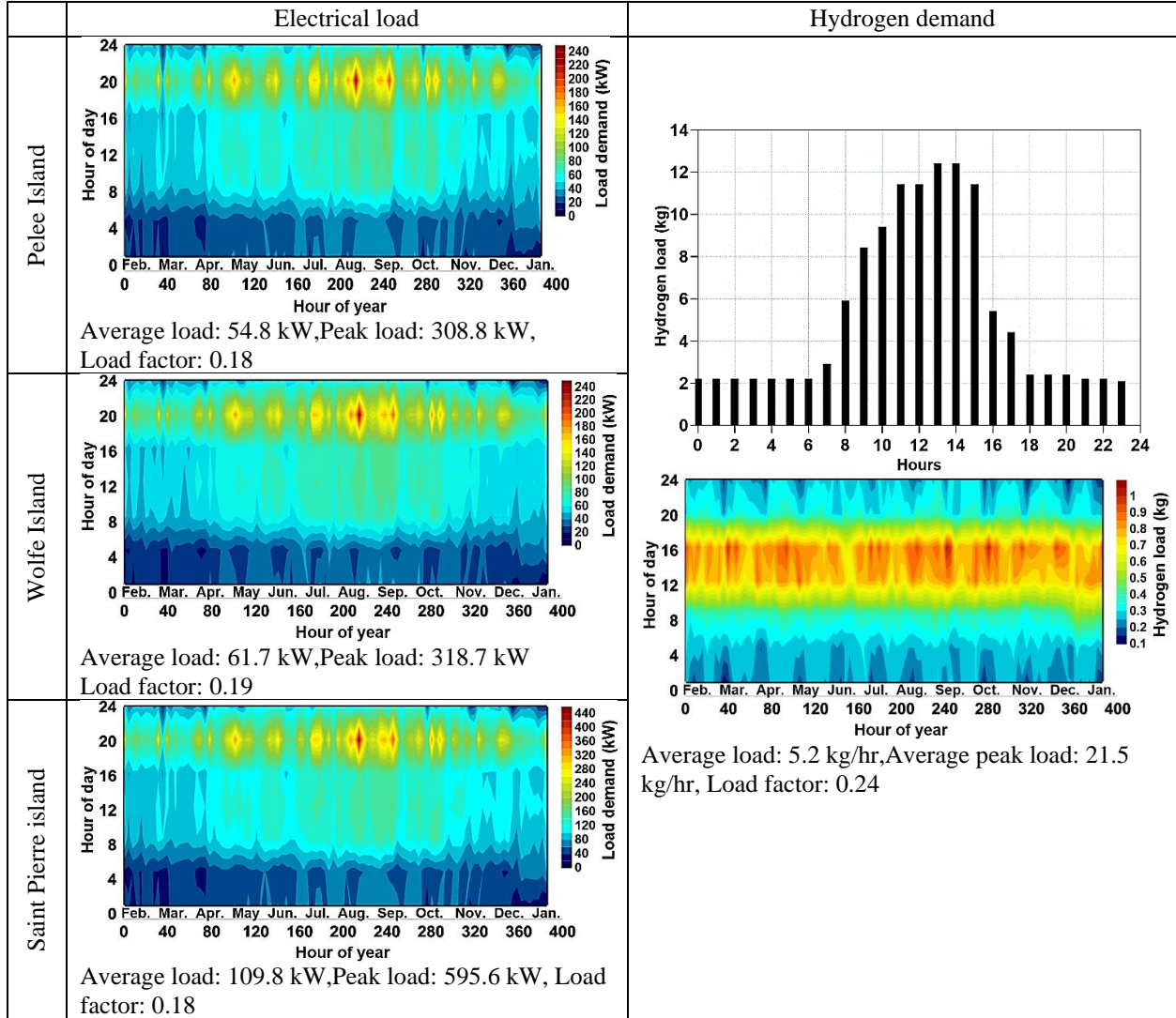
4.2.3. System description

An autonomous hybrid hydrogen/electricity refuelling station powered by a wind turbine and PV arrays power station is proposed in this work. This configuration is supposed to satisfy the electricity demand of 50 residential buildings and 25 hydrogen fuel cell vehicles in the target places. Fig. 4.4 illustrates the schematic diagram of the proposed system, consisting of a PV module(PV), wind farm(WT), electrolyzer(ELC), hydrogen storage tank (HST), fuel cell(FC),

battery and a converter. The red, blue and green arrows represent the electricity, water and hydrogen flow, respectively. The electricity produced by the WT/PV system can be categorized into two parts: one part is directly supplied to residential users, and the other part is used to produce hydrogen by using an electrolyzer. The hydrogen is then compressed into a hydrogen storage tank utilizing a compressor. The hydrogen storage tank delivers hydrogen to dispensers, and fuel cells produce electricity for households. Noted that whenever PV/WT output is inadequate, the fuel cell starts generating electricity. The size of the electrolyzer is dependent on the input power obtained from renewables. The capacity of the fuel cell stack also depends on the required energy of the unit. A bidirectional AC-DC/DC-AC converter is used for power-sharing of electric current between DC and AC bus.
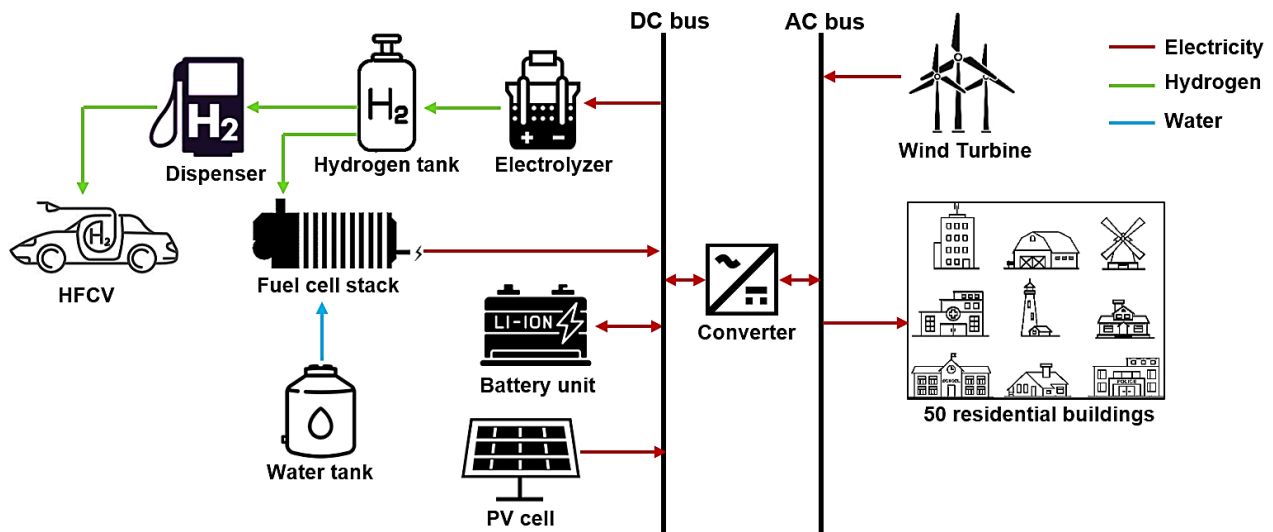
Fig. 4.4. Schematic diagram of a grid-isolated hybrid hydrogen refuelling/power charging station

4.3. Results and discussion

This section highlights the results and discussion of the proposed hydrogen-based microgrid utilized to satisfy the needs of residential communities in Canada. Three system solutions are examined to investigate the system performance by giving information on technical, economic, and environmental measures. Sensitivity evaluation is then conducted to analyze the impacts of uncertainty. Furthermore, a sensitivity analysis was performed on some important parameters that affect the performance of an economically optimal system. In this study, project lifetime, nominal discount rate, and expected inflation rate are assumed to be 25 years, 8%, and 2%, respectively. Several stand-alone hybrid power configurations are modelled to satisfy 50 buildings of three

islands by considering the real-time renewable resources and load demand over a year. The techno-environmental results of the optimal results in terms of the economic indicator are presented in Tables 4.3 to 4.5. Since optimal sizing and modelling hybrid energy solutions are highly site-specific and dependent on locally possible renewable resources and load demand, the optimization output reveals different values in each place.

4.3.1. *Case 1: Pelee Island (Southern Ontario)*

The scenarios that contained PV arrays are more cost-effective since the amount of solar radiation in Southern Ontario is favourable throughout the year. Table 4.3 presents the optimization tables of cases in Pelee Island. A combination of 249 kW PV,132 kW WT,634 battery units,700 kg H_2 tank, 250 kW ELC, and 450 kW FC is the optimal case, with LCOE and LCOH of 0.494$/kWh and 29.4 $/kg$H_2$, respectively. The second (without PV) and third(without WT) optimal cases have 9.8% and 25.2% higher NPC than the optimal case. Integration of PV panels and wind turbines into the hydrogen-based energy system minimizes NPC due to better coverage for the electricity peak consumption, ~25% decrease in batteries units, and lower PV panels.

4.3.2. *Case 2: Wolfe Island (Eastern Ontario)*

The meteorological condition of Wolfe Island is roughly similar to Pelee Island, with lower wind speed. Therefore, the arrangement for the optimum scenarios is influenced by the number of PV panels. The details of optimal sizing in Wolfe Island are shown in Table 4.4. the number of solar panels and wind turbines of this optimal case compared to Pelee Island increase by ~56% and reduce by more than two times, respectively. This variation of component capacities leads to a significant change in techno-economic results. Using the optimal configuration without wind turbine increases LCOE and LCOH by 31% and 85%. Wolfe Island is the worst option in lowering NPC due to weaker renewable resources and the intense need to store energy received in the higher batteries.

4.3.3. *Case 3: Saint Pierre Island (Eastern Newfoundland)*

Saint Pierre Island has higher wind intensity and expected inflation rate than the other islands, although solar radiation's potential is much lower. These factors directly impact the techno-economic results of the optimal solution in this area. Table 4.5 depicts the optimal results for all possible configurations in Saint Pierre Island. The number of wind turbines to satisfy the electrical

and hydrogen load in the optimal case is higher than solar panels, meaning that wind speed volatility significantly impacts energy generation and financial indicators on this island. Despite the fact that the expected inflation rate in Newfoundland province is ~1% higher than Ontario, the combination of 69 kW PV,88 kW WT,581 battery units,700 kg H_2 tank, 250 kW ELC, 450 kW FC, and 276 kW CNV which is selected as a winning solution based on the lowest NPC. Although it can be mainly due to the 200 kWh lower daily electricity load than the other two islands.

Table 4.3. Optimization results of the proposed solutions in Pelee Island

Configuration	PV	WT	ELC	FC	H_2 tank	BT	CNV	NPC	LCOE	LCOH
	kW	kW	kW	kW	kg	Unit	kW	M$	$/kWh	$/kgH_2
PV-WT-BT-H_2 tank-ELC-FC	249	132	250 (5,099 hrs/yr)	450 (131 hrs/yr)	700	634	297	3.58	0.494	29.4
WT-BT-H_2 tank-ELC-FC	-	254	250 (5,020 hrs/yr)	450 (85 hrs/yr)	700	1,154	380	3.97	0.548	37.5
PV-BT-H_2 tank-ELC-FC	950	-	250 (2,060 hrs/yr)	450 (55 hrs/yr)	700	2,535	420	4.79	0.661	56.8

Table 4.4. Optimization results of the proposed solutions in Wolfe Island

Configuration	PV	WT	ELC	FC	H_2 tank	BT	CNV	NPC	LCOE	LCOH
	kW	kW	kW	kW	kg	Unit	kW	M$	$/kWh	$/kgH_2
PV-WT-BT-H_2 tank-ELC-FC	575	60	250 (2,734 hrs/yr)	450 (103 hrs/yr)	700	1,274	301	3.98	0.549	37.7
WT-BT-H_2 tank-ELC-FC	954	-	250 (1,961 hrs/yr)	450 (34 hrs/yr)	700	3,356	697	5.21	0.719	69.8
PV-BT-H_2 tank-ELC-FC	-	535	250 (3,729 hrs/yr)	450 (17 hrs/yr)	700	4,003	419	6.68	0.921	85.2

Table 4.5. Optimization results of the proposed solutions in Saint Pierre Island

Configuration	PV	WT	ELC	FC	H_2 tank	BT	CNV	NPC	LCOE	LCOH
	kW	kW	kW	kW	kg	Unit	kW	M$	$/kWh	$/kgH_2
PV-WT-BT-H_2 tank-ELC-FC	69	88	250 (5,282 hrs/yr)	450 (132 hrs/yr)	700	581	276	2.99	0.374	21.9

| WT-BT- H$_2$ tank-ELC-FC | - | 105 | 450 (5,294 hrs/yr) | 597 (155 hrs/yr) | 700 | 597 | 335 | 3.07 | 0.385 | 21.2 |
| PV-BT- H$_2$ tank-ELC-FC | 1,298 | - | 250 (2,221 hrs/yr) | 450 (35 hrs/yr) | 700 | 597 | 332 | 5.30 | 0.664 | 62.0 |

4.3.4. *Comparison of optimal solutions*

Table 4.6 illustrates the details of the shared annual energy output of renewable components in each area's optimal case. The contribution of fuel cells in annual power generation is considerably lower than WT and PV in all islands. The highest average of energy production from wind turbines in Pelee and Saint Pierre islands is higher, while solar arrays in Wolfe island contribute to ~70% of yearly generation. PV panels in Saint Pierre island are responsible for supplying ~63% and ~14% lower energy production during a year. The energy produced from the fuel cell will not exceed 5% in each location. It can be concluded that using hydrogen-based components (FC/ELC/H$_2$ tank) for electrification may only add additional cost to the hybrid system while not capable of significant electricity generation (in relation to its expenses).

The profile of the H$_2$ tank enlightens active times over a year for the refueling station and indicates the system's reliability whether or not it can satisfy the station's hydrogen requirement. Table 4.7 represents the profile and cumulative density mass of stored hydrogen in the tank in each area. From late September to the end of the fall, the H$_2$ tank in Wolfe and Saint Pierre islands would have the least capacity of lower than 200 kg/hr. Although Pelee Island can confidently supply the hydrogen load over this period. The maximum frequency for the H$_2$ tank capacity occurs mainly in Pelee Island for 5500 hrs a year, which is 3000 and 1000 hours lower than Saint Pierre and Wolf Islands, respectively.

Table 4.6. The output power and shared annual energy of power generation components in optimum cases in three selected target areas

	PV output (kW)	WT output (kW)	FC output (kW)
Pelee	20.5% (328,075 kWh/yr)	76.1% (1,220,251 kWh/yr)	3.4% (55,803 kWh/yr)

	PV output	WT output	FC output
Wolfe	69.4% (727,930 kWh/yr)	26.2% (275,152 kWh/yr)	4.35% (45,565 kWh/yr)
Saint Pierre	6.65% (83,122 kWh/yr)	88.7% (1,108,927 kWh/yr)	4.65% (58,139 kWh/yr)
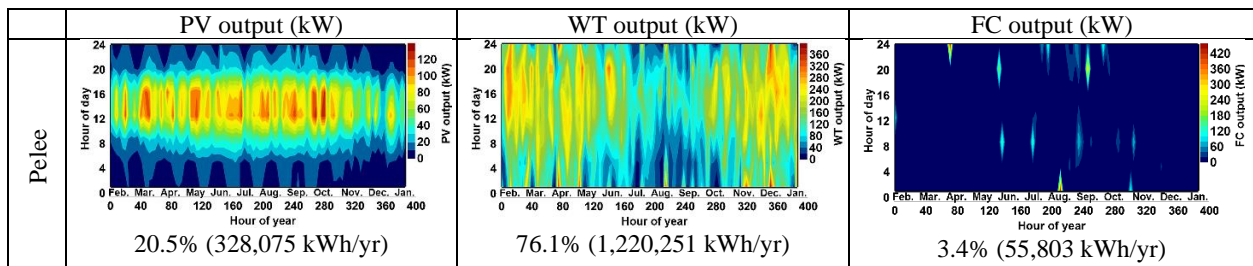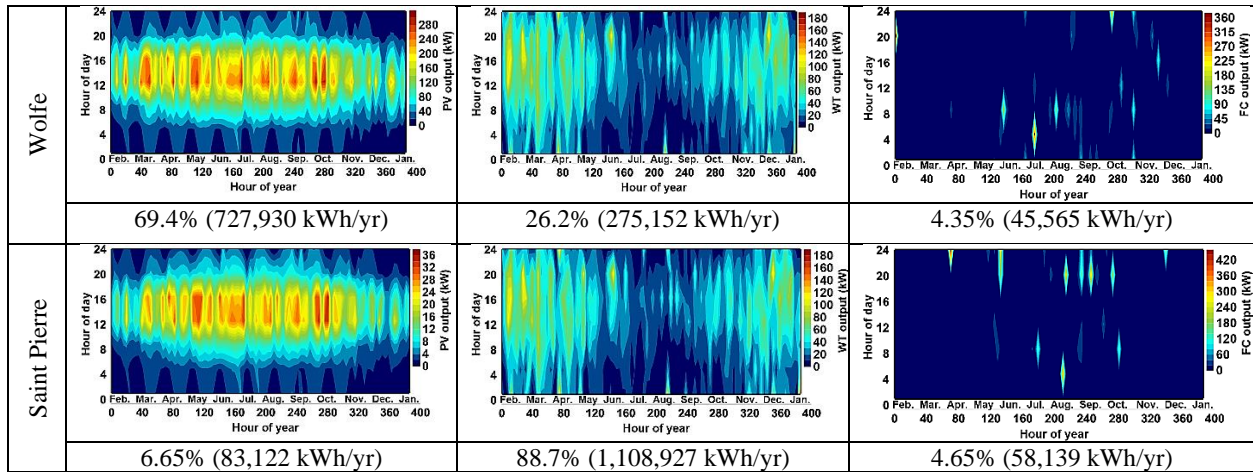
Table 4.7. Hourly profile and cumulative density mass of hydrogen production

	H$_2$ tank level (kg)	Cumulative density of hydrogen production
Pelee		
Wolfe		
Saint Pierre		
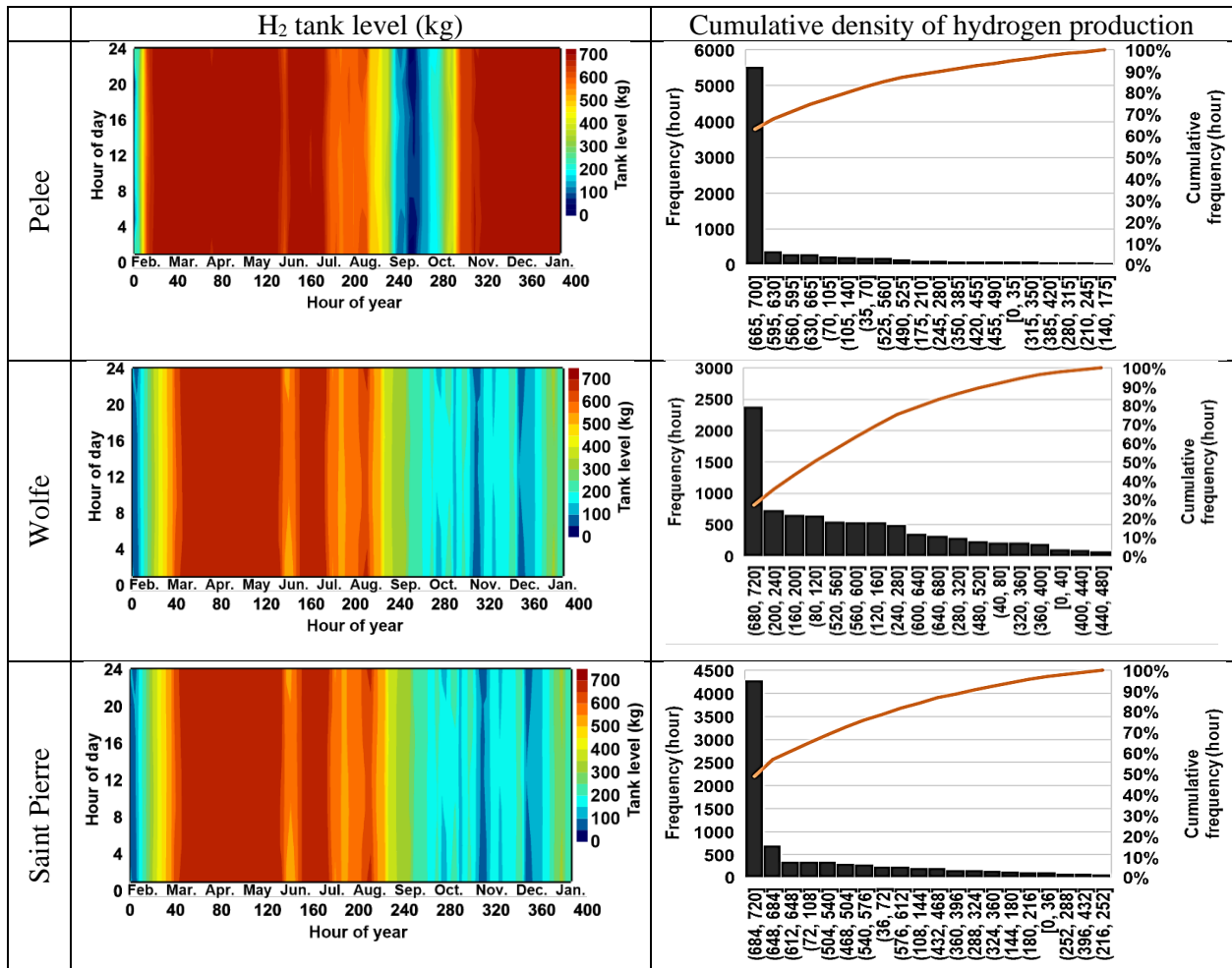
The cost breakdown of each optimal case is also displayed in Fig. 4.5. The most significant portion of project investment goes toward the capital cost of the components. The capital cost of a hybrid solution in Saint Pierre Island is $0.6M and $1.07M higher than the optimal case in Pelee and Wolfe Islands. Salvage cost is the value remaining in a system component at the end of a 25-year project lifetime. The salvage value is dependent on the replacement cost rather than the initial cost and involves prorated maintenance costs from the last event to the end of the project. Here, the salvage value in Wolfe Island is observed to be higher compared to other places.
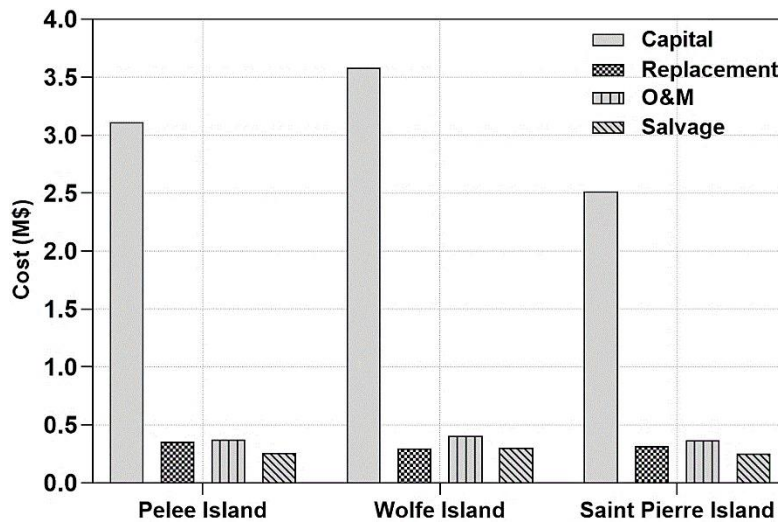
Fig. 4.5. Cost breakdown of the optimal case of optimal cases in the target areas

Hybrid design iterations that leave unmet electric load and the lack of capacity must be firmed up so that power is always available. Unmet electric load specifies information on the load that went unserved owing to insufficient production. The average unmet load can be utilized to measure the energy system's reliability in terms of load supply [20]. Moreover, the storage throughput (kWh) is expressed as the total energy that cycles through the battery units over a year. Battery throughput is approximated by the average energy (kWh) between energy in and out. Noted that battery throughput per battery gives information about the battery's operational lifetime; there is an indirect correlation between the annual throughput and the battery's lifespan. As displayed in Fig. 4.6, since all systems have unmet loads, they are assumed to be reliable with various values. The optimal option in Pelee Island is estimated to be the most reliable case due to their lowest unmet load. Conversely, the optimal case in Saint Pierre Island has the worst designs from this standpoint. It might be due to the highest dependence of this island on the one component(WT) in electricity

70

provision, increasing unreliability. Also, It is predicted that batteries in optimal Saint Pierre and Wolfe Islands cases, respectively, are more compatible to operate over a higher and lower lifetime efficiently.
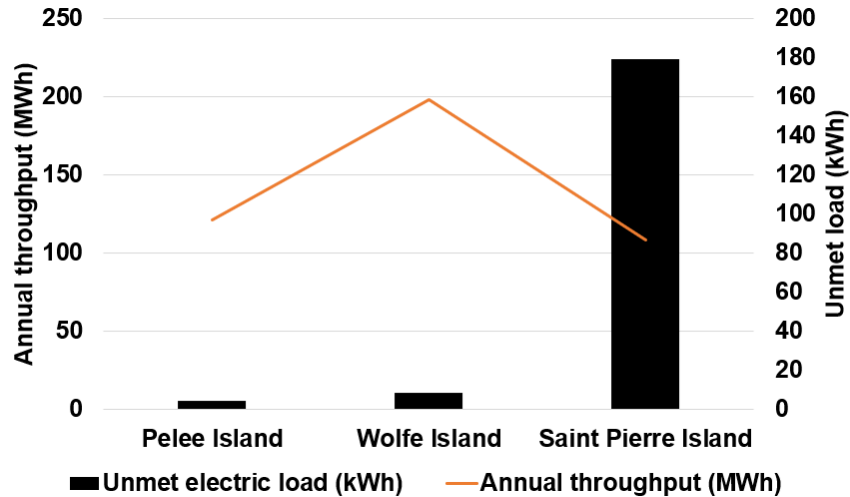
Fig. 4.6. Variation of annual throughput and unmet load under optimal option in each island

4.3.5. Sample of operation schedule under the optimal scheme

Fig. 4.7 depicts the operating schedules and energy flow of optimal system components over 48 hours (April 1st and 2nd). At 4 a.m., the wind turbine begins generating power, but it was not enough to meet the load; therefore, the batteries discharge their energy for a while to help wind turbines. When wind speed and solar irradiation can not be received by the WT/PV system, such as the period between 5 p.m. and 5 a.m, the batteries supply the load demand alone. Once the charge level reaches its SOC_{min} (hour 2189), the fuel cell operates to satisfy the load and charge batteries by its excess power simultaneously. Whenever solar irradiation is intense (9 a.m. to 3 p.m.), PV arrays start generating electricity to help wind turbines to fulfill all demands and charge the battery.

Fig. 4.7. Operations schedules and energy flow of the components over 48 hours

4.3.5. Sensitivity analysis

Following the modelling, introduction of optimal sizing, and techno-socio-economic evaluation of the best solutions in each area, a sensitivity analysis is performed to determine how much uncertainty of each techno-economic feature would influence the total system outputs. It evaluates the riskiness of the methodology by identifying how dependent the output is on various input values. The principal focus of the parameters examined 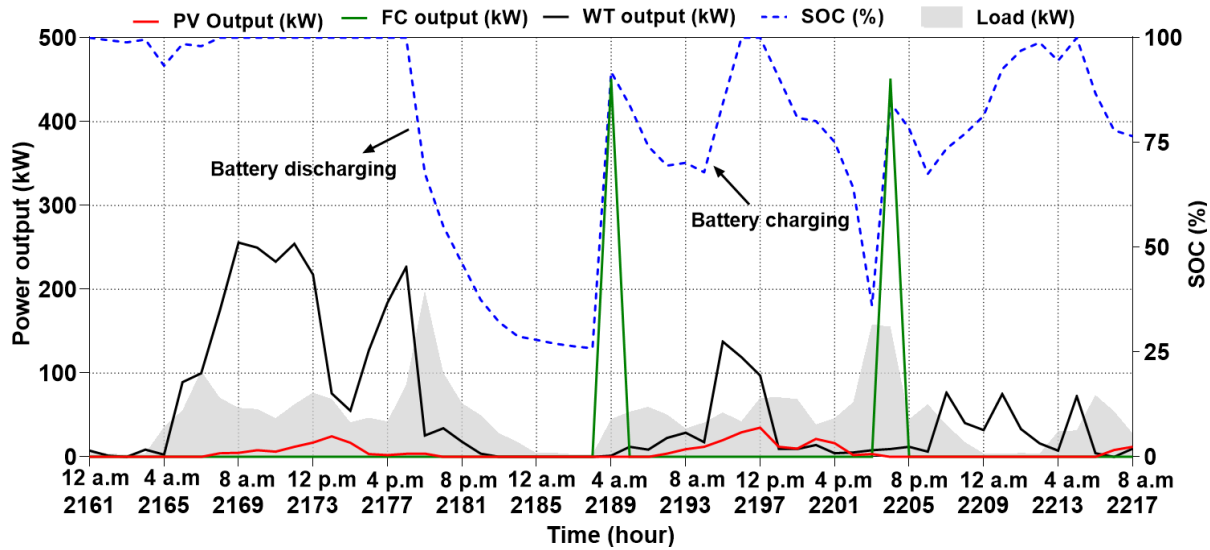in this study is to highlight the impacts of project lifetime and capital cost multiplier under the optimal cases or only the winning case(Saint Pierre Island)

4.3.5.1. Effects of capital cost multiplier

The stochasticity of the economic variables is discussed in this subsection. In this regard, if the initial(capital)cost of each equipment is assumed as Y, then a +50% and -50% change in the capital cost is 1.50Y and 0.5Y, respectively. Fig. 4.8 (a) and (b) display the variation NPC and LCOE against component's capital cost multiplier in each area. The devices assessed here are the most effective components, including wind turbine, solar array, fuel cell, and battery. Among the optimal cases, the LCOE in Pelee, Wolfe and Saint Pierre Island is more sensitive to fuel cells' market fluctuations than other components. It can be owing to the considerably lower price of the converter than other components. It can be due to the higher initial price of the fuel cells than other components. Among wind and solar components, wolf island is highly dependent on the financial

fluctuations of wind turbines. It is because the wind energy system has a major contribution to energy savings/generation on this island.
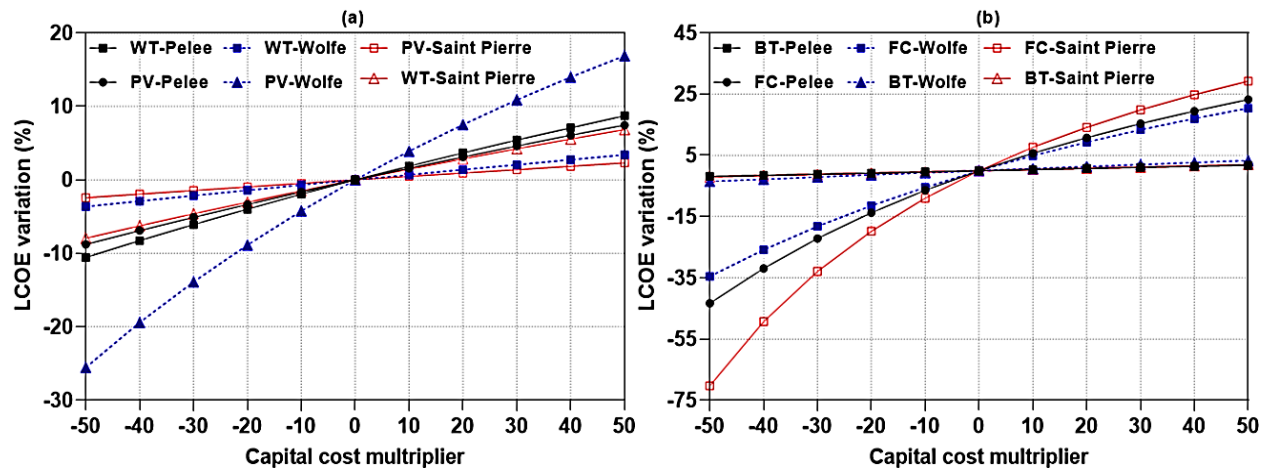
Fig. 4.8. Impacts of capital cost multiplier of (a) wind turbine/PV array and (b) fuel cell/battery on LCOE

4.3.5.2. Effects of the project lifetime on economic parameters

Fig. 4.9 presents the impacts of project lifetime on the economic indicators of each island. An increment in the project lifetime in all islands minimizes the COE, and the NPC of the final generated electricity increases. These lifetime modifications can be notable for the island with high solar radiation potential due to the higher economic benefits of employing solar panels and the lower salvage impact on these components. In this regard, a more significant reduction of energy cost(~63%)is observed when the optimal case in Pelee Island increases its lifetime by 28 years. As a result, given the minor effect of salvage, it might be inferred that long-term power/hydrogen generation is more cost-effective for the government.
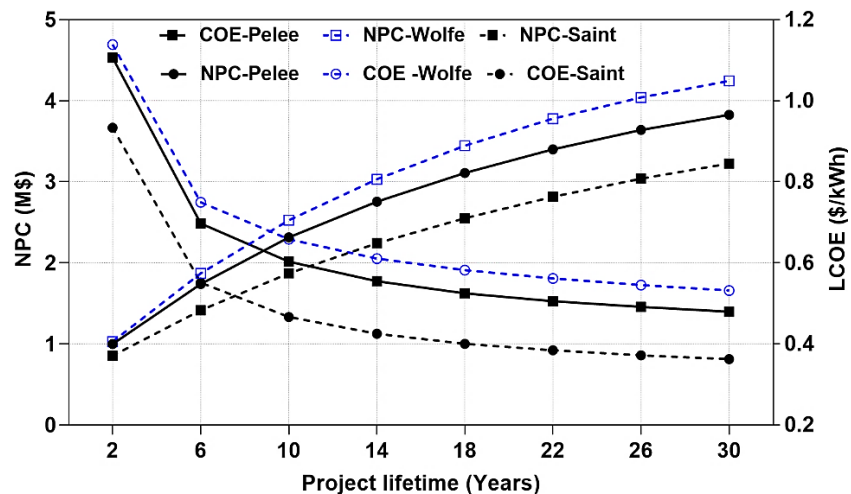
Fig. 4.9. The effect of project lifetime on the LCOE of the produced power in the winning solution

Meteorological data and climate change significantly influence the optimal architecture and energy costs of each hybrid system. Fig. 4.10(a) and (b) demonstrate the heatmaps indicating impacts of solar irradiation and wind speed versus LCOE of the winning case(Saint Pierre Island). Based on the heatmaps, average values of LCOE per specific radiation and wind speed are lower in the long-term project than that of the short-term project. It emphasizes that the accuracy of estimating resource assessment in the short-term project is highly critical during than long-term project. Therefore, in unpredictable climate circumstances, when there is insufficient time to evaluate the viability of renewable resources, predicting the energy cost of a short-term project is challenging. Furthermore, the potential spot here was drawn based on the average renewable data in Saint Pierre Island. It highlights that the winning case potentially observes $0.36/kWh≤LCOE≤$0.44/kWh within 1-1.5% of sensitivity changes.
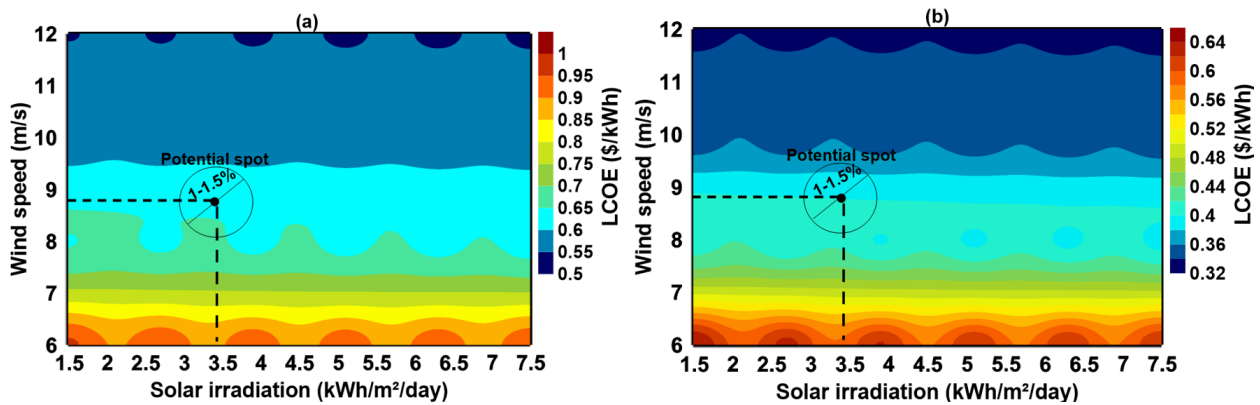
Fig. 4.10. Heat map of renewable resources potential versus energy cost in (a) short-term and (b) long-term project

The inflation rate is a factor causing money's purchasing power to weaken and the nominal value of revenue (i.e. cash inflows) and expenditures (cash outflows) to grow. The interest rate is also a fluctuating factor that seems more acute in developing countries where the interest rates could be as high as 15-25%. However, in Canada, it has been observed below 5%. Fig. 4.11(a) and (b) illustrate how the internet and nominal discount rate impact the LCOE of the short-term and long-term project. The number of phase changes on the heatmap for energy cost values is higher in the short-term project than in long-term projects. If the interest rates were to fluctuate by 1-2%,

electricity production costs would change higher than $0.1/kWh in the short-term project and lower than $0.8/kWh.
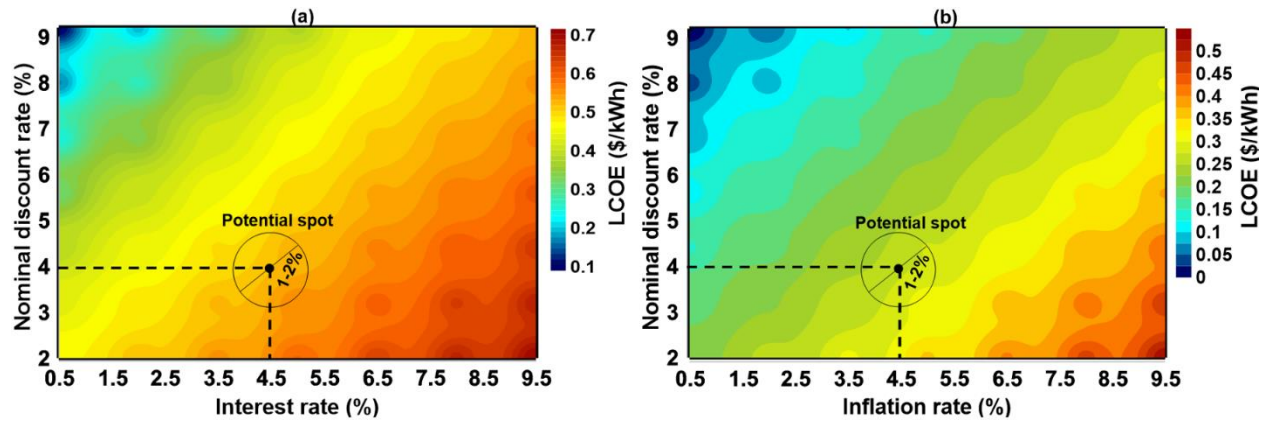
Fig. 4.11. Heat map regarding unstable economic indicators versus energy cost in (a) short-term and (b) long-term project

Fig. 4.12 (a) and (b) compare the variation of solar system and wind turbine selling prices in the retail market versus the energy cost over the short-term and long-term project lifetime. As expected, the short-term cases have expensive energy prices than the short-term ones. In the short-term period, the hybrid system will be highly sensitive to the initial cost of wind turbine than solar panels, while in the long-term project, both components have a similar impact on shifting energy costs. Energy cost in the short-term project mostly is fluctuated from $0.5/kWh to $0.75/kWh. This uncertainty in the calculations, related to the long-term projects, has a lower effect on financial indicators compared to the short-term project. Based on the potential spots,±0.2 change in initial costs of solar cells and wind turbines for the short-term project would raise uncertainties in energy cost than of that long-term project.
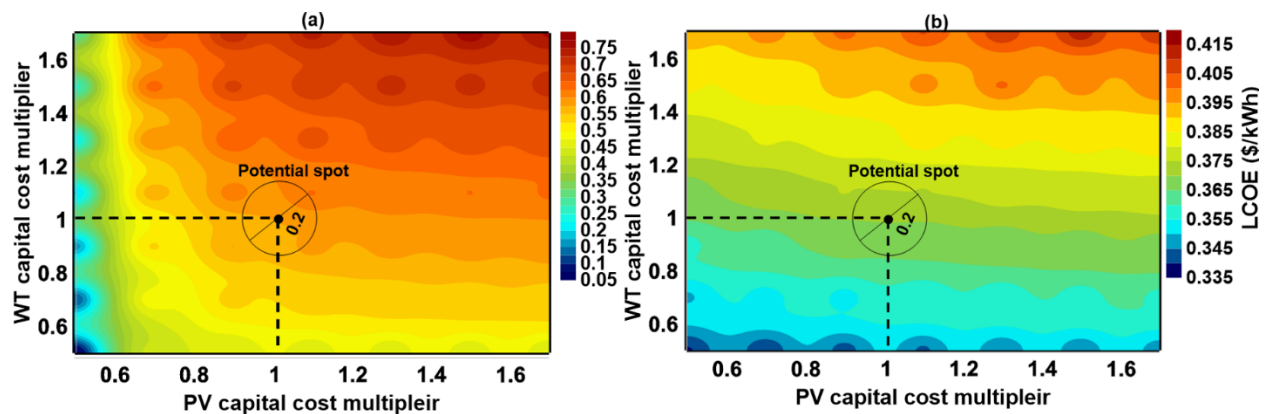
4.3.5.3. Comparison of salvage share

Fig. 4.13 shows the impacts of the project lifetime on the salvage share in the net present cost in the selected areas. The disparity in the volume of the bubbles in this diagram represents that the NPC would ascend as the project lifetime increases. However, the salvage ratio to the sum of total NPC and the salvage would decline as the project lifetime rises. The average ratio of salvage cost in Pelee and Saint Pierre islands is ~2.2% and ~1.5 lower than Wolfe Island. Based on these results, the share of salvage in the long-term project is more than that of the short-term project, indicating higher cost-effectiveness and reliability for the long-term project for the government. The reason for this trend is that, in the short-term project, the remaining lifetime of the components is considerable; thus, the uncertainty of the selling cost on the retail market would noticeably affect the outcomes. Fig. 4.14 illustrates the variation of project lifetime on LCOH in each island. Project lifetime minimizes the hydrogen cost of target islands during the long-term project. The highest and lowest decrement of LCOH is found under the optimal case of Wolfe Island($41.6/kg) and Saint Pierre($33.3/kg), respectively.

Fig. 4.13. The share of salvage value in the final NPC of the optimal cases in (a) Pelee, (b) Saint Pierre, and (c) Wolf Islands
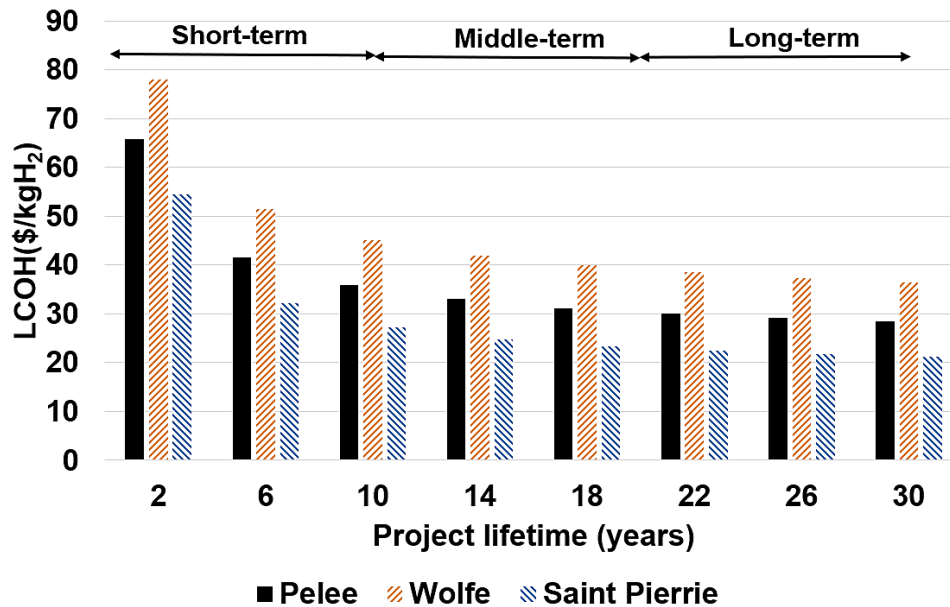
Fig. 4.14. Effect of project lifetime on the LCOH in the selected areas

References

[1]   N. Dalilah and H. Abdul, "Comparison of optimum design , sizing , and economic analysis of standalone photovoltaic / battery without and with hydrogen production systems," *Renew. Energy*, vol. 141, pp. 107–123, 2019, doi: 10.1016/j.renene.2019.03.090.

[2]   Hannah Ritchie and M. Roser, "Access to Energy," *Our World Data*, 2019.

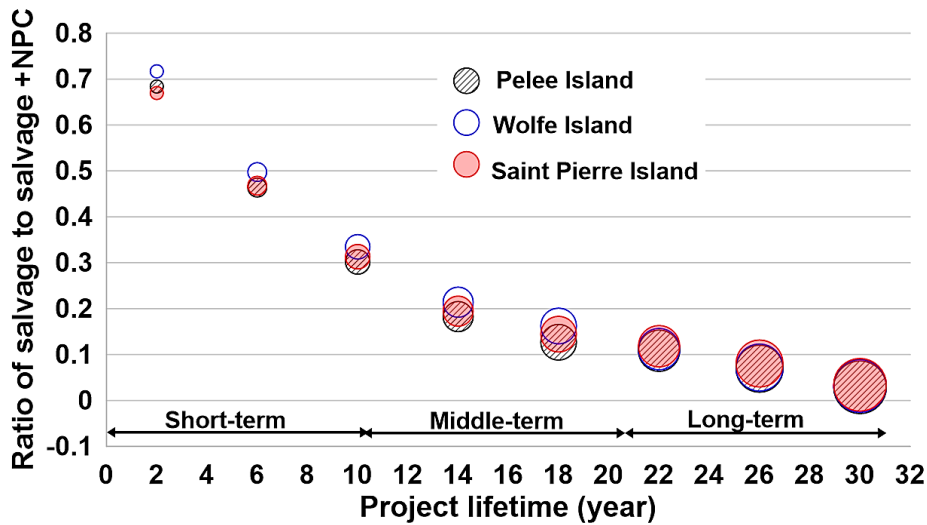[3]   S. Mandelli, J. Barbieri, R. Mereu, and E. Colombo, "Off-grid systems for rural electri fi cation in developing countries : De fi nitions , classi fi cation and a comprehensive literature review," vol. 58, pp. 1621–1646, 2016, doi: 10.1016/j.rser.2015.12.338.

[4]   F. Dawood, G. M. Shafiullah, and M. Anda, "Stand-alone microgrid with 100% renewable energy: A case study with hybrid solar pv-battery-hydrogen," *Sustain.*, vol. 12, no. 5, 2020, doi: 10.3390/su12052047.

[5]   K. Ghaib and F.-Z. Ben-Fares, "Power-to-Methane: A state-of-the-art review," *Renew. Sustain. Energy Rev.*, vol. 81, pp. 433–446, Jan. 2018, doi: 10.1016/j.rser.2017.08.004.

[6]   H. Blanco and A. Faaij, "A review at the role of storage in energy systems with a focus on Power to Gas and long-term storage," *Renew. Sustain. Energy Rev.*, vol. 81, pp. 1049–1086, Jan. 2018, doi: 10.1016/j.rser.2017.07.062.

[7]   C. Zhang, J. Wu, C. Long, and M. Cheng, "Review of Existing Peer-to-Peer Energy Trading Projects," *Energy Procedia*, vol. 105, pp. 2563–2568, May 2017, doi: 10.1016/j.egypro.2017.03.737.

[8]   F. Dawood, M. Anda, and G. M. Shafiullah, "Hydrogen production for energy: An overview," *Int. J. Hydrogen Energy*, vol. 45, no. 7, pp. 3847–3869, 2020, doi: 10.1016/j.ijhydene.2019.12.059.

[9]   J. Stansberry, A. Hormaza Mejia, L. Zhao, and J. Brouwer, "Experimental analysis of photovoltaic integration with a proton exchange membrane electrolysis system for power-to-gas," *Int. J. Hydrogen Energy*, vol. 42, no. 52, pp. 30569–30583, Dec. 2017, doi: 10.1016/j.ijhydene.2017.10.170.

[10] M. Boudellal, *Power-to-Gas:Renewable Hydrogen Economy for the Energy Transition*. De Gruyter, 2018.

[11] B. Endrődi, N. Simic, M. Wildlock, and A. Cornell, "A review of chromium(VI) use in chlorate electrolysis: Functions, challenges and suggested alternatives," *Electrochim. Acta*, vol. 234, pp. 108–122, Apr. 2017, doi: 10.1016/j.electacta.2017.02.150.

[12] D. Apostolou, P. Enevoldsen, and G. Xydis, "Supporting green Urban mobility – The case of a small-scale autonomous hydrogen refuelling station," *Int. J. Hydrogen Energy*, vol. 44, no. 20, pp. 9675–9689, 2019, doi: 10.1016/j.ijhydene.2018.11.197.

[13] C. Higgins and M. Ferguson, "Identifying and Characterizing Potential Electric Vehicle Adopters in Canada : A Two-stage Modelling Approach Moataz Mohamed Pavlos Kanaroglou," pp. 1–21.

[14] O. Ekren, C. Hakan Canbaz, and Ç. B. Güvel, "Sizing of a solar-wind hybrid electric vehicle charging station by using HOMER software," *J. Clean. Prod.*, vol. 279, p. 123615, 2021, doi: 10.1016/j.jclepro.2020.123615.

[15] N. P. | Docs, "POWER Data Methodology." [Online]. Available: https://power.larc.nasa.gov/docs/methodology/data/#meteorological.

[16] "Understanding your electricity bill," *Tiered price plan*, 2021. [Online]. Available: https://utilitieskingston.com/Electricity/About/YourElectricityBill.

[17] ENWIN, "Electricity, Water and District Energy for Windsor," 2021. [Online]. Available: https://enwin.com/electric-rates-residential/.

[18] WorldData.info, "Energy consumption in Saint Pierre and Miquelon," 2021. [Online]. Available: https://www.worlddata.info/america/stpierre-miquelon/energy-consumption.php.

[19] M. Gökçek and C. Kale, "Optimal design of a Hydrogen Refuelling Station (HRFS) powered by Hybrid Power System," *Energy Convers. Manag.*, vol. 161, no. December 2017, pp. 215–224, 2018, doi: 10.1016/j.enconman.2018.02.007.

[20] A. S. Aziz, M. F. N. Tajuddin, M. R. Adzman, M. F. Mohammed, and M. A. M. Ramli, "Feasibility analysis of grid-connected and islanded operation of a solar PV microgrid system: A case study of Iraq," *Energy*, vol. 191, p. 116591, Jan. 2020, doi: 10.1016/j.energy.2019.116591.

CHAPTER V

Conclusions and recommendations

5.1. Conclusions

This thesis conducted detailed feasibility, performance, and market evaluation to introduce stand-alone renewable technologies under various operation and component conditions. The summarized findings of chapters are listed below:

- Renewable fraction of LA-based systems than other options is more sensitive to fuel price volatility and solar irradiance. Although SBS-based systems have promising LCOE values, 1 kWh Li-Ion battery-based options keep their lowest LCOE over variation of required load, fuel price and irradiance. The values of NPC, LCOE, emissions and battery units of all hybrid alternatives increases as the ambient temperature rises.

- PV/WT/DG/100 kWh Li-Ion was the most reliable case due to having the lowest unmet load, estimated to be 286 kWh/year. However, PV/WT/2.5 kWh SBS was the worst option from this standpoint. Comparison of energy in/out predicted that 100 kWh Li-Ion than 2.5 kWh SBS batteries can efficiently operate at a higher service lifetime. PV/WT configurations also are more compatible with their batteries over a longer lifetime.

- SOC_{min} fluctuation revealed that the most sensitive cases to SOC_{min} variation are the NPC of HMA and COE of HVA-based trackers controlled by CC dispatch strategies. The highest and lowest energy cost reductions were detected in the HVA and DA trackers controlled by the CC dispatch strategy, respectively. In order for the results to be comparable to that of the VCA tracker with the original initial value, the cost of the DA tracker in CC and LF-based systems must be reduced by at least 41% and 43%, respectively.

- When ground reflectance (albedo) varies, LF-controlled systems show more volatility than CC-controlled systems. An albedo of about 60% achieves the most desirable results compared to all other ground cover types. As a result of albedo growth, LF-based systems equipped with HVA and HMA tracking options showed the greatest reduction in PV capacity and RF values, respectively.

- For hydrogen/electricity production, the integration of 69 kW PV,88 kW WT,581 battery units,700 kg H_2 tank, 250 kW ELC, 450 kW FC, and 276 kW CNV was identified as a winning solution due to the lowest NPC. Wind speed volatility significantly impacts energy generation and financial indicators in the selected islands. For example, using the optimal option without WT in Wolfe Island increases LCOE and LCOH by 31% and 85%.

- Fuel cell costs are more sensitive to market changes in LCOE than other energy components in all islands. The highest energy cost reduction(~63%) was obtained when the optimal case in Pelee Island increases its lifetime by 28 years. The long-term project is more cost-effective for the government due to its higher salvage costs than the short-term.

- Over a short-term period, the hybrid system was highly sensitive to the capital cost of wind turbines than solar panels, while in the long-term project, both components had a similar effect on changing energy costs. Changes in initial costs of solar cells and wind turbines for the short-term project would raise uncertainties in energy cost than of that long-term project.

5.2. Recommendations

The following points offer several optimization guidance for cost reduction and better technical operation of hybrid energy solutions based on previous chapters presented.

- Using 1 kWh Li-Ion batteries is superior to 1 kWh Lead-acid, 2.5 kWh SBS and 100 kWh Li-Ion battery designs in minimizing NPC of hybrid energy systems.

- In order to satisfy the accurate amount of load, the PV/WT/DG/100kWh Li-Ion and PV/WT/1 kWh Li-Ion systems have the highest and lowest reliability, respectively.

- If the irradiance and fuel price are highly fluctuating in the area, 1 kWh LA-based and 1 kWh Li-Ion systems are highly recommended from the technical and economic stand of point, respectively.

- The highest service lifetime of battery units is predicted using 100 kWh Li-Ion in the hybrid energy systems.

- Combining hybrid energy systems with vertical-axis PV trackers controlled by the CC controller achieves the lowest NPC than other tracking modules.

- For HMA and HVA-based systems controlled with CC strategy, It is recommended to use the battery units having the lowest change in SOC_{min}.

- Keeping albedo within the lower values is more desirable from an economic perspective.

- The CC-controlled systems witness higher compatibility with changing albedo than LF-controlled systems.

- The intensity of renewable resources and load data can play a more pivotal role in changing NPC than interest and inflation rates. Based on the last chapter, although Newfoundland's expected inflation rate was higher than in Ontario, the lowest net present cost(NPC) of the hybrid solution was found in Saint Pierre Island, Newfoundland, due to lower load demand and higher wind speed.

- Among renewable components, LCOE is more sensitive to market changes of the fuel cell. Then, an area with the highest variation of fuel cells is not recommended for using this component from an economic perspective.

- The hydrogen tank in Pelee Island has the lowest reliability to satisfy the required hydrogen of more cars due to its lowest hydrogen frequency than Saint Pierre and Wolfe Islands.

- The hybrid energy options are recommended to maintain within the long-term project lifetime due to more profitability at the end of the project and higher accuracy to predict energy/hydrogen cost.

- It is recommended to study the impact of the project lifetimes and salvage values on the techno-economic results of the optimal hybrid configurations to achieve more accurate results.

5.3. Comparisons

It can be challenging to collate the present case study with relevant literature due to the specificity of system structures, sizes, load demands, and renewable resources. However, some economic parameters can serve as a metric to assess our results against similar efforts in other research works. The following tables compare the findings of the winning battery and tracker technology worldwide with regard to their economic indicators.

5.3.1. Comparison of battery technologies

Table 5.1 presents a synoptic comparison between NPC, LCOE, and winning component selection of the present research and some literature findings. Li-Ion batteries are more interoperable with hybrid solutions in many localities. Furthermore, since NPC is determined based on the local

81

capital costs and HES sizes, the value is meaningfully unequal from area to area. Instead, LCOE obtained from dividing the annualized cost of producing electricity by the total electric load served can be a valuable indicator for comparing the cost-effectiveness of the hybrid energy systems. The tabulated data shows that Leopard Beach (Western China), Punjab(Pakistan) and Odisha state(India) have the smallest LCOE, while energy cost is higher in Lanzhou (China). One of the effective parameters that change LCOE is diesel and biomass price. It is evident that that country located in/near the Middle East, due to having cheaper fuel prices, obtains lower LCOE values. The energy cost of the optimal solution in the present work (0.321 \$/kWh) compared to other regions indicates the promising economic feasibility of HES in Canada. Several measures from the government can be performed to lower the current LCOE in Pelee Island, such as up-front grants or cash rebates for installing renewable energy equipment, low-interest or interest-free loans to organizations that install renewable energy, and exclude the value of distributed renewable energy systems from property tax assessments.

Table 5.1. Comparison data with the relevant works worldwide

Reference Location	HES	Winning battery type				Winning NPC (M\$)	Winning LCOE (\$/kWh)
		LA	Li	Ni-Fe	Other		
[1], Streaky Bay, Australia	PV/ICE		✓			0.02	0.30
[2], Lanzhou, China	DG/WT				✓	7.73	0.471
[3], Chorasariadho, Bangladesh	PV/WT/DG	✓				0.335	0.370
[4], Odisha state, India	PV/WT/Bio generator/DG			✓		0.633	0.238
[5], Leopard Beach, Western China	PV/WT/bio generator	✓				0.587	0.201
[6], Layyah, Punjab, Pakistan	PV/ Bio generator		✓			0.61	0.10
Pelee Island, Canada	**PV/WT/DG**		✓			**3.67**	**0.321**

5.3.2. Comparison of solar tracking modules

Comparing the present optimal tracker-based design with results in the literature can help establish the applicability of these different tracker technologies across various places worldwide. Table 5.2 presents the winning tracking technology and NPC comparison for various locations featured in the literature. It is evident that similar to this study, in most cases, the vertical-axis PV trackers

(VCA) have been highlighted as a winning solution to satisfy the required load regardless of the geographic location. Discrepancies of NPC growth rates in both cases in Saudi Arabia (Makkah and Alkharj city) are observed higher than the rest of the options. Comparing NPC growth rates between Pelee Island, Ontario, Canada, and Concordia University, Montreal, Canada, reveals that after HVA, DA tacking options can be more reliable and cost-effective in Canadian regions with a similar climate pattern.

Table 5.2. Comparison of the present results with literature findings

	Ref., Location	HES[1]	Winning tracker[2]	NPC growth rate (%)[3]				
				Fixed-tilt	HMA	HCA	VCA	DAT
Grid-connected design	[7], Concordia University, Canada	PV/WT/BT	VCA	-	-	17.70	Optimal	16.14
	[8], Makkah, Saudi Arabia	PV	DAT	Optimal	20.63	20.00	1.00	19.95
	[9], Eight cities in Iran	PV/BT	VCA	0.70	2.06	3.40	Optimal	0.70
	[10], Alkharj city, Saudi Arabia	PV/ELC/FC	VCA	38.00	-	78.00	Optimal	84.00
	Pelee Island, Canada	**PV/BG/DG/ BT**	**VCA**	**-**	**20.00**	**25.58**	**Optimal**	**18.36**
Off-grid design	[11], Hilly terrain, India	PV/WT/BT	VCA	-	2.00	3.86	Optimal	9.77
	[12], South of Iran	PV/PSH	DAT	6.84	-	12.80	-	Optimal
	[13], Healthcare building, India	PV/BT	VCA	-	7.50	16.31	Optimal	13.90

[1]BG= bio gasifier, DG= diesel generator,BT=battery,PV= solar system,WT=wind farm,PSH= Pump storage hydroelectric, ELC=electrolyzer
[2]VCA=Vertical-axis,HCA=Horizontal axis,VCA=Vertical axis,DAT=Dual-axis tracker
[3]NPC growth rate (%)= $\frac{NPC_{\text{selected tracker}} - NPC_{\text{winning tracker}}}{NPC_{\text{selected tracker}}}$

References

[1]   N. Dalilah and H. Abdul, "Comparison of optimum design, sizing, and economic analysis of standalone photovoltaic / battery without and with hydrogen production systems," *Renew. Energy*, vol. 141, pp. 107–123, 2019, doi: 10.1016/j.renene.2019.03.090.
[2]   Hannah Ritchie and M. Roser, "Access to Energy," *Our World Data*, 2019.

[3]   S. Mandelli, J. Barbieri, R. Mereu, and E. Colombo, "Off-grid systems for rural electri fi cation in developing countries : De fi nitions , classi fi cation and a comprehensive literature review," vol. 58, pp. 1621–1646, 2016, doi: 10.1016/j.rser.2015.12.338.

[4]   F. Dawood, G. M. Shafiullah, and M. Anda, "Stand-alone microgrid with 100% renewable energy: A case study with hybrid solar pv-battery-hydrogen," *Sustain.*, vol. 12, no. 5, 2020, doi: 10.3390/su12052047.

[5]   K. Ghaib and F.-Z. Ben-Fares, "Power-to-Methane: A state-of-the-art review," *Renew. Sustain. Energy Rev.*, vol. 81, pp. 433–446, Jan. 2018, doi: 10.1016/j.rser.2017.08.004.

[6]   H. Blanco and A. Faaij, "A review at the role of storage in energy systems with a focus on Power to Gas and long-term storage," *Renew. Sustain. Energy Rev.*, vol. 81, pp. 1049–1086, Jan. 2018, doi: 10.1016/j.rser.2017.07.062.

[7]   C. Zhang, J. Wu, C. Long, and M. Cheng, "Review of Existing Peer-to-Peer Energy Trading Projects," *Energy Procedia*, vol. 105, pp. 2563–2568, May 2017, doi: 10.1016/j.egypro.2017.03.737.

[8]   F. Dawood, M. Anda, and G. M. Shafiullah, "Hydrogen production for energy: An overview," *Int. J. Hydrogen Energy*, vol. 45, no. 7, pp. 3847–3869, 2020, doi: 10.1016/j.ijhydene.2019.12.059.

[9]   J. Stansberry, A. Hormaza Mejia, L. Zhao, and J. Brouwer, "Experimental analysis of photovoltaic integration with a proton exchange membrane electrolysis system for power-to-gas," *Int. J. Hydrogen Energy*, vol. 42, no. 52, pp. 30569–30583, Dec. 2017, doi: 10.1016/j.ijhydene.2017.10.170.

[10]   M. Boudellal, *Power-to-Gas:Renewable Hydrogen Economy for the Energy Transition*. De Gruyter, 2018.

[11]   B. Endrődi, N. Simic, M. Wildlock, and A. Cornell, "A review of chromium(VI) use in chlorate electrolysis: Functions, challenges and suggested alternatives," *Electrochim. Acta*, vol. 234, pp. 108–122, Apr. 2017, doi: 10.1016/j.electacta.2017.02.150.

[12]   D. Apostolou, P. Enevoldsen, and G. Xydis, "Supporting green Urban mobility – The case of a small-scale autonomous hydrogen refuelling station," *Int. J. Hydrogen Energy*, vol. 44, no. 20, pp. 9675–9689, 2019, doi: 10.1016/j.ijhydene.2018.11.197.

[13]   C. Higgins and M. Ferguson, "Identifying and Characterizing Potential Electric Vehicle Adopters in Canada : A Two-stage Modelling Approach Moataz Mohamed Pavlos Kanaroglou," pp. 1–21.

[14]   O. Ekren, C. Hakan Canbaz, and Ç. B. Güvel, "Sizing of a solar-wind hybrid electric vehicle charging station by using HOMER software," *J. Clean. Prod.*, vol. 279, p. 123615, 2021, doi: 10.1016/j.jclepro.2020.123615.

[15]   N. P. | Docs, "POWER Data Methodology." [Online]. Available: https://power.larc.nasa.gov/docs/methodology/data/#meteorological.

[16]   "Understanding your electricity bill," *Tiered price plan*, 2021. [Online]. Available: https://utilitieskingston.com/Electricity/About/YourElectricityBill.

[17]   ENWIN, "Electricity, Water and District Energy for Windsor," 2021. [Online]. Available: https://enwin.com/electric-rates-residential/.

[18]   WorldData.info, "Energy consumption in Saint Pierre and Miquelon," 2021. [Online]. Available: https://www.worlddata.info/america/stpierre-miquelon/energy-consumption.php.

[19]   M. Gökçek and C. Kale, "Optimal design of a Hydrogen Refuelling Station (HRFS) powered by Hybrid Power System," *Energy Convers. Manag.*, vol. 161, no. December

2017, pp. 215–224, 2018, doi: 10.1016/j.enconman.2018.02.007.

[20] A. S. Aziz, M. F. N. Tajuddin, M. R. Adzman, M. F. Mohammed, and M. A. M. Ramli, "Feasibility analysis of grid-connected and islanded operation of a solar PV microgrid system: A case study of Iraq," *Energy*, vol. 191, p. 116591, Jan. 2020, doi: 10.1016/j.energy.2019.116591.

VITA AUCTORIS

NAME: Mohammadreza Babaei Jamnani

PLACE OF BIRTH: Mazandaran, Iran

YEAR OF BIRTH: 1996

EDUCATION: Shahed high school, Mazandaran, Iran, 2014

University of Mazandaran, Mazandaran,Iran,
B.A.Sc.,Mechanical Engineering, 2018

University of Windsor, Windsor, Ontario,
M.A.Sc., Mechanical Engineering, 2021